CORONARY ARTERY DISEASE IN METABOLIC SYNDROME:

A ROLE FOR THE SARCOPLASMIC RETICULUM Ca^{2+} ATPASE

Stacey Dineen Rodenbeck

Submitted to the faculty of the University Graduate School
in partial fulfillment of the requirements
for the degree
Doctor of Philosophy
in the Department of Cellular & Integrative Physiology,
Indiana University

July, 2016

Accepted by the Graduate Faculty, Indiana University, in partial fulfillment of the requirements for the degree of Doctor of Philosophy.

_____

Michael S. Sturek, Ph.D., Chair

_____

Richard N. Day, Ph.D.

Doctoral Committee

_____

Carmella Evans-Molina, M.D./Ph.D.

May 10, 2016

_____

Kieren Mather, M.D.

_____

Johnathan D. Tune, Ph.D.

DEDICATION

To my grandfather, Dr. Eldon LaVerne Haselwood, who has been a constant source of personal and professional wisdom and guidance, and to my grandmother, Mrs. Joan McQuiddy Haselwood, who was instrumental in my development of critical thinking skills during childhood, thank you both. You continue to be inspiration and encouragement at each step along the way. It is to both of you, with deep and abiding love, utmost respect, and complete gratitude, that I dedicate this work.

ACKNOWLEDGEMENTS

To my advisor, Dr. Mike Sturek, thank you. Thank you for encouraging me, for convincing me that “negative data are still data,” for believing in me when I didn’t believe in myself, and for pushing me to be better than I thought I could be. Thank you for the meetings, the pep talks, and the general support that you’ve provided. Your dedication to strong mentorship is evident, and I am so grateful to have been the beneficiary of it.

To my research committee, Dr. Richard N. Day, Dr. Carmella Evans-Molina, Dr. Kieren Mather, and Dr. Johnathan D. Tune, thank you for the meetings, support, guidance, and constructive criticisms that have been invaluable contributions to this research.

To my labmates: Mouhamad Alloosh, Jill Badin, Becky Bruning, Jim Byrd, Ayeeshik Kole, John Martin, Mikaela McKenney-Drake, Brandy Sparks, and Josh Sturek, thank you for the laughter, friendships, conversations, and general happy work environment. Thank you for being such an excellent and supportive team.

To Cassie Gohn, Jill Noblet, Kaela Varberg, and Emily Waskow, thank you for connecting during our first year, and for our continued friendships. Thank you for the girls’ nights out, the laughter, and the mutual support. You have truly made this journey enjoyable, and I don’t think I could have done it without you.

To the Department of Cellular & Integrative Physiology at Indiana University School of Medicine, thank you for the collaborations, the smiles in the hallway, and for welcoming me to such an incredible group of researchers.

To the Indiana University School of Medicine Biomedical Gateway (IBMG) program, thank you for providing the classes and rotation opportunities during the first year at Indiana University School of Medicine.

To my undergraduate mentors in the School of Natural Sciences at Indiana University Southeast, Dr. Pamela Connerly, Dr. Subhranil De, Dr. Kent Edmonds, Gail Emmert, Dr. Jan Fleischer, Dr. Elaine Haub, Dr. Teresa Hickerson, Dr. Randy Hunt, Dr. Gretchen Kirchner, Dr. Ben Nassim, Dr. Beth Rueschhoff, Dr. Aaron Setterdahl, Dr. David Taylor, Dr. David Treves, and Dr. Michele Zimmerman, thank you for excellent undergraduate training, continued mentorship, and ongoing friendships. You are continued sources of inspiration and courage.

To the friends I made in the School of Natural Sciences at Indiana University Southeast, Cory Dixon, Jeremy Eberle, Adam Groves, Media Lewandowski, Andrew Stillman, Ben Stillman, and Samantha Strom, thank you for the game nights, the laughter, for introducing me to silly YouTube videos, for group dinners at New Albany Brewing Company, and for your continued friendships and support.

To my church family at the Brownsburg Church of Christ, thank you for your friendships, your support, and your prayers. You have been my family for the past four years, and I love you all.

To my parents, John and Karen Dineen, thank you for your constant love and support. Thank you for teaching me to work hard, to love learning, and to be kind. You are my heroes, and I love you. To my siblings, Elizabeth Shearer, John Dineen, James Dineen, Joshua Dineen, Jacob Dineen, Joseph Dineen, Jared Dineen, Josiah Dineen, Nancy Dineen, and Jason Dineen, thank you for keeping me humble, and for your love. To my niece, Haelley Shearer, and nephews, Brennan Shearer and Cameron Shearer, thank you for your constant sunshine.

To my forever friend, Stephanie Davis, thank you for being interested in my journey, for pulling me back to reality, for reminding me that there is life outside of graduate school, for grounding me, and for your constancy. Your friendship is one I treasure dearly.

To my husband, Jim Rodenbeck, I love you. Thank you for loving me through this journey, for drying my eyes, and for pushing me to succeed. Thank you for your support, your loyalty, your patience, and your undying love. I can't want to do the next phase of life with you.

To my God, thank you for life and for seeing me through the best and worst parts of it. Thank you for every new morning and every opportunity. Thank you for second chances and for saving me from myself. Thank you for walking by my side through this leg of life's journey.

This research was supported by the American Heart Association (15PRE25280001) and by the National Institutes of Health (HL062552).

Stacey Dineen Rodenbeck

CORONARY ARTERY DISEASE IN METABOLIC SYNDROME: A ROLE FOR THE SARCOPLASMIC RETICULUM Ca^{2+} ATPASE

Coronary artery disease (CAD) is a leading cause of death among Americans and is fueled by underlying metabolic syndrome (MetS). The prevalence and lethality of CAD necessitates rigorous investigations into its underlying mechanisms and to facilitate the development of effective treatment options. Coronary smooth muscle (CSM) phenotypic modulation from quiescent to synthetic, proliferative, and osteogenic phenotypes is a key area of investigation, with underlying mechanisms that remain poorly understood. Using a well-established pre-clinical model of CAD and MetS, the Ossabaw miniature swine, we established for the first time the time course of Ca^{2+} dysregulation during MetS-induced CAD progression. In particular, we used the fluorescent Ca^{2+} dye, fura-2, to examine alterations in CSM intracellular Ca^{2+} regulation during CAD progression, as perturbations in intracellular Ca^{2+} regulation are implicated in several cellular processes associated with CAD pathology, including CSM contractile responses and proliferative pathways. These studies revealed that the function of several CSM Ca^{2+} handling proteins is elevated in early CAD, followed by loss of function in severe atherosclerotic plaques. Decreased intracellular Ca^{2+} regulation occurred concurrently with reductions in CSM proliferation, measured with Ki-67 staining. In particular, alterations in sarcoplasmic reticulum (SR) Ca^{2+} store together with altered function of the sarco/endoplasmic reticulum Ca^{2+} ATPase (SERCA) were associated with induction of proliferation. Organ culture of coronary arterial segments revealed that culture-induced medial thickening was prevented by SERCA inhibition with cyclopiazonic acid (CPA). Activation of SERCA with the small molecule activator,

CDN1163, increased CSM proliferation, which was attenuated by treatment with CPA, thus establishing upregulated SERCA function as a proximal inducer of CSM proliferation. Further, we demonstrated that *in vitro* treatment of CSM from lean Ossabaw swine with the glucagon-like peptide-1 (GLP-1) receptor agonist, exenatide, increased SERCA function. However, *in vivo* treatment of Ossabaw swine with MetS with the GLP-1 receptor agonist, AC3174, had no effect on CAD progression and *in vitro* examination revealed resistance of SERCA to GLP-1 receptor agonism in MetS. These findings further implicate SERCA in CAD progression. Collectively, these are the first data directly linking SERCA dysfunction to CSM proliferation and CAD progression, providing a key mechanistic step in CAD progression.

Michael Sturek, Ph.D., Chair

TABLE OF CONTENTS

LIST OF TABLES

LIST OF FIGURES

LIST OF ABBREVIATIONS

ANOVA – Analysis of variance

BMI – Body mass index

CAC – Coronary artery calcification

CAD – Coronary artery disease

cAMP – Cyclic adenosine monophosphate

CFX – Circumflex artery

CPA – Cyclopiazonic acid

CSM – Coronary smooth muscle

DMEM – Dulbecco's modified eagle medium

DPP-IV – Dipeptidyl-peptidase IV

E-C – Excitation-contraction

ERK1/2 – Extracellular signal-related kinase

FBS – Fetal bovine serum

GLP-1 – Glucagon-like peptide-1

IP_3 – Inositol 1,4,5-trisphosphate

IVUS – Intravascular ultrasound

LAD – Left anterior descending artery

LDL – Low density lipoprotein

MAPK – Mitogen activated protein kinase

MetS – Metabolic syndrome

NCX – Sodium-calcium exchanger

PDGF – Platelet-derived growth factor

PIP_2 – Phosphatidylinositol diphosphate

PKA – Protein kinase A

PKCζ – Protein kinase Cζ

PLC – Phospholipase C

PMCA – Plasmalemma Ca^{2+} ATPase

RCA – Right coronary artery

RUNX2 – runt-related transcription factor-2

RyR – Ryanodine receptor

SERCA – Sarco-endoplasmic reticulum Ca^{2+} ATPase

SM-MHC – Smooth muscle myosin heavy chain

SOCE – Store operated Ca^{2+} entry

SR – Sarcoplasmic reticulum

TC – Masson's trichrome

TRP – Transient receptor potential

TRPC1 – Transient receptor potential canonical 1

VGCC – Voltage-gated Ca^{2+} channel

VSM – Vascular smooth muscle

VVG – Verhoeff van-Gieson

WHO – World Health Organization

CHAPTER 1: INTRODUCTION

Obesity

Currently, nearly 35% of adults in the United States are obese, as shown by a body mass index (BMI) ≥ 30 kg/m^2 (1). Globally, in 2014 39% of adults were overweight (BMI ≥ 25 kg/m^2) and obesity affected 11% of men and 15% of women (2). Even in developing countries, well-meaning philanthropic efforts have increased supply of sweeteners and oils and have unfortunately contributed to global rises in obesity (3). In addition to the vast numbers of adults suffering from obesity, nearly 17% of children in the United States are classified as obese (1). Worldwide, the proportion of overweight and obese children has increased from 5% in 2000 to 9% in 2014 (2). Juvenile obesity is of special concern because during childhood obesity occurs through both adipocyte hyperplasia and hypertrophy (4), while in adults obesity occurs primarily through adipocyte hypertrophy (5). The presence of adipocyte hyperplasia in childhood indicates that juvenile obesity actually increases potential for greater obesity in adulthood. In addition to the rising numbers of obese individuals, we must contend with ever-increasing medical costs. Obesity alone is estimated to cost the United States $147 billion in medical costs (6).

An understanding of the origins of obesity provides clues to potential underlying mechanisms of disease etiology. During the early hunter-gatherer phase of human evolution our species was exposed to the “feast or famine” food availability associated with seasonal cycles. This environment served as the selective pressure by which the “thrifty genotype” was propagated. During times of plenty, the thrifty genotype enabled efficient storage of excess calories in various fat depots (7). These fat depots could then be mobilized as energy sources during “famine” times, when food supply was restricted. Modern food preservation options have eliminated the cyclical pattern of food availability, providing a constant, plentiful supply. Today, a sedentary lifestyle combined with

abundant food supply renders this “thrifty genotype” harmful (8). We live in an “obesogenic environment” of constant “feast,” signaling our bodies to build fat depots. In the absence of “famine,” these fat depots continue to grow unchecked, resulting in growing waistlines and many obesity-related complications (9).

Metabolic Syndrome

Closely related to the obesity crisis is an ever-increasing incidence of metabolic syndrome (MetS). Alberti *et al.* (10) defines the word “syndrome” as “simply a clustering of factors that occur together more often than by chance alone and for which the cause is often uncertain.” Using this definition of “syndrome,” MetS is easily defined as a clustering of metabolic conditions, all of which are risk factors for cardiovascular disease or diabetes. Because of the vague nature of these definitions, there has been much disagreement regarding proper criteria for diagnosis. Beginning with World Health Organization (WHO) consortium in 1998 (11), attempts have been made to reconcile differences in diagnostic criteria. The most recent standard for diagnosis is the presence of 3 of the 5 risk factors listed in Table 1.1 (10; 12). Hypertension and insulin resistance are also often included as independent risk factors in the diagnosis of MetS (11). Indeed both insulin resistance and glucose intolerance contribute to the hyperglycemia shown in Table 1.1.

In addition to the thrifty genotype hypothesis surrounding development of obesity and MetS, a “thrifty phenotype” hypothesis has also been proposed (13; 14) which states that, during fetal and early postnatal development, undernutrition may trigger fetal programming of adaptive mechanisms. These fetal adaptations are rendered harmful when the postnatal environment is healthy and nutrition is adequate. Whether inherited (thrifty genotype hypothesis), or environmentally triggered (thrifty phenotype hypothesis), a propensity toward MetS may contribute to overall decline of metabolic health and lead to additional complications, including diabetes and cardiovascular disease.

Although many controversies exist surrounding the development and components of MetS, it is well-established that the presence of MetS confers elevated risk for the development of diabetes and cardiovascular disease. Indeed, the presence of MetS doubles risk of cardiovascular disease development (10; 15-17). While each component of MetS is an individual risk factor for cardiovascular disease, the presence of the MetS cluster confers greater risk than any individual component (18). Risk for developing type 2 diabetes mellitus is increased 5 times by presence of MetS (10). Ultimately, MetS increases risk of all-cause mortality 1.5-fold (17).

Several animal models have been developed to recapitulate many of the risk factors for MetS. The Ossabaw miniature swine is an excellent model for MetS, as they display a “thrifty phenotype,” and naturally develop all of the human risk factors for MetS. Table 1.2 (adapted from (19)) describes Ossabaw miniature swine as a superior model of MetS compared to Yucatan miniature swine, which are leaner and are resistant to development of MetS.

Type 2 Diabetes

In 2011, 366 million individuals worldwide were affected by diabetes mellitus (20), defined by the American Diabetes Association as “a group of metabolic diseases characterized by hyperglycemia resulting from defects in insulin secretion, insulin action, or both (21).” Diabetes mellitus is sub-classified into two forms: Type 1 diabetes mellitus that is initiated through an auto-immune attack on the β-cells of the endocrine pancreas resulting in diminished insulin production, while type 2 diabetes mellitus is a progressive disease, resulting from prolonged glucose intolerance and insulin resistance, and accounts for 90-95% of diabetes mellitus cases in North America (22). Diabetes mellitus cost the United States $245 billion in 2012 in direct and indirect medical costs (23; 24).

The etiology of type 2 diabetes mellitus is complex, often riddled with other confounding metabolic factors. In normal physiology, a post-prandial rise in plasma

glucose is sensed by the pancreatic beta cell, and insulin secretion is initiated. Circulating insulin binds to receptors on peripheral tissues (liver, skeletal muscle, adipose), initiating intracellular signaling cascades resulting in glucose uptake. In early type 2 diabetes mellitus (Fig. 1.1) (25), elevated fasting blood glucose levels result from reduced insulin sensitivity in the peripheral tissues. This reduced sensitivity occurs through multiple signaling pathways, including a lack of receptor binding of insulin or through aberrant post-receptor signaling in the peripheral tissues. The incidence of insulin resistance is elevated with increasing age, obesity, and a sedentary lifestyle. The resultant rise in plasma glucose sparks a compensatory rise in insulin secretion, giving rise to the hyperinsulinemia closely associated with the etiology of type 2 diabetes mellitus. Over time, as insulin sensitivity decreases, the ever-increasing demand on the pancreatic beta cell for more insulin creates an impossible feed-forward loop. The beta cell, unable to compensate for the growing demands, can no longer produce adequate insulin and ultimately fails.

Many options exist for the treatment of type 2 diabetes mellitus (26; 27). In addition to initial recommendations for diet modification and exercise, most individuals diagnosed with type 2 diabetes mellitus are also treated with glucose-lowering drugs. This can be accomplished through insulin-sensitization (biguanides) (28-30), enhancement of insulin secretion from the pancreatic beta cell (sulfonylureas) (31; 32), or through combined increase of insulin sensitivity and insulin secretion (glucagon-like peptide-1 receptor agonists) (33; 34). Following beta cell failure, insulin therapy is often necessary.

Coronary Circulation

One of the major long-term complications of poorly controlled type 2 diabetes is coronary artery disease, which ultimately causes the greatest morbidity and mortality in type 2 diabetes patients. Accordingly, fundamental knowledge of the regulation of the coronary circulation in health and disease is essential.

The coronary arteries branch from the proximal aorta, wrapping around the heart and branching deep into the myocardium. The coronary circulation delivers oxygen and other substrates to the tirelessly working heart. Because resting myocardial oxygen consumption is high, its oxygen delivery must be efficient. Hindrances to coronary blood flow can have far-reaching and serious consequences.

The right and left main coronary arteries originate from the left and right ostia (Fig. 1.2; (35)) in the proximal aorta, just distal to the aortic semilunar valve. The left main coronary artery branches soon after leaving the ostium into the left anterior descending (LAD) artery, and the circumflex (CFX) artery. The LAD travels along the anterior interventricular groove, while the CFX wraps around the heart in the left atrioventricular groove. The right coronary artery (RCA) wraps around the heart in the right atrioventricular groove. In ~90% of humans (right-dominant), once the RCA reaches the posterior interventricular groove, it turns downward, becoming the posterior descending artery (35). In the remaining ~10% (left-dominant), the CFX becomes the posterior descending artery.

The coronary arteries can be subdivided into macrovascular conduit coronary arteries (described above), and microvascular resistance arterioles (36). The large conduit coronary arteries branch extensively, giving rise to first, second, and third order resistance arterioles. These branches dive deep into the myocardium, providing the tight control over blood flow necessary to regulate substrate delivery to the myocardium.

Histological examinations reveal the cell types and extracellular matrix of the conduit coronary artery (Fig. 1.3). Arteries are comprised of three layers, the adventitia, the media, and the intima. The adventitial layer, comprised primarily of collagen and other connective tissue, provides the tough outer layer surrounding most arteries. The medial layer comprises the bulk of the artery wall and is composed primarily of vascular smooth muscle. The intimal layer lies adjacent to the lumen and is comprised primarily of a single layer of endothelial cells. The media is bounded by two layers of elastin, termed the internal elastic lamina between the media and the intima and the external elastic lamina between the media and the adventitia. Resistance arterioles are primarily comprised of a medial layer, which provides them the ability for the tight regulation of circumference necessary to regulate blood flow to the myocardium.

Coronary Artery Disease

Cardiovascular disease accounted for 23.6% of all deaths in the United States in 2012 (37), maintaining its rank as the leading cause of death. Incidence of cardiovascular disease is predicted to rise to 40.5% of the United States population by 2030 (38). Estimated costs for cardiovascular disease in the United States from 2011-2012 were $316.6 billion, including both direct and indirect medical costs (6). These totals have significantly decreased since 2006, when cardiovascular disease medical costs were estimated at $403.1 billion (39).

Coronary artery disease (CAD) is one of the many forms of cardiovascular disease. An estimated 15.5 million adults in the United States suffer from CAD and 1 out of every 7 deaths has CAD as an underlying cause (6). The etiology and progression of CAD is complex and still under investigation. In 1995, Stary *et al.* (40) introduced a system for the classification of CAD stages (detailed in Fig. 1.4, edited from (41; 42)). In the early, clinically insignificant stages of CAD, fatty streaks develop as lipids infiltrate the intimal region of the coronary artery. CAD progresses with recruitment of circulating

leukocytes from the bloodstream and of coronary smooth muscle (CSM) cells from the medial layer of the artery. Further progression of CAD involves apoptosis, leading to the accumulation of lipids and cellular debris within the core of the atherosclerotic plaque. Plaques with large lipid-laden and/or necrotic cores and thin fibrous caps (types 4-6) are prone to rupture, resulting in thrombosis, embolism, and acute myocardial infarction. The current understanding of the cellular biology underlying atherosclerosis has recently been summarized in excellent reviews by Tabas *et al.* (43) and McEvoy *et al.* (42).

The relationship between MetS and CAD is both complicated and convincing. Lakka *et al.* (44) examined development of CAD in 1,209 Finnish middle-aged men over the course of 11 years. None of the patients displayed cardiovascular disease at the beginning of the study. The presence of MetS significantly increased incidence of CAD. The presence of MetS not only increases risk of CAD, but also increases CAD severity (18). In one study of 632 individuals, multivariate analysis revealed that, as the number of MetS components present increased, severity of CAD, as assessed by Gensini scoring, was elevated (45) (Fig. 1.5). Gensini scoring assigns values for CAD severity based on the amount of stenosis and the "importance" of the location of the atherosclerotic lesion in the coronary anatomy (e.g.: a lesion in the left main coronary artery would affect more myocardium than would a lesion in the distal LAD and would be assigned a higher score) (45). Ultimately, MetS exacerbates both risk for and severity of CAD, presenting a variety of targets for CAD treatment and prevention. Type 2 diabetes also contributes to CAD risk; however, the focus of this work will be on the role of MetS in CAD development.

Vascular Smooth Muscle

CSM cells play a key role in CAD progression, functioning both in plaque stabilization and outward remodeling to maintain arterial lumen diameter. Smooth muscle cells are generally small (diameter ~5-6 μm) with an elongated spindle-shape

(length ~20-50 μm) and display profound heterogeneity in both cellular and molecular physiology. First, depending on location and function, smooth muscle may display either phasic (non-vascular and some venous smooth muscle, such as in the portal vein) or tonic (most vascular) contraction patterns (36; 46; 47). Vascular smooth muscle (VSM) must sustain some level of tone throughout the life of the organism, while gastrointestinal smooth muscle must participate in peristaltic contractions. These differences in function highlight the need for differential contraction patterns. The focus here will be on VSM, and in particular, coronary smooth muscle (CSM).

The most dramatic difference in the subcellular organization of smooth muscle as compared to striated muscle is the lack of organized contractile filament sarcomeres. Rather, thin filaments attach at the sarcolemma to membrane plaques and within the cytosol to “floating” dense bodies, which are analogous to the z-lines in striated muscle (36; 48; 49). These thin filaments associate with myosin filament groups to form “mini-sarcomeres” (49). The thin filaments are composed primarily of actin and tropomyosin, which course along in a lattice arrangement (36), which has shown ability to rapidly adapt, providing the wide working length range necessary in smooth muscle (50; 51).

Smooth muscle cells are connected to one another by gap junctions, forming a functional syncytium (36; 49). This coupling allows ion flow from one cell to the next, resulting in the concerted, controlled contraction and relaxation necessary to modulate blood flow. Smooth muscle, contracting together, result in reduction in arterial diameter, which restricts blood flow. Simultaneous, controlled relaxation of smooth muscle results in arterial dilation, which increases blood flow. This ability is crucial to the organism’s ability to modulate substrate delivery according to specific need.

Excitation-Contraction (E-C) coupling may occur in smooth muscle via two different mechanisms: electromechanical coupling and pharmacomechanical coupling (49), both functioning through a rise in cytosolic Ca^{2+} to trigger contraction.

Electromechanical coupling evokes contraction through changes in membrane potential, such as membrane depolarization. Pharmacomechanical coupling refers to any E-C coupling event which evokes contraction independent of alterations in membrane potential, i.e. largely without depolarization. The trigger for this kind of E-C coupling is either ligand-gated Ca^{2+} influx, intracellular Ca^{2+} release, or modulation of the Ca^{2+} sensitivity of the contractile proteins (49). Physiologically, electromechanical and pharmacomechanical coupling often occur in concert (52; 53), providing the CSM means by which to obtain greater contraction or relaxation than would be possible with only one stimulus.

Smooth Muscle Phenotypic Modulation

Under normal, healthy conditions, CSM cells maintain a quiescent, contractile phenotype. However, under conditions of vascular injury or atherosclerotic CAD, CSM cells will modulate phenotype to respond to the changing environment. Identification of phenotypic markers has proven difficult, because smooth displays remarkable diversity, and because many markers of smooth muscle differentiation are also expressed in other cell types (54). Still, a variety of markers have been identified. In addition to the normal, quiescent phenotype, two primary abnormal phenotypes have been described - the proliferative CSM and the osteogenic CSM.

The first abnormal CSM phenotype, proliferative CSM is implicated in a variety of disease states, and functions in CAD progression both to stabilize atherosclerotic plaque and in lumen expansion via outward arterial remodeling. Experimental identification of proliferative CSM is difficult. However, based on observations in cell culture, proliferative CSM cells do not express normal contractile proteins (49; 55). Thus, identification of the proliferative CSM phenotype can be done by observation of the loss of a number of contractile CSM markers, such as smooth muscle myosin heavy chain (SM-MHC), smoothelin, smooth muscle α-actin, or calponin. Additionally, proliferative smooth muscle

cells possess the ability to secrete elevated amounts of collagen and other extracellular matrix proteins, which functions to assist in atherosclerotic plaque stabilization.

The second abnormal CSM phenotype is the osteogenic smooth muscle phenotype. These CSM underlie arterial calcification, expelling molecules, largely by secretion of matrix vesicles (exosomes) to form hydroxyapatite crystals (56). Osteogenic CSM cells, like proliferative CSM cells, lack markers of mature, contractile CSM, such as SM-MHC (57). However, unlike proliferative CSM, osteogenic CSM express bone marker proteins, such as runt-related transcription factor-2 (RUNX2) (57). Calcification during CAD progression most often occurs in the neointimal layer of coronary arteries, while calcification induced by kidney disorders most often occurs within the arterial media (56; 57). The detailed mechanisms underlying calcification are still under investigation. While the experiments contained in this thesis do not directly examine coronary artery calcification, it is likely that perturbations in CSM intracellular Ca^{2+} regulation contribute to the phenotypic switch to an osteogenic phenotype, and future studies will undertake the establishment of these links.

Coronary Smooth Muscle Intracellular Ca^{2+} Regulation

In CAD, the Ca^{2+} handling mechanisms in CSM cells are profoundly altered. Intracellular Ca^{2+} is a ubiquitous second messenger and regulator of a number of critical processes in CSM cells, including excitation-contraction coupling, excitation-transcription coupling, and proliferation. Therefore, a variety of Ca^{2+} handling proteins are employed to keep cytoplasmic Ca^{2+} under tight regulation (Fig. 1.6), to maintain average cytoplasmic Ca^{2+} concentration at ~100 nM. Ca^{2+} regulating proteins can be loosely divided into three categories: cytoplasmic Ca^{2+} binding proteins, such as calmodulin, membrane bound Ca^{2+} transporting proteins, and sarcoplasmic reticulum (SR) Ca^{2+} binding proteins, such as calreticulin and calsequestrin. The membrane bound Ca^{2+} transporting proteins function to bring Ca^{2+} into the CSM cells from the extracellular

environment (influx mechanisms), transport Ca^{2+} out of the cytosol to the extracellular environment (efflux mechanisms), transport Ca^{2+} into intracellular Ca^{2+} stores from the cytosol, and transport Ca^{2+} out of the cytosol into intracellular Ca^{2+} stores.

Ca^{2+} influx mechanisms are mediated by voltage-gated Ca^{2+} channels (VGCC) and transient receptor potential (TRP) channels. VGCCs are controlled by membrane potential and open in response to membrane depolarization. These channels are the target of many blood pressure lowering, arrhythmia correcting drugs, such as verapamil, nifedipine, and diltiazem. Inhibition of VGCCs results in attenuation of contraction, thus maintaining lower arterial pressures. In contrast, TRP channels mediate store-operated Ca^{2+} entry (SOCE), which partly compensates for depletion of internal Ca^{2+} stores (58). Following both VGCC and TRP channel opening, Ca^{2+} enters the CSM cells passively, flowing down its electrochemical gradient.

Ca^{2+} efflux involves active transport, as Ca^{2+} moves out of the CSM cell against its electrochemical gradient. The Na^{+}/Ca^{2+} exchanger (NCX) harvests the energy from the movement of two Na^{2+} ions flowing down their gradient into the CSM, and transports a single Ca^{2+} ion out of the CSM cell. The plasmalemma Ca^{2+} ATPase (PMCA) uses the energy gained by ATP hydrolysis to pump Ca^{2+} out of the CSM cell.

Alterations in SR Ca^{2+} beyond an optimal set point likely play a pivotal role in SR CSM phenotypic modulation during CAD progression. Internal Ca^{2+} stores serve a crucial role in CSM Ca^{2+} regulation, providing the bulk of the Ca^{2+} required for CSM contraction. The SR occupies 1-7.5% of cell volume in smooth muscle (49), and is the primary intracellular Ca^{2+} store, contiguous with the nuclear envelope. Additionally, interactions between SR and mitochondrial Ca^{2+} stores have been observed, with mitochondria contributing to SR Ca^{2+} refilling following SR Ca^{2+} store depletion (59), although details of this mechanism remain unknown. Total SR luminal Ca^{2+} concentrations are estimated to be 2-5 mM (60) with the majority of luminal Ca^{2+} bound

by SR Ca^{2+}-binding proteins, such as calreticulin and calsequestrin. Luminal free [Ca^{2+}] fluctuates with store filling and depletion, and estimates in non-smooth muscle cells suggest that luminal free [Ca^{2+}] ranges from 60-400 μM in the full state to 1-50 μM in the depleted state (61). The tight regulation of SR [Ca^{2+}] is necessary for healthy CSM function. Studies in cardiac muscle reveal that overloading of the SR with Ca^{2+} results overload-induced Ca^{2+} store release (62), resulting in cardiac arrhythmias. Early studies from our lab in CSM indicate a similar phenomenon, termed SR Ca^{2+} unloading (63-65). While much of this "unloaded" Ca^{2+} may be preferentially released toward the sarcolemma for extrusion (63-65), other studies in SMC monolayer cultures indicate that increased SR Ca^{2+} stores are responsible for the elevations in bulk cytosolic Ca^{2+} necessary for induction of SMC de-differentiation and proliferation (66-68). Therefore, elevated luminal SR Ca^{2+} results in loss of the differentiated, contractile phenotype, leading to the increased CSM proliferation observed in early CAD. Conversely, decreases in SR luminal Ca^{2+} are sensed by Ca^{2+} binding chaperones within the SR, such as Grp78, which trigger induction of endoplasmic reticulum stress pathways, which, if unchecked, result in apoptosis (61). Thus, CSM apoptosis induced by reductions in SR Ca^{2+} store may contribute to the increased necrotic core observed in advanced atherosclerotic lesions in late CAD.

Two Ca^{2+} release channels, located in the contiguous sarcoplasmic reticulum (SR) and nuclear envelope membranes, are responsible for release of Ca^{2+} from the internal store; however, the results of release are wildly divergent. Ryanodine receptors (RyR), while important in striated muscle for Ca^{2+} induced Ca^{2+} release and muscle contraction, have a lesser role in initiating contraction of CSM. In the CSM, localized Ca^{2+} sparks resulting from RyR release of SR Ca^{2+} elicits spontaneous transient outward K^+ currents, hyperpolarizing the sarcolemma, closing VGCCs, and ultimately relaxing the CSM (36; 69). Conversely, the release of Ca^{2+} that is mediated by inositol 1,4,5-

trisphosphate (IP_3) receptors is mediated through hormone binding to G protein coupled receptors. Activation of the hormone receptor results in phospholipase C cleavage of phosphatidylinositol diphosphate, liberating IP_3. Liberated IP_3 functions, in part, to initiate Ca^2 release from the SR through IP_3 receptors located on the SR membrane. While RyRs are the primary means of Ca^{2+}-induced Ca^{2+} release, IP_3 activity is largely mediated by contracting factors from the coronary endothelium, such as endothelin-1 (70).

A major mechanism of relaxation of CSM is mediated through Ca^{2+} uptake by the sarco-endoplasmic reticulum Ca^{2+} ATPase (SERCA). Using energy gained from ATP hydrolysis, SERCA pumps Ca^{2+} out of the cytosol into the SR, thus removing the stimulus for contraction, ultimately resulting in relaxation. The affinity of SERCA for Ca^{2+} is regulated by phospholamban. Phosphorylation of phospholamban results in its dissociation from SERCA, leading to an increased affinity of SERCA for Ca^{2+}, and efficient removal of Ca^{2+} from the cytosol. The phosphorylation of phospholamban is mediated through the activity of cyclic adenosine monophosphate (cAMP) and cyclic guanosine monophosphate – dependent protein kinases.

Mammalian SERCA 1, 2, and 3 are homologous proteins encoded by three distinct genes (71). Alternative splicing of these genes results in more than ten mammalian SERCA isoforms. Broadly, SERCA1 is primarily expressed in skeletal muscle, SERCA2 is ubiquitously expressed, and SERCA3 is expressed primarily in non-muscle cells. Alternative splicing of SERCA2 results in three distinct SERCA2 isoforms. SERCA2a is largely expressed in cardiac and slow-twitch skeletal muscle (71), although recent studies have implicated loss of SERCA2a in VSM as a potential contributor to proliferation in arterial organ culture conditions (72-74). SERCA2b is ubiquitously expressed, both in muscle and non-muscle cells (71). SERCA2c was more recently identified in cardiac muscle (75).

In CAD, almost all of these described Ca^{2+} handling mechanisms are altered. Table 1.2 summarizes the changes in intracellular Ca^{2+} handling with diabetic dyslipidemia or MetS-induced CAD. However, there are several discrepancies in the literature regarding these changes in Ca^{2+} handling. In particular, there is disagreement regarding the up- vs. downregulation of VGCC and SERCA function. Several studies by our research group have demonstrated increased VGCC function and expression in CAD (76-78), while additional studies from ours and other groups have shown decreased VGCC function in CAD (79; 80). We have demonstrated both increased (79; 81) and decreased (82) SERCA function in CAD. Differences in breed, MetS/CAD duration, and systemic milieu (i.e. diabetic dyslipidemia vs. MetS) between studies demonstrate the need for studies in a common animal model examining alterations in Ca^{2+} handling during CAD/MetS progression, linking these changes to specific facets of CAD progression.

Glucagon-like Peptide-1 Actions on the Coronary Vasculature

Modulation of intracellular Ca^{2+} handling processes is hypothesized to result in prevention of CSM phenotypic switching, disallowing CAD progression. Thus, efforts toward drug discovery and development to this end are crucial. Glucagon-like peptide-1 (GLP-1) is an endogenous hormone, secreted in a postprandial manner, which functions to increase insulin sensitivity and to increase insulin biosynthesis and secretion (33). The GLP-1 receptor is a G protein-coupled receptor activated upon ligand binding. Several downstream intracellular signaling pathways have been implicated in the propagation of GLP-1 receptor activation. The most well characterized of the GLP-1 receptor pathways is as follows: GLP-1 receptor activation results in the generation of cAMP by adenylate cyclase (83; 84), triggering the activation of protein kinase A (PKA) (85), which has a number of phosphorylation targets, including VGCCs (86; 87) and the negative regulator of SERCA, phospholamban (88; 89). Additional pathways have also been elucidated,

including phosphatidylinositol 3-kinase activation of extracellular signal-related kinase (ERK) 1/2 and p38 mitogen-activated protein kinase (MAPK) (90; 91), or protein kinase Cζ (PKCζ) (92), and through activation of PLC (84).

Endogenous, native GLP-1 is rapidly degraded by dipeptidyl-peptidase IV (DPP-IV) (93; 94). Because of this rapid degradation, GLP-1 demonstrates a half-life *in vivo* of ~1-2 minutes (94). Thus, a number of DPP-IV resistant GLP-1 analogs and GLP-1 receptor agonists were developed for therapeutic use. The discovery of DPP-IV resistant Exendin-4 in the saliva of *Heloderma suspectum* (95), and its verification as a GLP-1 receptor agonist (96) and insulinotropic agent (97; 98), triggered the synthesis of a number of GLP-1 receptor agonists which are resistant to cleavage by DPP-IV. Currently, there are five GLP-1 receptor agonists approved for treatment of type 2 diabetes, and variations in the structure of these synthetic agonists contribute to variations in half-life and dosing interval (99). Exenatide was the first of GLP-1 receptor agonist to be developed and approved for use in humans, and continues to be used both in treatment of patients and in basic research (100-102). A number of other agonists are in various phases of development, and are used in basic research. For example, AC3174 demonstrates similar pharmacokinetic and pharmacodynamics profiles as exenatide, and has been used in a number of basic research studies (34; 103; 104).

Early studies of GLP-1 activity in the pancreatic β-cell revealed a role for GLP-1 receptor modulation of intracellular Ca^{2+} handling, resulting in heightened glucose-stimulated insulin secretion (105). Specifically, GLP-1 receptor agonists increase Ca^{2+} current through VGCCs, both through plasma membrane depolarization resulting from inhibition of K_{ATP} channels (106-108) and through increased VGCC sensitivity to a depolarizing event (105; 109). Further, GLP-1 receptor activation assists in mobilization of internal Ca^{2+} stores via both IP_3R and RyR activation (110; 111). Thus, GLP-1 receptor activation in pancreatic β-cells contributes to enhanced glucose-stimulated

insulin secretion through elevations in cytosolic Ca^{2+} by increasing both Ca^{2+} influx across the plasma membrane and by increasing release of internal Ca^{2+} stores.

GLP-1 receptor agonists have also garnered much interest as potential cardioprotective agents. Indeed, exenatide has been demonstrated to reduce myocardial infarct size following ischemia/reperfusion injury in swine (112). Exendin-4 was shown to protect against neointimal thickening following vascular injury (113). AC3174 improved cardiac function and remodeling during chronic heart failure (103) and partially relieved hypertension in rats (104). GLP-1 receptor agonists have also demonstrated a number of intracellular and Ca^{2+} handling effects, signaling both through ERK1/2 and cAMP pathways to reduce endoplasmic reticulum stress in macrophages (114) and cardiomyocytes (115), in part through increased SERCA function and/or protein expression. Further, GLP-1 receptor agonists enhance SERCA function in vascular endothelial cells (116). Thus, GLP-1 has potential for a protective role in the coronary vasculature. In this thesis, we examined the effect of GLP-1 receptor agonists on MetS-induced CAD progression, and on CSM intracellular Ca^{2+} handling in health and MetS/CAD.

The prevalence and severity of obesity, MetS, and T2D, and their contribution to CAD incidence and severity necessitate detailed investigation into the underlying mechanisms propagating this deadly disease cocktail. This thesis work tackles an examination of CSM Ca^{2+} handling changes during the progression of CAD, specifically dissects a causal role for SERCA in CSM proliferation, and examines the effect of a specific glucose-lowering agent on SERCA function in health and MetS/CAD.

Major Hypotheses

1. Intracellular CSM Ca^{2+} handling, specifically SR Ca^{2+} buffering by SERCA, is increased in early MetS/CAD and decreased in late MetS/CAD. This pattern in SR Ca^{2+} buffering is paralleled by changes that occur in CSM proliferation during CAD progression.

2. Acute SERCA activation increases the SR Ca^{2+} store and causes CSM proliferation, consistent with increased SR Ca^{2+} contribution to CSM proliferation in early stages of CAD.

3. Metabolic syndrome confers cardiovascular resistance to GLP-1 receptor agonism, and this effect is mediated, at least in part, by lack of SERCA responsiveness to GLP-1 receptor activation.

Tables and Figures

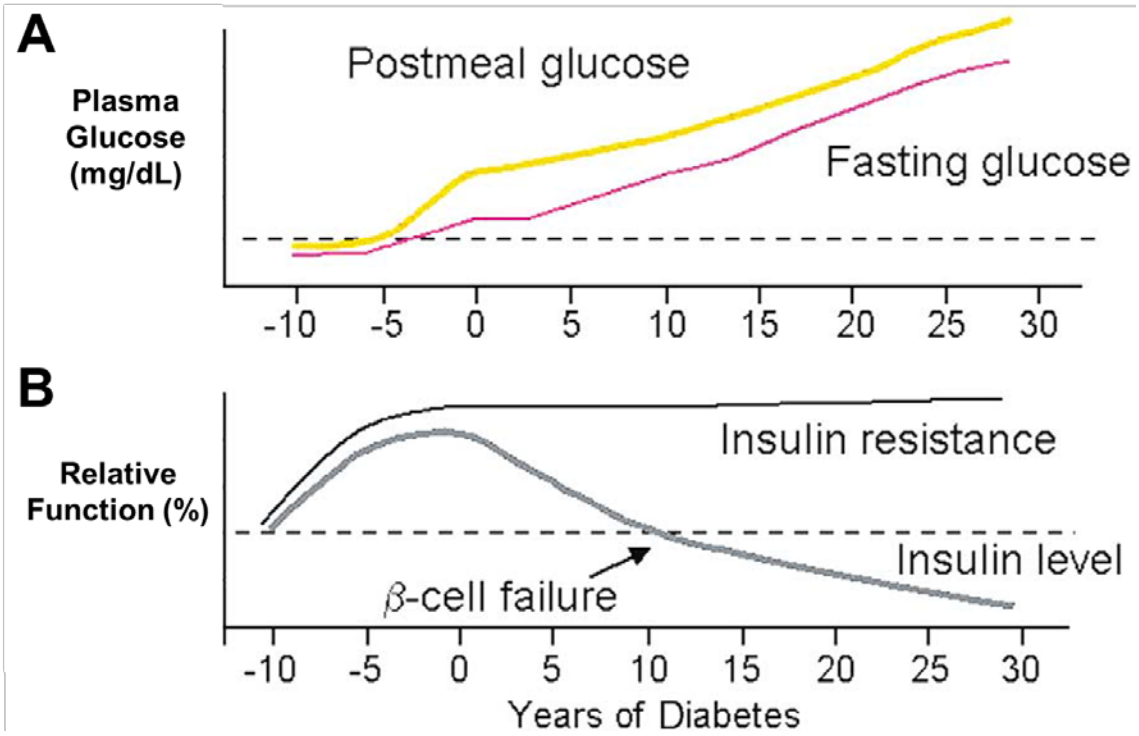

Figure 1.1: A time course of type 2 diabetes mellitus progression in humans (25). A. Fed and fasting plasma glucose levels become elevated prior to diabetes diagnosis ("prediabetes" or "metabolic syndrome") at "Time 0." **B.** Insulin resistance, together with the elevated plasma glucose levels in panel A, initiate compensatory elevations in beta cell function. However, with prolonged insulin resistance and hyperglycemia, the over-worked beta cells fail, resulting in drastically decreased insulin production.

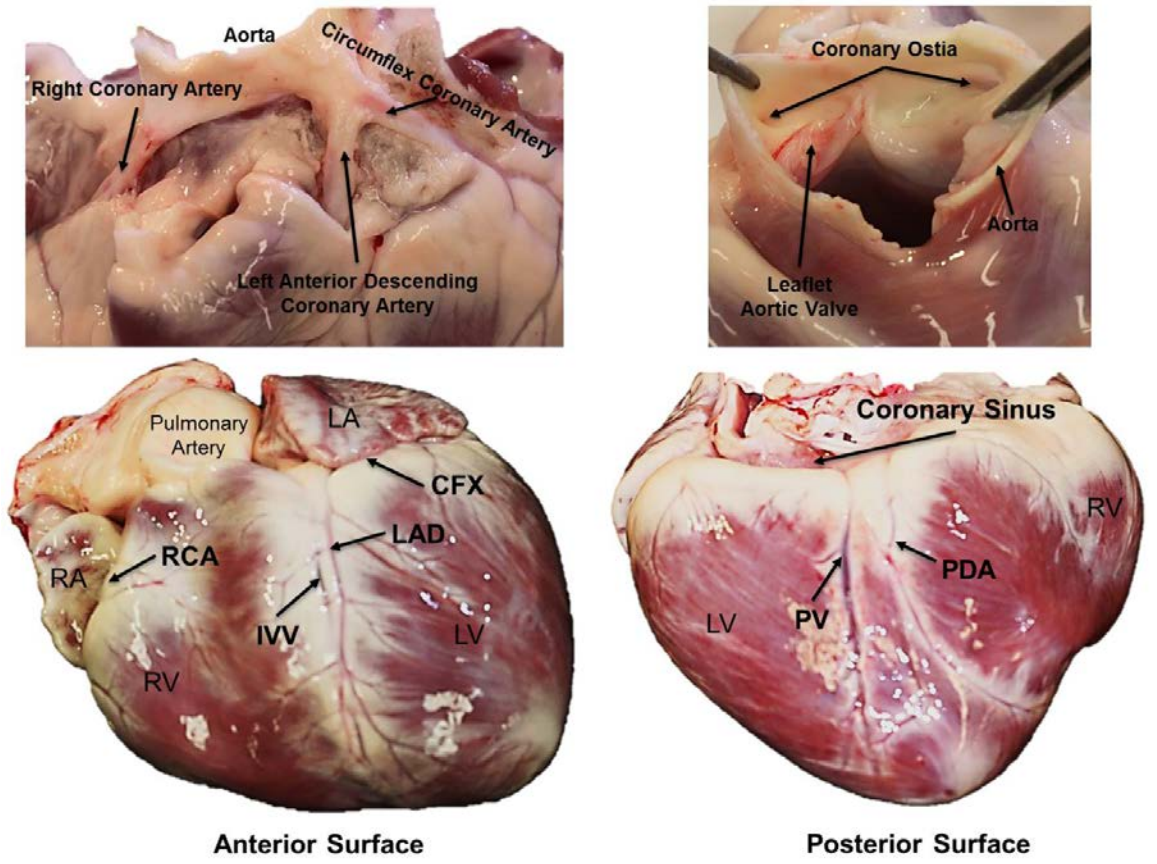

Figure 1.2: Anatomy of the coronary circulation (35). LA = Left atrium; CFX = Circumflex artery; LAD = Left anterior descending artery; LV = Left ventricle; IVV = Interventricular vein; RV = Right ventricle; RCA = Right coronary artery; RA = Right atrium; PV = Posterior vein; PDA = Posterior descending artery.

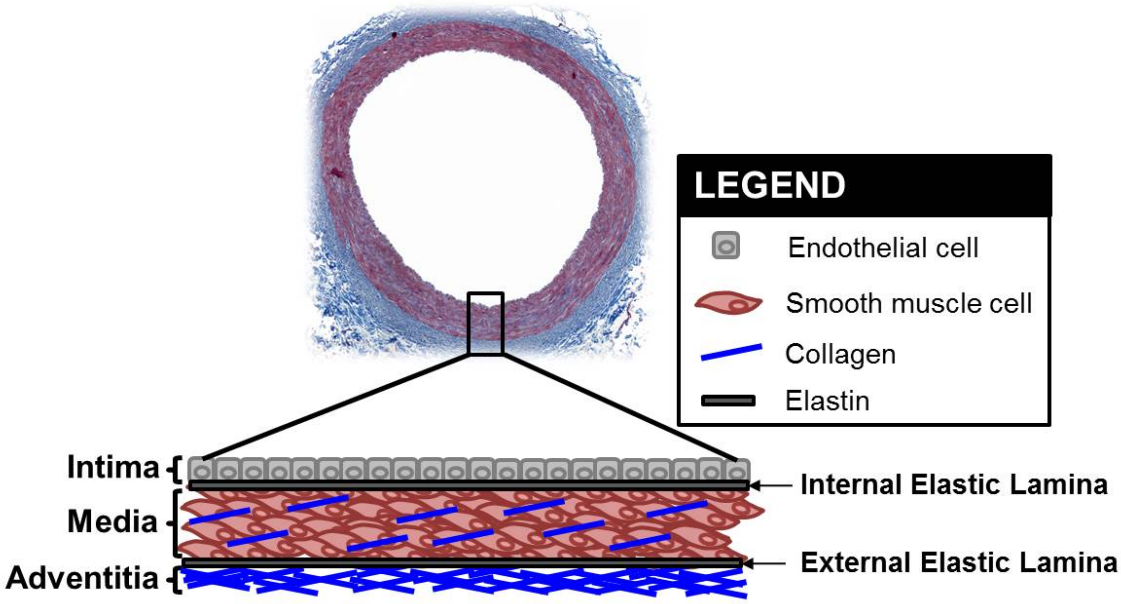

Figure 1.3: Cross-sectional anatomy of a coronary artery. The coronary artery is comprised of three main regions: the intima, the media, and the adventitia. The media is bounded by two elastic lamina: the internal elastic lamina and the external elastic lamina. On the luminal side of the internal elastic lamina, the intimal layer contains primarily endothelial cells. The media is comprised primarily of smooth muscle cells and extracellular matrix proteins, such as collagen. On the outer side of the external elastic lamina is the protective adventitial layer, comprised of collagen and various other extracellular matrix proteins.

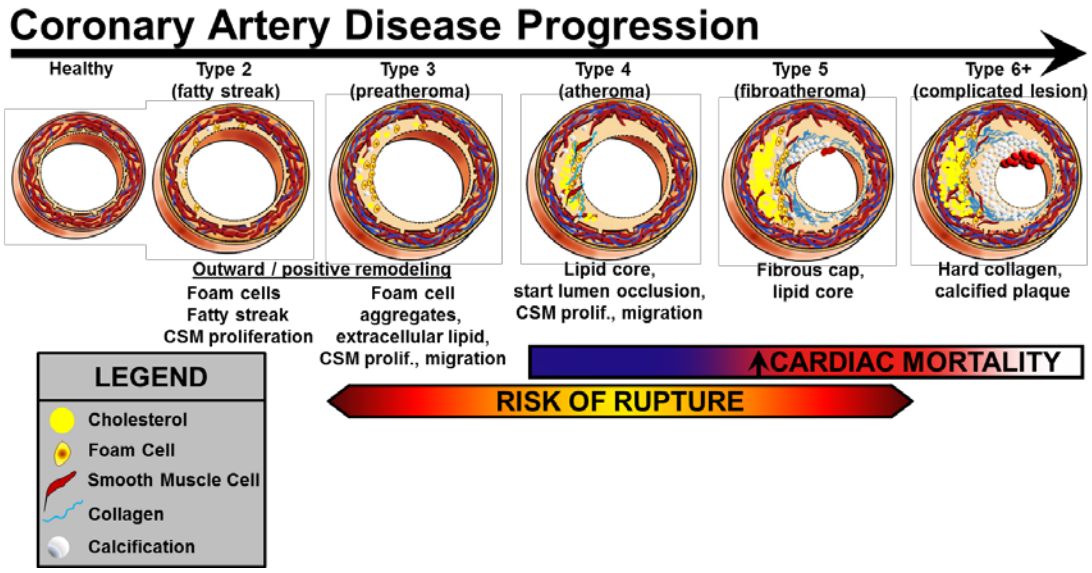

Figure 1.4: A time course of coronary artery disease progression (Adapted from (41; 42)). Following initial insult, recruitment of circulating leucocytes, deposition of lipids, and initiation of smooth muscle cell proliferation initiates the coronary artery disease (CAD) cascade, beginning with a thin fatty streak (Type 2 lesions). Cholesterol deposits are engulfed by infiltrated macrophages, thus forming foam cells. Type 3 atherosclerotic lesions are characterized by aggregation of foam cells, together with induction of CSM proliferation and migration into the forming atherosclerotic lesion. As CAD progresses into type 4 and 5 atherosclerotic lesions, proliferative CSM secrete extracellular matrix proteins to stabilize the growing lesion. Further lipid and foam cell accumulation, together with apoptosis of CSM and other cell types initiate the formation of a necrotic lipid core. Additionally, the deposition of hydroxyapatite crystals into the plaque contributes to coronary artery calcification, which, in early microcalcification stages, can serve to de-stabilize the growing plaque. Thin-walled, necrotic atheromas are susceptible to rupture, resulting in acute myocardial infarction.

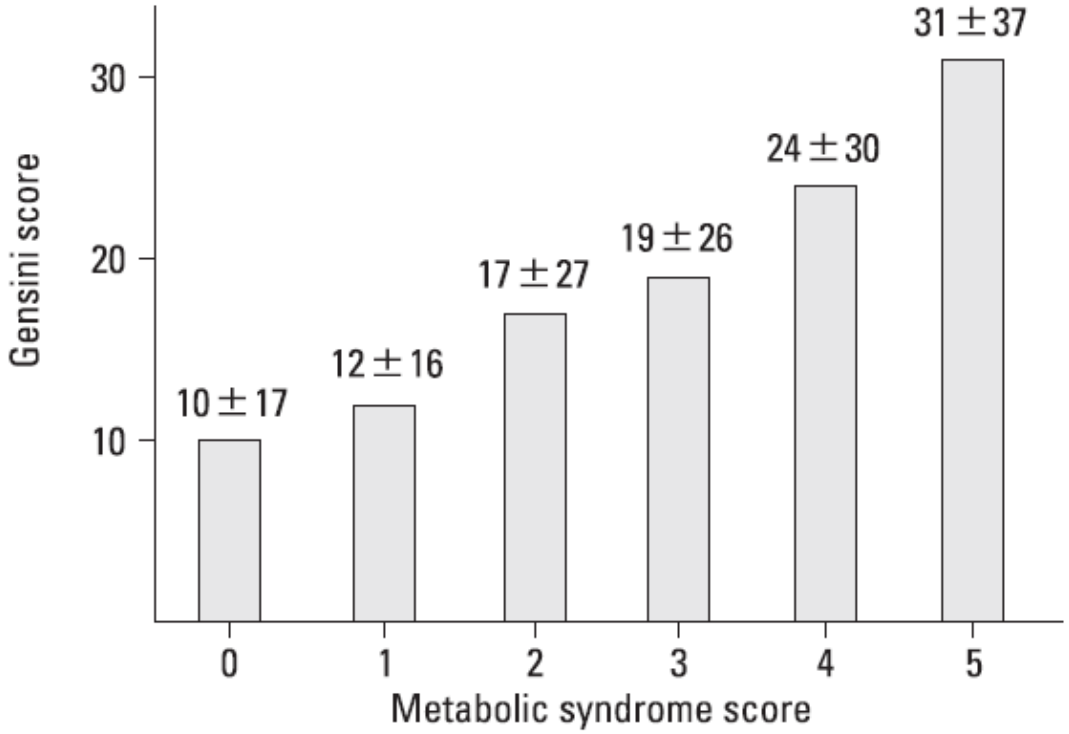

Figure 1.5: Metabolic syndrome increases severity of coronary artery disease in an additive fashion (45). Metabolic syndrome (MetS) scores were assigned to 632 patients, based on the number of MetS risk factors present (0-5). CAD severity was assessed in each of these cases, using the Gensini scoring system. The Gensini scoring system classifies severity based on the extent of luminal narrowing, as well as the location of the atherosclerotic lesion. Lesions with greater luminal narrowing, and in "crucial" regions, such as the left main coronary artery, receive higher Gensini scores. Gensini scores were increased in a "dose-dependent" manner with increasing number of MetS risk factors.

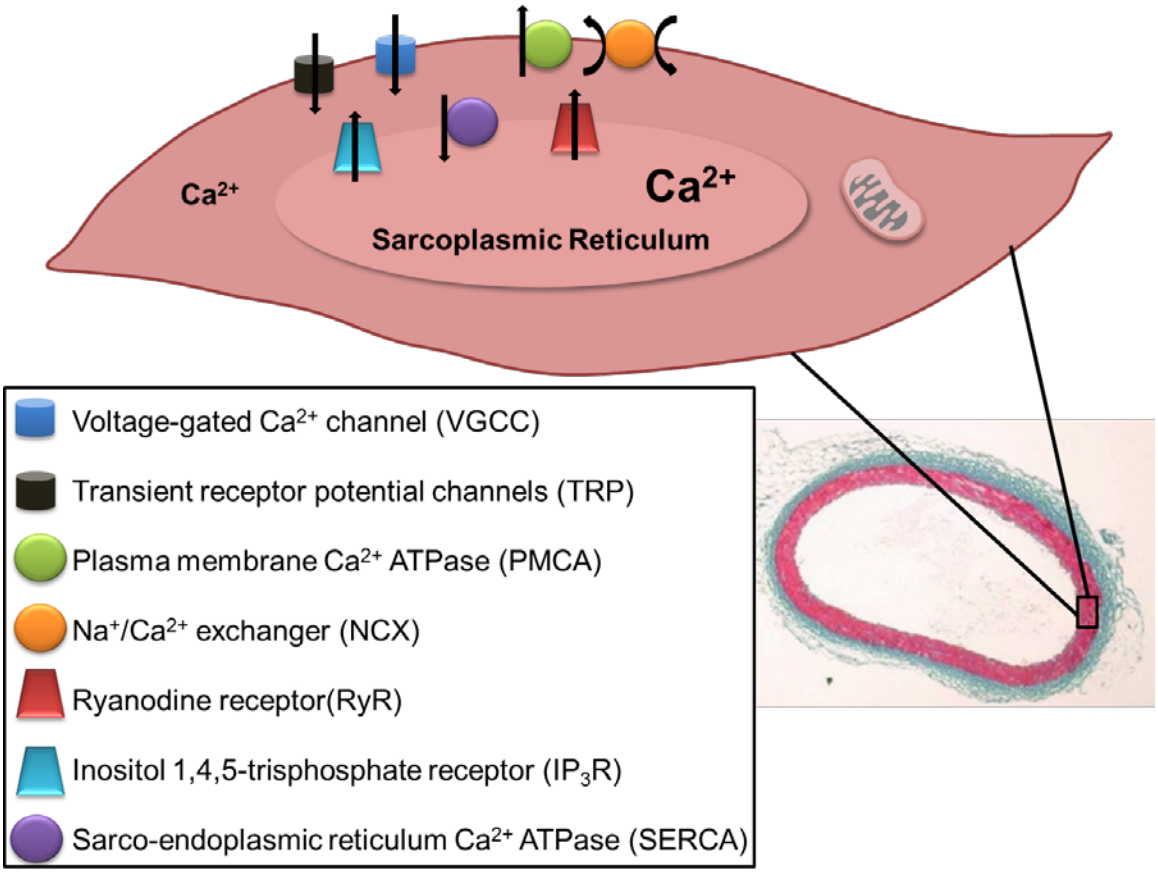

Figure 1.6: Membrane-bound Ca^{2+} regulatory proteins in coronary smooth muscle. Influx mechanisms include voltage-gated Ca^{2+} channels (VGCC) and transient receptor potential (TRP) channels. Efflux mechanisms include the plasma membrane Ca^{2+} ATPase (PMCA) and the sodium-calcium exchanger (NCX). Sarcoplasmic reticulum (SR) Ca^{2+} release channels include the ryanodine receptor (RyR) and the inositol 1,4,5-trisphosphate receptor (IP_3R). Ca^{2+} is returned to the SR via the sarco-endoplasmic reticulum Ca^{2+} ATPase (SERCA).

Table 1.1: Criteria for Clinical Diagnosis of the Metabolic Syndrome†

Component	*Term*	*Categorical Cutoff*	
		Men	Women
Elevated waist circumference	Abdominal Obesity	≥102 cm	≥88 cm
Elevated fasting triglycerides	Dyslipidemia	≥ 150 mg/dL	≥ 150 mg/dL
Reduced high-density lipoprotein cholesterol	Dyslipidemia	<40 mg/dL	<50 mg/dL
Elevated blood pressure	Hypertension	≥130/85 mmHg	≥130/85 mmHg
Elevated fasting plasma glucose	Hyperglycemia	≥100 mg/dL	≥100 mg/dL

†Adapted from Alberti *et al*. (10)

Table 1.2: Comparison of metabolic syndrome in Yucatan and Ossabaw swine†

Component	*Yucatan*	*Ossabaw*	*References*
Obesity	No	Yes	(76; 82; 91; 117-155)
Insulin resistance	No	Yes	(82; 117; 124-126; 128; 129; 132-140; 142; 144; 147; 152; 155-160)
Glucose intolerance	No	Yes	(76; 79; 82; 117; 118; 121; 122; 124-127; 129; 132-137; 139; 140; 143; 146; 147; 152; 154; 156; 158-163)
Dyslipidemia (↑LDL/HDL)	Yes	Yes	(76; 79; 82; 91; 117; 119; 122; 123; 125; 126; 134-136; 138; 139; 141; 142; 151; 152; 155; 156; 159; 161; 162; 164-167)
Dyslipidemia (↑ triglycerides)	No	Yes	(81; 91; 117; 122-126; 132; 134-136; 139; 140; 143; 152; 154-156; 159-161; 163; 165; 167)
Hypertension	No	Yes	(76; 91; 119; 122; 124-127; 129; 134-136; 139; 143; 152; 155; 158)

†Adapted from Sturek *et al.* (19)

Table 1.3: Changes in Intracellular Ca^{2+} Handling in Coronary Artery Disease

Ca^{2+} Transporter	*Change in Function*	*References*
Voltage-gated Ca^{2+} channel (VGCC)	↑,↓	(76-80; 168)
Transient receptor potential channel (TRP)	↑	(79; 126)
Na^{+}/Ca^{2+} Exchanger (NCX)	↓	(79; 82; 160)
Plasmalemma Ca^{2+} ATPase (PMCA)	↓	(79; 82; 160)
Sarco-endoplasmic reticulum Ca^{2+} ATPase (SERCA)	↑,↓	(79; 82; 160)

CHAPTER 2: BIPHASIC ALTERATIONS IN CORONARY SMOOTH MUSCLE Ca^{2+} REGULATION IN A REPEAT CROSS-SECTIONAL STUDY OF CORONARY ARTERY DISEASE SEVERITY IN METABOLIC SYNDROME

(Published in *Atherosclerosis* 249:1-9, 2016.
doi: 10.10.16/j.atherosclerosis.2013.03.032)

Abstract

Background and Aims

Coronary artery disease (CAD) is progressive, classified by stages of severity. Alterations in Ca^{2+} regulation within coronary smooth muscle (CSM) cells in metabolic syndrome (MetS) have been observed, but there is a lack of data in relatively early (mild) and late (severe) stages of CAD. The current study examined alterations in CSM Ca^{2+} regulation at several time points during CAD progression.

Methods

MetS was induced by feeding an excess calorie atherogenic diet for 6, 9, or 12 months and compared to age-matched lean controls. CAD was measured with intravascular ultrasound (IVUS). Intracellular Ca^{2+} was assessed with fura-2.

Results

IVUS revealed that the extent of atherosclerotic CAD correlated with the duration on atherogenic diet. Fura-2 imaging of intracellular Ca^{2+} in CSM cells revealed heightened Ca^{2+} signaling at 9 months on diet, compared to 6 and 12 months, and to age-matched lean controls. Isolated coronary artery rings from swine fed for 9 months followed the same pattern, developing greater tension to depolarization, compared to 6 and 12 months (6 months= 1.8 ± 0.6 g, 9 months= 5.0 ± 1.0 g, 12 months= 0.7 ± 0.1 g). CSM in severe atherosclerotic plaques showed dampened Ca^{2+} regulation and decreased proliferation compared to CSM from the wall.

Conclusion

These CSM Ca^{2+} regulation data from several time points in CAD progression and severity help to resolve the controversy regarding up- vs. down-regulation of CSM Ca^{2+} regulation in previous reports. These data are consistent with the hypothesis that alterations in sarcoplasmic reticulum Ca^{2+} contribute to progression of atherosclerotic CAD in MetS.

Background

Obesity affects more than one-third of adults in the United States (1). The human propensity for obesity has been attributed to a “thrifty genotype” (7). This “thrifty genotype” was adaptive during the early stages of human evolution, when humans were easily affected by the “feast or famine” environment associated with changing seasons and a lack of modern food preservation and storage. Now, a consistent and abundant food supply, coupled with a sedentary lifestyle, has propelled the obesity epidemic, resulting in the coining of such terms as “obesogenic environment” (9) and tongue-in-cheek references to a new species with the name “*Homo sedentarius*” (8). Obesity often appears in connection with the metabolic syndrome (MetS), which is classically defined as the clustering of three or more of the following risk factors: central obesity, hypertension, dyslipidemia, insulin resistance, and glucose intolerance (169). Together, obesity and MetS double the risk of coronary artery disease (CAD), the leading killer of Americans (15).

CAD is a progressive disease with stages typically classified according to the Stary classification system (40). Early, clinically insignificant neointimal thickening due to lipid deposition in the artery wall worsens with increasing lipid and inflammatory cell infiltration (170; 171). Further progression involves recruitment of coronary smooth muscle (CSM) cells from the media into the growing plaque. Such mobilization is accompanied by a shift in CSM phenotype from healthy, contractile CSM cells to synthetic, proliferative CSM cells (54), whose secretory capabilities result in the deposition of collagen and other fibers into the developing lesion. The presence of CSM cells in the atherosclerotic plaque stabilizes the early lesion. As atherosclerotic CAD progresses, however, increased apoptosis and accumulation of lipids and cellular debris within the plaque results in thinning of the fibrous cap surrounding the lesion. This

thinning of the fibrous cap may lead to rupture and thrombosis, often resulting in myocardial infarction and sudden cardiac death.

Ca^{2+} is a ubiquitous second messenger known to be involved in smooth muscle contraction (54; 172), proliferation (54; 173-175), migration (176; 177), and gene transcription (178; 179). Therefore, alteration in CSM Ca^{2+} regulation in CAD is an important area of study. Alterations in many Ca^{2+} transporters, including voltage-gated Ca^{2+} channels (76; 79), sarco-endoplasmic reticulum Ca^{2+} ATPases (79; 81; 82), transient receptor potential channels (126), plasma membrane Ca^{2+} ATPases (79), and Na^{+}/Ca^{2+} exchangers (79), have been described in CAD (180). However, there is a paucity of data regarding time-dependent changes in CSM Ca^{2+} handling in the setting of obesity/MetS. This study utilized the well-characterized Ossabaw miniature swine model of MetS and CAD (19; 82; 125; 126; 136; 181) to examine the changes in CSM Ca^{2+} regulation during obesity-induced CAD progression, providing a much needed longitudinal assessment of Ca^{2+} regulation over time and with increasing severity. Further, we examined differences in Ca^{2+} regulation in CSM harvested specifically from plaque vs. vascular wall.

Methods

Animal care and experimental groups

All experimental procedures involving animals were approved by the Institutional Animal Care and Use Committee at Indiana University School of Medicine with the recommendations outlined by the National Research Council and the American Veterinary Medical Association Panel on Euthanasia (182; 183). Six month old Ossabaw miniature swine were fed 1 kg of an excess-calorie atherogenic diet daily for 6 (n=6), 9 (n=7), or 12 (n=9) months in the repeat cross-sectional study (Figs. 2.1 and 2.2). The 6 and 9 month time points were considered “early” and the 12 month time point “late” CAD for comparison to Lean healthy pigs. For comparison, an additional subset of Ossabaw

miniature swine were fed the same excess-calorie atherogenic diet above for 11 months to provide coronary arteries for comparison of CSM in “mild CAD” and “severe CAD” defined as arteries with less than 30% and greater than 30% plaque burden, respectively, as assessed by IVUS (Figs. 2.3-2.5). Plaque vs. vascular wall components were dissected from the same artery segments in severe CAD to compare CSM properties (Fig. 2.4). Lean control swine for this dataset (n=6) were fed the standard diet mentioned above.

Metabolic Phenotyping

Final body weights and blood were obtained at time of sacrifice for lipid analysis (ANTECH Diagnostics, Fishers, IN).

Intravascular ultrasound (IVUS) for quantification of coronary artery disease

Swine were anesthetized and intravascular ultrasound was performed as described previously (82; 126; 139; 148).

Still frame IVUS pullback images were obtained offline at 1 mm intervals (Fig. 2.1). Percent plaque burden measures were obtained using Image J software (1.48v, National Institutes of Health, USA).

Fluorescent imaging for assessment of CSM intracellular Ca^{2+} signaling from freshly harvested coronary arteries

CSM cells from Ossabaw swine were enzymatically isolated from freshly dissected coronary arteries and loaded with fura-2 AM (2.5 mmol/l Molecular Probes, Life Technologies, Eugene, OR) as previously described (79; 82; 126; 184).

Isometric tension studies for functional assessment of freshly harvested coronary arteries

Isometric tension was examined in isolated coronary artery rings (2-4 mm in length) as described previously (141).

Isolation of atherosclerotic plaques from coronary arteries with severe CAD

Following IVUS and sacrifice, coronary arteries were excised and cleaned of adherent tissue. Arteries were segmented and opened longitudinally. Artery segments with plaque burden greater than 30% as measured by IVUS were selected and labeled as “severe CAD” (n=5). Plaques such as those labeled as intima (I) in Fig. 2.4I “Severe CAD” histology were trimmed away from the artery wall and placed in conical tubes containing the same collagenase solution previously described for isolation of CSM cells from the coronary artery wall (media) (79; 82; 126; 184). The plaque cell population was then isolated through a series of enzymatic washes. Plaque cells were loaded with fura-2/AM for 45 minutes, washed, and placed on ice prior to being imaged as described above.

Histology

Coronary artery segments (2-4 mm in length) were placed in 10% phosphate-buffered formalin for 24-48 hours, and then transferred to 70% ethanol. Histology was performed in the Department of Anatomy and Cell Biology at Indiana University School of Medicine (Indianapolis, IN).

Immunohistochemistry

Coronary artery segments embedded in paraffin (described above) were transported the Department of Pathology at Indiana University School of Medicine and were processed as previously described (139). Immunostaining was performed using Ki-67 as a proliferation marker. Images were captured using a LEICA DM 300 inverted microscope and analyzed with ImageJ software.

Statistical Analysis

Statistical analysis was performed using GraphPad Prism 5.0 (San Diego, CA). One-way analysis of variance (ANOVA) or two-way ANOVA with Bonferroni post hoc analysis was performed. Data are represented as mean ± SEM. $p<0.05$ was considered statistically significant.

Results

Metabolic Characteristics

Swine fed an excess-calorie atherogenic diet developed MetS as indicated by increased body weight, hypertension, and elevated total cholesterol and triglycerides, (see Table 1 in associated Data in Brief article (185)). Plasma triglycerides and total cholesterol were decreased at 12 months of diet in the initial, repeat cross-sectional study. In contrast, total cholesterol was not different between mild and severe CAD groups in the 11-month diet study (data not shown).

Coronary artery disease (CAD) severity increases during prolonged MetS duration.

Analysis of IVUS still-frames revealed increased coronary artery plaque burden MetS swine with time on atherogenic diet (Fig. 2.1D), but did not significantly increase until 12 months on diet. Percent wall coverage increased early in MetS-induced CAD, plateauing later (Fig. 2.1D; Solid line), indicating that atherosclerotic plaques expand around the circumference of the artery prior to encroachment upon the lumen. These data support our statement that percent wall coverage is a strong tool for quantification of early intimal CAD prior to the stage of more intimal plaque burden. These quantification methods suggest that swine on 6-9 months of atherogenic diet present with “early stage” CAD (representative IVUS still frame in Fig. 2.1B), whereas 12 months on atherogenic diet results in “late stage” CAD (representative still frame in Fig. 2.1C).

Coronary smooth muscle Ca^{2+} responses to depolarization are biphasically altered during disease progression.

Fura-2/AM assessment of intracellular Ca^{2+} handling in response to depolarization revealed a biphasic pattern in CSM from swine with MetS, in which responses were heightened in “early state” CAD, followed by dampened responses in “late stage” CAD. Fig. 2.2A provides a representative tracing to demonstrate the experimental protocol. CSM from swine with “early stage” CAD after nine months of atherogenic feeding demonstrated greater Ca^{2+} influx through voltage-gated Ca^{2+} channels (VGCC) after activation by K^+ (80 mmol/l; Green shading; Fig. 2.2A) compared to cells from age-matched lean swine as quantified by area under the curve. This increased VGCC activation was absent in CSM from swine with “late stage” CAD (Fig. 2.2B).

Coronary artery responses to depolarization are biphasically altered during disease progression.

Functional assessment of coronary rings from lean pigs revealed no effect of age on tension development to KCl (20 mM) (Fig. 2.2C; Black Bars). Rings from swine with MetS revealed a biphasic change in tension development to 20 mM KCl as CAD progressed (Fig. 2.2C; White Bars). When compared to age-matched leans, rings from swine with “early stage” CAD after 9 months of atherogenic feeding developed significantly more tension to KCl (20 mM). Following 12 months of atherogenic diet feeding, tension development dramatically decreases below that of rings from lean age-matched swine (Fig. 2.2C).

Sarcoplasmic reticulum Ca^{2+} store capacity is altered during CAD progression.

Release of the SR store with caffeine (5 mmol/l)-triggered activation of ryanodine receptors is observed as a transient, robust increase in cytosolic [Ca^{2+}] (Blue Arrow; Fig. 2.2A). This transient increase was significantly greater in CSM from swine with “early stage” CAD compared to CSM from age-matched lean swine. As observed with

depolarization responses, this increased Ca^{2+} signal in CSM from swine with “early stage” CAD was absent in CSM from swine with “late stage” CAD (Fig. 2.2D).

Recovery of cytosolic [Ca^{2+}] following SR Ca^{2+} store release is biphasically altered during CAD progression

Finally, Ca^{2+} buffering impairment along with simultaneously store-operated Ca2+ influx was assessed after SR store depletion. This is observed as a sustained Ca^{2+} signal above baseline levels following SR Ca^{2+} store depletion with caffeine (Red Arrow; Fig. 2.2A). While this revealed the same pattern of Ca^{2+} alterations during the time course of CAD progression, no significant changes from age-matched lean swine were observed (Fig. 2.2E).

Plaque burden and collagen content are increased with CAD severity

Arteries with greater than 30% plaque burden as assessed by IVUS were classified as having “severe” CAD, while arteries with less than 30% plaque burden were classified as having “mild” CAD. To further classify disease severity for more detailed analysis of plaque composition, histological analysis was performed. See lumen (L), intima (I), and media (M) layers labeled in Fig. 2.3A-C. Plaque burden in the “severe CAD” group was increased compared to that in the “mild CAD” group (Fig. 2.3G). An additional measure of intimal plaque growth is obtained when the intimal/medial area ratio (I/M) is assessed. I/M was significantly increased in severe CAD, compared to mild (Fig. 2.3H). Further, to assess progression of plaque fibrosis, collagen content within the plaque was examined and was increased ~30% in severe disease, compared to mild (Fig. 2.3I). Medial collagen content trended toward increase with severe CAD, but this was not significant (Fig. 2.3J; $p = 0.08$).

Sarcoplasmic reticulum Ca^{2+} handling is altered with CAD severity

To examine steady-state SR [Ca^{2+}], the SR Ca^{2+} store was released with caffeine (5 mmol/l) in the absence of extracellular Ca^{2+} (See Fig. 2.4A for representative

tracing/experimental protocol; “Caf-sensitive SR Ca^{2+} store”; bi-directional arrow) and the transient increase in cytosolic [Ca^{2+}] was measured. In CSM isolated from arterial segments with mild CAD a dramatic increase in caffeine-sensitive steady-state SR [Ca^{2+}] was observed (Fig. 2.4B). In contrast, CSM isolated from plaques of arteries with severe CAD showed depletion of the caffeine-sensitive steady-state SR [Ca^{2+}] compared to CSM isolated from both healthy and mild CAD swine. Following an increase in cytosolic [Ca^{2+}] resulting from caffeine stimulation, a number of extrusion/buffering mechanisms are employed to restore cytosolic [Ca^{2+}]. SERCA buffering activity is assessed by measuring the cytosolic [Ca^{2+}] undershoot below baseline levels during recovery from caffeine stimulation (see Fig. 2.4A; “SERCA Activity”; downward arrow). The cytosolic [Ca^{2+}] undershoot (SERCA activity) was increased in mild CAD and was dramatically decreased in CSM of arterial segments from severe CAD (Fig. 2.4C).

To provide an intra-arterial comparison, intracellular Ca^{2+} regulation in CSM harvested specifically from the intima (plaque) region was compared to CSM from the wall (media) of arteries with severe CAD. The caffeine-sensitive steady-state SR Ca^{2+} store was depleted in CSM from intima (plaque) compared to CSM from the artery wall (media) (Fig. 2.4D). Correspondingly, when CSM from the intima (plaque) was compared with the adjacent artery wall (media), plaque cells demonstrated a decreased undershoot, i.e. decreased SERCA activity (Fig. 2.4E).

L-type voltage-gated channel function is altered with CAD severity

To further and more specifically assess VGCC function, Ba^{2+}-containing depolarizing solution with low Na^{+} was employed. Ca^{2+} influx through VGCC immediately triggers activation of Ca^{2+} extrusion and buffering mechanisms, which makes direct assessment of VGCC activity difficult. Fura-2 binds Ba^{2+} with similar affinity as to Ca^{2+}. Substitution of Ca^{2+} with Ba^{2+} allows Ba^{2+} entry through VGCC upon depolarization. Ba^{2+} is not buffered by SERCA or transported by the plasma membrane Ca^{2+} ATPase. Low

extracellular Na^+ inhibits Na^+/Ca^{2+} exchange, preventing Ba^{2+} extrusion by this pathway, thereby providing a pure measure of VGCC function. For a representative tracing and experimental protocol, see Fig. 2.4F.

The rate of Ba^{2+} entry was assessed as the slope of the rise in the F_{340}/F_{380} signal following depolarization. Rate of Ba^{2+} entry through VGCCs was dramatically increased in CSM from swine with mild CAD compared to Healthy and severe CAD (Fig. 2.4G). We also examined rate of Ba^{2+} entry following depolarization in the arterial wall (media) adjacent to the excised intima (plaque). VGCC activity was not different in CSM from plaques compared to CSM in their adjacent arterial media (Fig. 2.4H). The Healthy, Mild CAD, and Severe CAD histology with schematic illustrations of normal SR, increased SR, and decreased SR Ca^{2+} stores, respectively, are shown in Fig. 2.4I. The figure shows the proposed changes in Ca^{2+} handling associated with CSM phenotypic modulation during CAD progression.

Cell proliferation declines with CAD severity

To determine whether proliferation follows Ca^{2+} handling patterns, Ki-67 expression was measured as an index of proliferative activity within coronary artery sections (Fig. 2.5A-D). The number of proliferative cells within the intimal region of coronary arteries with severe CAD was dramatically reduced, compared to arteries with mild CAD (Fig. 2.5E).

Discussion

There is a paucity of literature on a time course analysis of the connection between MetS-induced CAD and CSM Ca^{2+} regulation. This study steps into the gap and provides insight into the transitory, biphasic nature of CSM Ca^{2+} regulation during the progression of CAD. Using *in vivo* intravascular ultrasound imaging we showed increased circumferential neointimal wall coverage in early CAD and more severe increased plaque burden in late CAD. The power of IVUS is that after the highly

sensitive analysis of CAD progression the arteries are viable for interrogation of cellular Ca^{2+} signaling. We found increased Ca^{2+} influx and Ca^{2+} release and buffering by the sarcoplasmic reticulum in early CAD and a surprising reversal of these Ca^{2+} signaling events in more severe, late state CAD. By separating overt plaques away from medial CSM in the artery wall, we provide novel insight into heterogeneity of intracellular Ca^{2+} regulation in the different regions of severely diseased arteries.

This clarity is important because there has been confusion regarding differences in intracellular Ca^{2+} regulation observed in several studies of CAD. For instance, Witczak *et al.* (79) and Hill *et al.* (81) reported increases in SERCA expression and function. Witczak *et al.* and others (80) also demonstrated decreases in VGCC function with disease. However, Neeb *et al.* (82) demonstrated a decrease in SERCA function with disease, and several studies (76-78) reported an increase in VGCC function with disease. One possible explanation for the apparent discrepancy in the data is duration of diet and/or severity of disease. Indeed, diet duration is different in each of these studies, causing differences in disease severity. An additional factor in these discrepancies may be the swine model. Witczak (79) and Hill (81) utilized diabetic dyslipidemic Yucatan swine that had no primary insulin resistance, while Berwick (76) utilized MetS Ossabaw swine with primary insulin resistance, hypertension, and increased aldosterone as major characteristics. Neeb (82) used both Ossabaw and Yucatan swine. Indeed, Neeb's work highlights model differences in SERCA function (82), underscoring the need for time-dependent studies in the same model. Specific components of the Ossabaw swine model that may contribute to differences in Ca^{2+} regulation include primary insulin resistance and increased aldosterone (186). The current study provides a repeat cross-sectional examination of intracellular Ca^{2+} regulation in MetS Ossabaw swine during CAD progression, reconciling the discrepant results in the reports mentioned above.

Here, we report that function of VGCC and SERCA is enhanced with early, mild CAD and that these functions decrease with increased CAD severity. These data explain, in part, the discrepancies in the reports mentioned above. During early, MetS-induced CAD, VGCC activity is increased, as observed by Berwick *et al.* (76) At the same time, SERCA activity is increased, as observed by Witczak *et al* (79). As MetS and CAD progress, however, VGCC and SERCA function are greatly diminished, which corresponds to the findings of Witczak (79) and Neeb (82). This decrease in VGCC and SERCA function appears to occur concurrently with a reduction in cell proliferation, as measured by Ki-67 expression. Future studies will seek to determine whether these phenomena are causally linked.

Interestingly, in the repeat cross-sectional study, plasma triglycerides and total cholesterol were decreased after 12 months on atherogenic diet vs. 6 and 9 months, suggesting that plasma cholesterol could play a role in Ca^{2+} handling differences observed over CAD progression. This is unlikely, however, because the plasma cholesterol at 12 months was still increased ~4-fold above that in healthy lean pigs. Further, in the eleven month subset of swine used for analysis of Ca^{2+} handling in atherosclerotic plaque vs. media, total plasma cholesterol was not different in the mild vs. severe CAD groups, yet the decreases in SERCA and VGCC function persisted. These data suggest that the plasma cholesterol decrease in the repeat cross-sectional study did not explain the decrease in CSM Ca^{2+} handling in late CAD.

Additionally, this study provides new insight on intracellular Ca^{2+} regulation *within atherosclerotic plaque.* In the repeat cross-sectional study, CSM isolated from coronary arteries with “late” CAD were a mixed population of cells from the arterial wall and cells from the plaque. Here, for the first time isolating atherosclerotic plaques away from the artery wall, we provided a close-up look at CSM Ca^{2+} regulation within a plaque. Fig. 2.4D, E, and H provide strong evidence that SR Ca^{2+} handling is decreased in the

intima (plaques) of arteries with severe CAD, compared to its adjacent wall (media). This finding prompts several questions: 1) Does a shift in Ca^{2+} regulation within atherosclerotic plaques signal a shift in the dominant cell phenotype within an atherosclerotic plaque? 2) If so, can intracellular Ca^{2+} handling provide insight regarding plaque stability and phenotypic modulation? These questions are beyond the scope of the current project, but are interesting areas of future investigation.

Together, the data in this report provide a much needed study of CAD progression in metabolic syndrome, providing insight on IVUS determinants of CAD severity and histological analysis of cellular components of CAD progression. The study also highlights the need for additional studies to further solidify causal links between intracellular Ca^{2+} regulation, CSM proliferation, and alterations in atherosclerotic plaque morphology during CAD progression.

Acknowledgements

The authors wish to acknowledge James P. Byrd, Josh Sturek, and Brandy Sparks for wonderful technical support during the metabolic phenotyping phase of this study. This study was supported by National Institutes of Health (HL062552 and T32 DK064466), American Heart Association (15PRE25280001), Indiana CTSI Predoctoral TL1 Training Fellowship (TR000162), the Fortune-Fry Ultrasound Research Fund, and the Cardiometabolic Disease Research Foundation.

Conflict of Interest

There are no conflicts of interest to disclose.

Figures

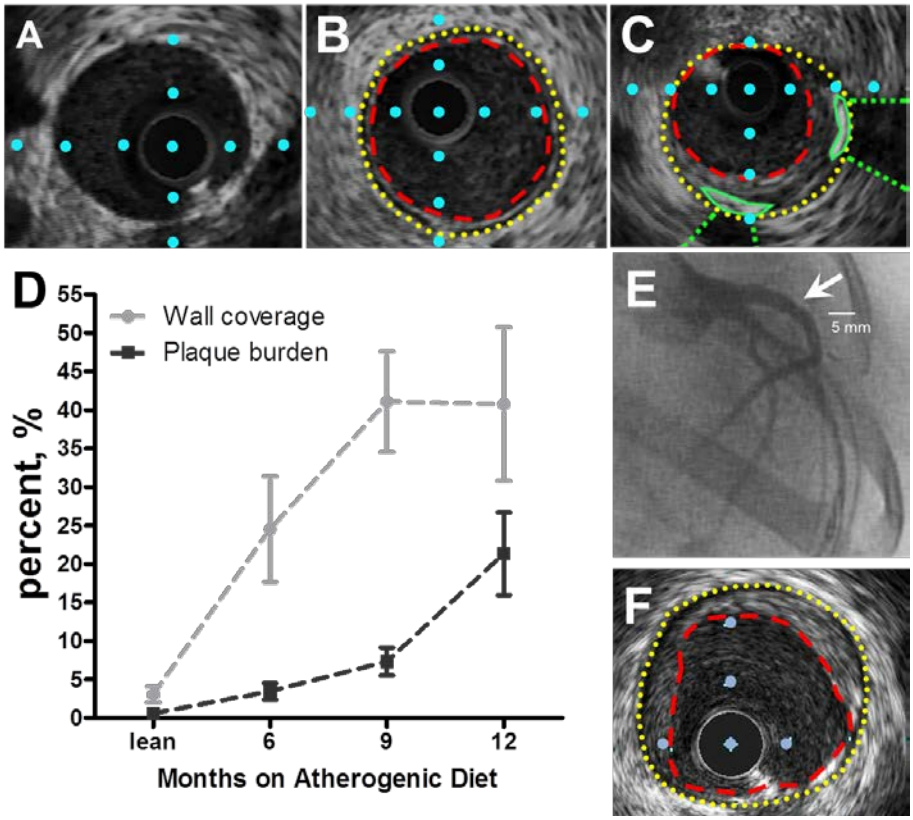

Figure 2.1: Intravascular ultrasound imaging of coronary arteries with varying stages of coronary artery disease in the repeat cross-sectional study. A. Cross-sectional view of a coronary artery from a lean pig. **B.** Cross-sectional view of a coronary artery from a MetS pig with "early stage" CAD. Internal elastic lamina = yellow dotted line; lumen = red dashed line. **C.** Cross-sectional view of a coronary artery from a MetS pig with "late stage" CAD. Distance between blue dots in A-C is 1 mm. **D.** Wall coverage significantly increases in "early stage" CAD (0-9 months). Plaque burden does not increase until "late stage" CAD (>9 months). (lean= 4 pigs, MetS 6 months= 5 pigs, MetS 9 months= 5 pigs, MetS 12 months= 7 pigs). **E.** Right anterior oblique coronary angiogram indicating lumen stenosis (arrow) in the left anterior descending artery. **F.** IVUS still frame which corresponds to lumen stenosis in panel E.

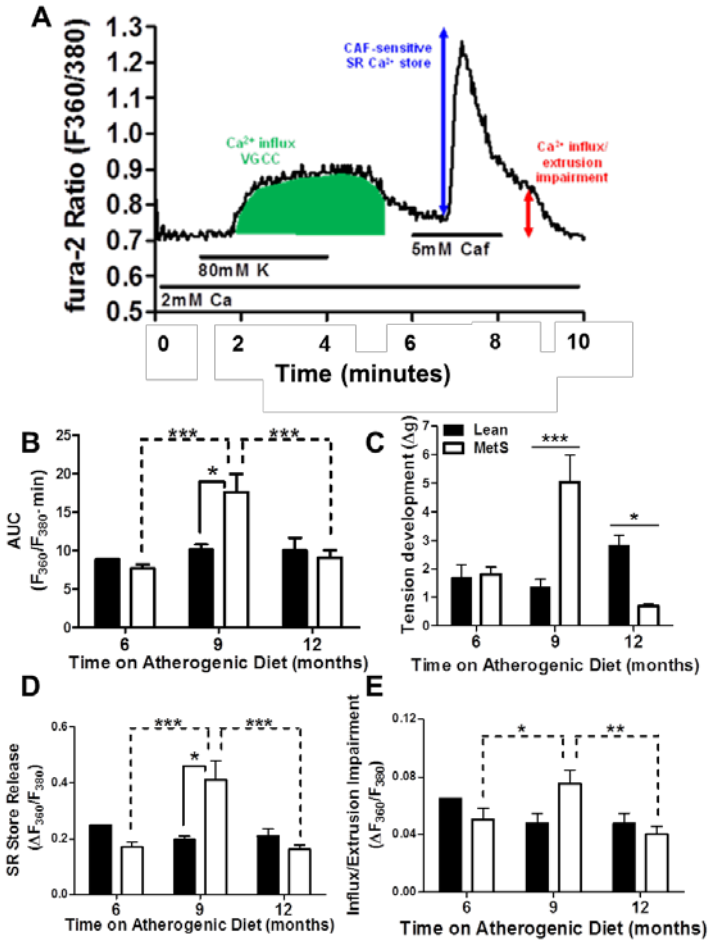

Figure 2.2: Intracellular Ca^{2+} signaling is biphasically altered in coronary smooth muscle cells during CAD progression in the repeat cross-sectional study. A. Representative tracing of CSM cytosolic Ca^{2+} flux. Labels indicate solution changes through superfusion chamber with duration shown by the horizontal lines. VGCC = voltage-gated Ca^{2+} channel; Caf = caffeine; green area under the curve = Ca^{2+} after 80 mM K+ membrane depolarization; blue double-headed arrow = SR Ca^{2+} store release; red double-headed arrow = delayed recovery to basal Ca^{2+} levels due to impaired Ca^{2+} buffering and store-operated influx. **B.** 9 month duration of diet results in elevated Ca^{2+} influx following depolarization, compared to 6 and 12 months (dashed lines indicating significant differences) and to age-matched lean pigs (solid lines indicating significant differences). **C.** Tension development to KCl (20 mM) in isolated coronary rings paralleled the changes in K depolarization-induced Ca^{2+} in panel B. **D.** SR Ca^{2+} store release is elevated at 9 months on atherogenic diet, compared to 6 and 12 months (dashed lines indicating significant differences), and to age-matched lean pigs. **E.** 9 months of atherogenic diet results in an increase in sustained Ca^{2+} signal, compared to 6 and 12 months, but not to age-matched leans. (Lean = 9 pigs, cells = 60; MetS 6 months = 6 pigs, cells = 56; MetS 9 months = 7 pigs, cells = 68; MetS 12 months = 9 pigs, cells = 92).

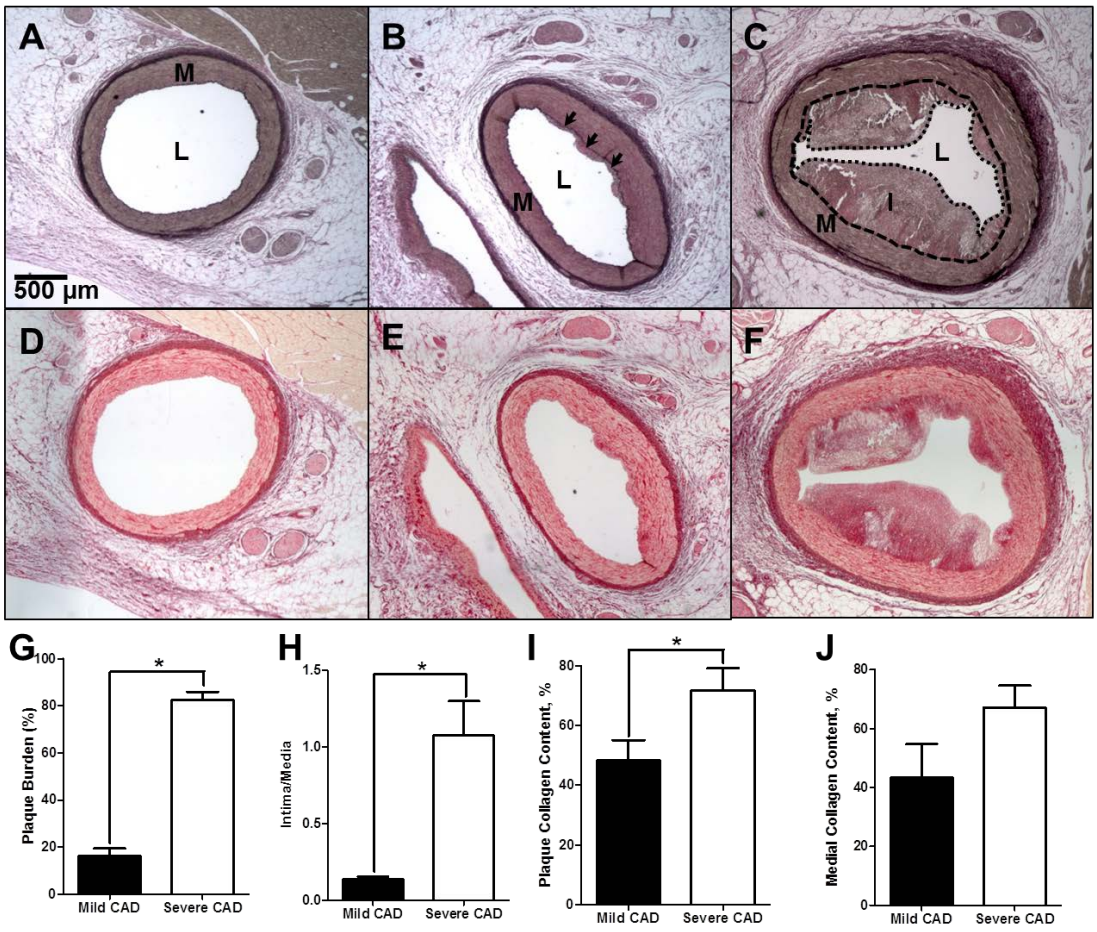

Figure 2.3: Histological assessment of mild and severe CAD and collagen deposition. A-C Verhoeff-Van Gieson staining of elastin in a coronary arterial ring in lean **(A)**, mild CAD (IVUS-detected plaque burden < 30%) **(B)**, and severe CAD (IVUS-detected plaque burden > 30%) **(C)**. L = Lumen; M = Media (Wall). I = Intima (plaque). Black arrows indicate the internal elastic lamina adjacent to early atherosclerotic lesion. **D – F.** Picrosirius red staining of collagen deposition in lean (D), mild CAD (E), and severe CAD (F) coronary arterial rings. **G.** % plaque burden is increased with severe CAD. **H.** Intima/media ratio is increased with severe CAD. **I.** Intimal collagen deposition is increased in severe CAD. **J.** Medial collagen deposition demonstrates a trend ($p = 0.08$) toward increase in severe CAD. (Mild CAD = 9 pigs; Severe CAD = 5 pigs) *$p<0.05$.

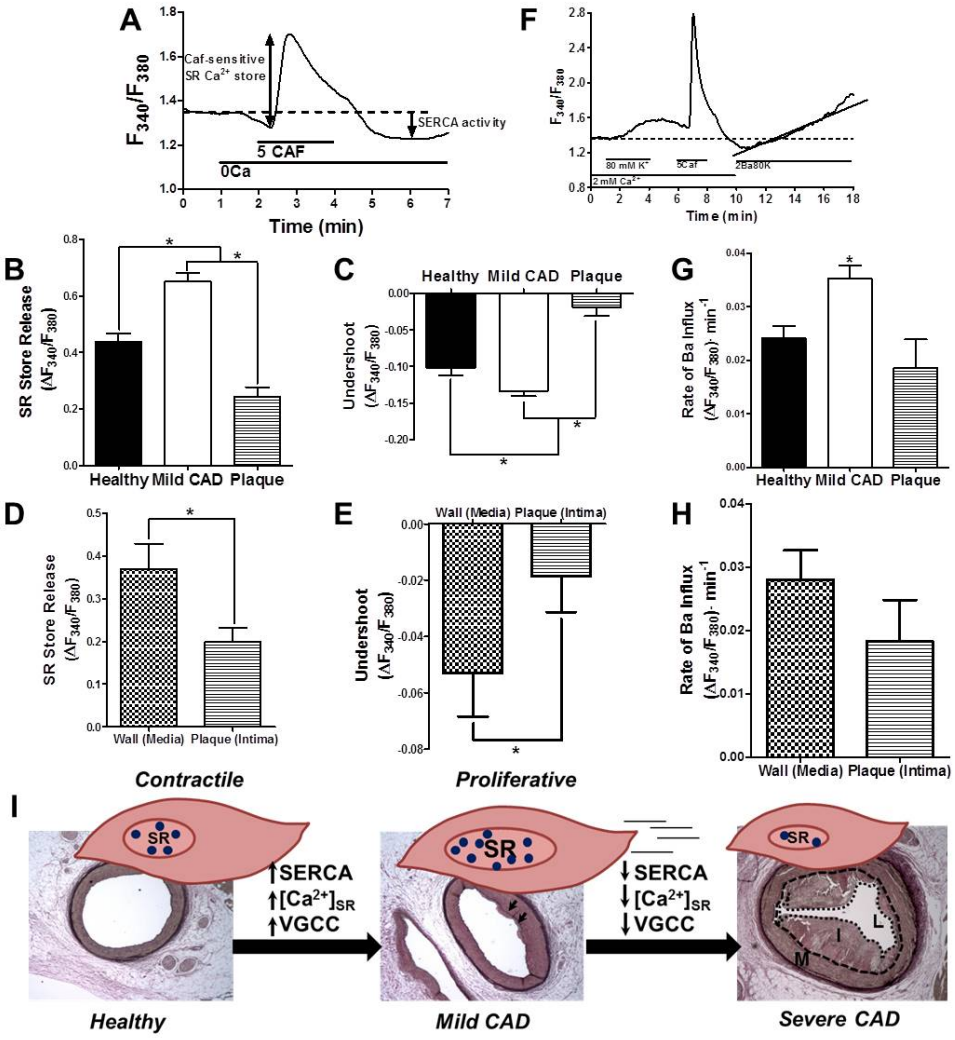

Figure 2.4: Intracellular Ca^{2+} handling is biphasically altered with CAD severity. A. Experimental protocol for panels B-E. **B.** The caffeine-sensitive steady-state SR store is increased in mild CAD compared to both healthy lean and severe CAD. **C.** The undershoot of cytosolic Ca^{2+} during recovery following removal of caffeine (SERCA activity) is increased in mild CAD compared to both healthy lean and severe CAD. **D.** When compared with CSM isolated from the adjacent arterial media (wall), intimal (plaque) CSM display decreased caffeine-releasable steady-state SR Ca^{2+} store. **E.** When compared with CSM isolated from the adjacent arterial media (wall), intimal (plaque) CSM display decreased SERCA activity. (Healthy = 6 pigs, cells = 67; Mild CAD = 9 pigs, cells = 156; Plaque = 5 pigs, cells = 29; Wall = 5 pigs, cells = 27). **F.** Experimental protocol for panels G-H. **G.** Rate of Ba^{2+} influx following depolarization is increased in CSM from mild CAD vs. Healthy and Severe CAD. **H.** When compared to CSM from the media (wall) adjacent to the plaque, intimal (plaque) cells do not demonstrate a difference in Ba^{2+} influx. (Healthy = 6 pigs, cells = 72; Mild CAD = 9 pigs, cells = 151; Plaque = 5 pigs, cells = 25; Wall = 5 pigs, cells = 42). **I.** Schematic depicting proposed changes in Ca^{2+} handling associated with CSM phenotypic modulation during CAD progression. Blue circles = Ca^{2+}.

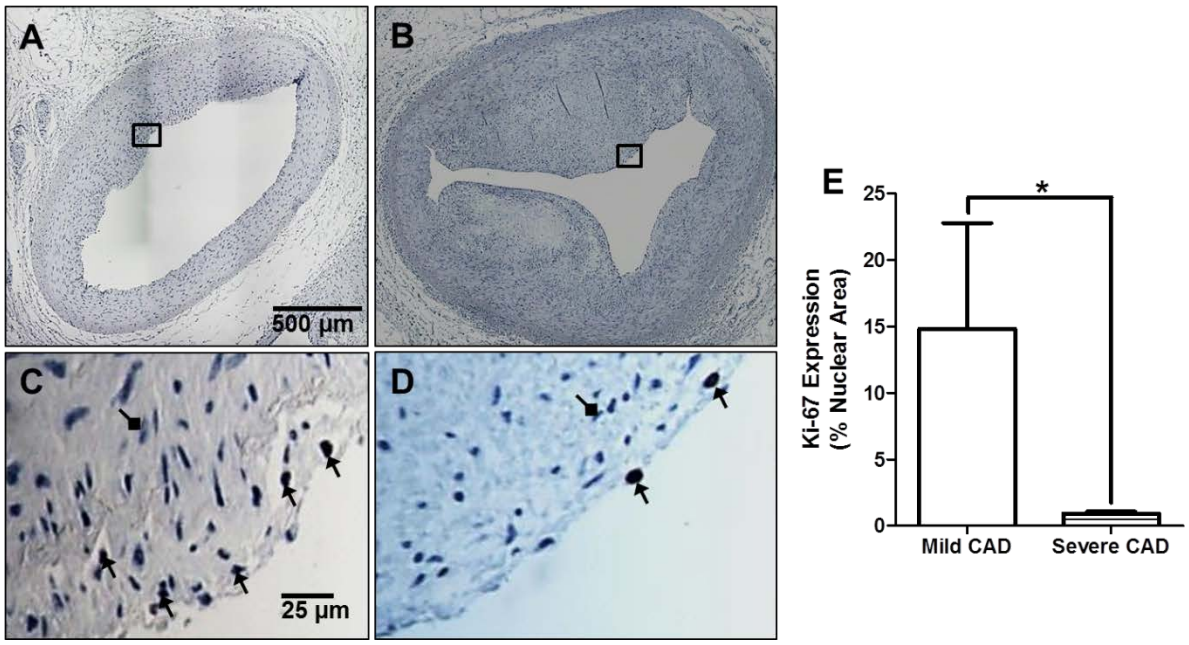

Figure 2.5: Cellular proliferation is decreased in severe CAD. A. Arterial ring from swine with mild CAD, interrogated with an antibody against Ki-67. **B.** Arterial ring from swine with severe CAD, interrogated with an antibody against Ki-67. **C-D.** Zoomed-in regions of rings in panels A and B. Black arrows indicate positive Ki-67 staining. Diamond arrows indicate negative Ki-67 stain. **E.** Ki-67 expression is decreased in severe CAD. (Mild CAD = 8 pigs; Severe CAD = 5 pigs).

Data-in-Brief

Metabolic characteristics observed during a repeat cross sectional study of coronary artery disease progression in Ossabaw miniature swine

(Published in *Data in Brief* 7:1393-1395, 2016
doi:10.1016/j.dib.2016.04.023)

Abstract

This repeat cross sectional study examined metabolic characteristics in Ossabaw miniature swine at different time points during atherogenic diet feeding. Briefly, metabolic syndrome was induced in Ossabaw miniature swine by feeding of an excess calorie, atherogenic diet for 6, 9, or 12 months. Ossabaw swine developed metabolic syndrome as indicated by increased body weight, hypertension, and increased plasma cholesterol and triglycerides, compared to lean controls. For more detailed explanations, see our associated research study (187).

Specifications Table

Subject area	*Physiology*
More specific subject area	*Metabolic syndrome development*
Type of data	*Table*
How data was acquired	*Plasma biochemical analysis*
Data format	*Analyzed*
Experimental factors	*Metabolic syndrome was induced by atherogenic diet feeding for 6, 9, and 12 months.*
Experimental features	*Repeat cross sectional study of metabolic syndrome induction at different time points of atherogenic diet feeding.*
Data source location	*Indianapolis, IN, United States of America.*
Data accessibility	*With this article*

Value of the data

- These data could assist researchers in study design for induction of metabolic syndrome.
- Provide previously unreported time-dependent aspects of metabolic syndrome.
- May provide insight toward development of therapies at different time points of metabolic syndrome progression.

Data

Metabolic syndrome has previously been defined as the presence of three or more of these risk factors: Obesity, hypertension, dyslipidemia (both LDL/HDL and triglyceride), insulin resistance, and glucose intolerance (169), and has been shown to double risk of developing coronary artery disease (15). Here, we conducted a repeat cross sectional analysis of metabolic syndrome development in Ossabaw swine during atherogenic diet feeding for 6, 9, and 12 months. Ossabaw swine developed metabolic syndrome, as indicated by increased body weight, hypertension, and dyslipidemia, compared to lean controls **(Table 2.DiB.1)**.

Table 2.DiB.1: Metabolic characteristics of Ossabaw miniature swine groups

	Lean	**MetS (6 months)**	**MetS (9 months)**	**MetS (12 months)**	**Significance**
Body weight (kg)	62 ± 5	89 ± 2	87 ± 7	116 ± 2	12 > 9, 6 > lean
Fasting Blood Glucose (mg/dL)	84 ± 6	75 ± 2	82 ± 7	81 ± 2	NS
Systolic Blood Pressure (mmHg)	131 ± 7	150 ± 9	143 ± 4	170 ± 7	12, 9, 6 > lean
Diastolic Blood Pressure (mmHg)	63 ± 2	77 ± 5	85 ± 4	89 ± 5	12, 9 > 6, lean
Total Cholesterol (mg/dL)	57 ± 5	383 ± 39	546 ± 66	247 ± 17	9 > 12, 6 > lean
Triglycerides (mg/dL)	25 ± 4	34 ± 4	98 ± 34	43 ± 6	9 > 12, 6, lean

NS = not significant.

Experimental Design, Materials and Methods

Animal Care

All experimental procedures involving animals were approved by the Institutional Animal Care and Use Committee at Indiana University School of Medicine with the recommendations outlined by the National Research Council and the American Veterinary Medical Association Panel on Euthanasia (182; 183). Six month old Ossabaw miniature swine were fed 1 kg of an excess-calorie atherogenic diet (KT-324, Purina Test Diet, Richmond, IN; 16% kcal from protein, 41% kcal from complex carbohydrates, 19% kcal from fructose, and 43% kcal from fat). The feed was supplemented with cholesterol (2.0%), hydrogenated coconut oil (4.70%), hydrogenated soybean oil (8.40%), cholate (0.70%), and high fructose corn syrup (5.0%) by weight (82; 126; 134; 148; 181)) daily for 6 (n=6), 9 (n=7), or 12 (n=9) months. Lean control swine (n=9) were fed 725 g of a standard diet (5L80, Purina Test Diet, Richmond, IN; 18% kcal from protein, 71% kcal from complex carbohydrates, and 11% kcal from fat). Swine were housed individually with free access to drinking water and on a 12-hour light/dark cycle.

Metabolic Phenotyping

Final body weights and blood were obtained at time of sacrifice. Plasma was obtained from heparinized whole blood by centrifugation at 2000 RPM for 20 minutes. Lipid and glucose biochemistry was performed by ANTECH Diagnostics (Fishers, IN).

Statistical Analysis

Statistical analysis was performed using GraphPad Prism 5.0 (San Diego, CA). One-way analysis of variance (ANOVA) with Bonferroni post hoc analysis was performed. Data are represented as mean ± SEM. $p<0.05$ was considered significant.

Acknowledgements

The authors wish to acknowledge James P. Byrd, Josh Sturek, and Brandy Sparks for wonderful technical support during the metabolic phenotyping phase of this study. This study was supported by National Institutes of Health (HL-062552 and T32DK064466), American Heart Association (15PRE25280001), Indiana CTSI Predoctoral TL1 Training Fellowship (TR000162), the Fortune-Fry Ultrasound Research Fund, and the Cardiometabolic Disease Research Foundation.

CHAPTER 3: SERCA ACTIVATOR CDN1163 INDUCES CORONARY SMOOTH MUSCLE PROLIFERATION IN AN ORGAN CULTURE MODEL OF CORONARY ARTERY DISEASE

Abstract

Coronary artery disease (CAD) is characterized in part by de-differentiation and proliferation of coronary smooth muscle cells (CSM). Elevated sarcoplasmic reticulum (SR) Ca^{2+} stores and sarco-endoplasmic reticulum Ca^{2+} ATPase (SERCA) function are increased in proliferating cells. Although elevated SERCA function is tightly associated with early CAD, a direct causal role has not been shown. The current study used the specific SERCA activator, CDN1163, to determine whether direct SERCA activation causes CSM proliferation in an organ culture model of medial thickening and cell proliferation. Coronary arterial rings were cultured for seven days in the presence and absence of the SERCA inhibitor, cyclopiazonic acid, then stained with Verhoeff Van-Gieson's elastin stain for assessment of medial thickening and with Masson's trichrome for assessment of collagen deposition. Cell proliferation was assessed in the presence and absence of CDN1163 following serum starvation. Positive Ki-67 staining was used as an index of cell proliferation. Cyclopiazonic acid (CPA) prevented recovery of cytosolic Ca^{2+} to below baseline following depletion of the SR Ca^{2+} store, verifying the use of these cytosolic Ca^{2+} flux parameters as measures of SERCA activity. CPA treatment prevented culture-induced medial thickening, but not collagen deposition, during seven days of culture. CDN1163 induced cell proliferation in coronary arterial segments. Selective SERCA stimulation by CDN1163 increased CSM proliferation, while inhibition of SERCA activity by CPA prevented culture-induced medial thickening. Taken together, these results provide a much needed causal link between SERCA activation and CSM proliferation, providing a potential target for prevention of CAD.

Background

The coronary circulation is responsible for the delivery of oxygen and other crucial substrates to the myocardium. The tireless functioning of the heart is the impetus for high resting myocardial oxygen consumption, which requires efficient, unhindered oxygen delivery. Impediments to coronary blood flow result in long-lasting, drastic consequences, often as severe as myocardial infarction and death.

Coronary artery disease (CAD) is often referred to as a "silent killer." Because of the heart's remarkable autoregulatory capacity, adequate myocardial blood flow can be maintained until restrictions in arterial lumen diameter exceed ~75-80% of the original lumen diameter (188). This means that CAD often progresses undetected for many years. Indeed, many studies have confirmed early atherosclerotic CAD in the conduit arteries of children and young adults (189-194), although it does not often clinically manifest until middle age (194). The silent nature of the disease necessitates greater understanding of early CAD, early detection, prevention, and/or treatment.

One of the hallmarks of CAD progression is coronary smooth muscle (CSM) phenotypic modulation. In health, CSM cells are predominantly quiescent and contractile, exhibiting extremely low proliferative capacity. However, during early CAD and via mechanisms that are not fully defined, CSM cells are triggered to de-differentiate, proliferate, and migrate toward the forming plaque (170), where they secrete extracellular matrix proteins such as collagen and elastin, thereby assisting in formation of a stabilized "cap" for the growing plaque (170).

Intracellular Ca^{2+} handling mechanisms have often been implicated in induction of CSM cell proliferation. Indeed, elevated cytosolic Ca^{2+} is necessary for induction of cell cycle gene transcription via the nuclear factor of activated T-lymphocytes (NFAT) signaling pathway (72; 195). These elevations in cytosolic Ca^{2+} may be mediated either through Ca^{2+} influx or through Ca^{2+} release from internal Ca^{2+} stores (196-198). Indeed,

several pivotal studies conducted in the DDT_1 MF-2 smooth muscle cell line by Gill's group in the early 1990's demonstrated that sarcoplasmic reticulum (SR) Ca^{2+} content is directly related to smooth muscle cell growth and proliferation (66-68). The sarco-endoplasmic reticulum Ca^{2+} ATPase (SERCA) serves as the sole means by which the SR is populated with Ca^{2+}, and Waldron *et al* (68) demonstrated that intact SERCA function is necessary for serum-induced smooth muscle cell proliferation. Indeed, SERCA expression is increased in pig aorta smooth muscle cell monolayer subcultures during platelet-derived growth factor (PDGF)-induced smooth muscle cell proliferation (199), specifically immediately prior to entrance into the S phase of the cell cycle (196).

Our lab has demonstrated upregulation of SERCA function and expression in early CAD (79; 81; 82; 168), during peak proliferation within atherosclerotic plaques (187), but in the absence of specific SERCA activators, a causal link between SERCA activation and CSM proliferation has been elusive. Recently, CDN1163 has been identified as a specific activator of SERCA (200). The current study employed both SERCA activation and inhibition in an organ culture model of medial thickening and CSM proliferation (201-203) to test the hypothesis that increased SERCA function induces CSM de-differentiation and proliferation, thereby driving medial thickening.

Methods

Fluorescence imaging for assessment of cyclopiazonic acid action on sarco-endoplasmic reticulum Ca^{2+}-ATPase function

CSM cells were enzymatically isolated from freshly dissected conduit coronary arteries and loaded with fura-2/AM (2.5 mmol/l Molecular Probes, Life Technologies, Eugene, OR) as previously described (79; 82; 126; 184). Fura-2 loaded cells were placed in physiologic salt solution composed of the following (in mM): $2CaCl_2$, 138 NaCl, 1 $MgCl_2$, 5 KCl, 10 HEPES, 10 glucose; pH 7.4) containing 0.02% bovine serum albumin and were kept on ice until experiments were performed. 20-25 µl fura-2 loaded CSM cell

suspension was placed on a coverslip contained in a constant-flow superfusion chamber mounted on an inverted epifluorescence microscope (model TMS-F, Nikon, Melville, NY), with flow maintained at 1-2 ml/min. Whole cell intracellular Ca^{2+} levels were expressed as the 360 nm (F360)/380 nm (F380) excitation ratio of the 510 nm fura-2 emission at room temperature (22-25°C), using the InCa++ Imaging System Intracellular Imaging, Cincinnati, OH). Sarcoplasmic reticulum (SR) Ca^{2+} stores were released with 5 mM caffeine in Ca^{2+}-free solution (138 NaCl, 1 $MgCl_2$, 5 KCl, 10 HEPES, 10^{-5} M K^+-EGTA, 10 glucose; pH 7.4) in the presence and absence of cyclopiazonic acid (CPA; 10 µM; Santa Cruz Biotechnology, Dallas, TX). SERCA activity was assessed in the absence of extracellular Ca^{2+} as recovery of the F360/F380 signal relative to baseline following removal of caffeine.

Organ culture of epicardial conduit coronary arteries

Epicardial coronary arteries were excised under sterile conditions from domestic swine hearts similar to previous reports (201-203). Arteries were cleared of adherent connective tissue and sectioned into arterial rings of 2-4 mm in length. Rings were cultured for seven days in 12-well plates at 37°C with 4.6% CO_2 in a base media of Dulbecco's modified eagle medium (DMEM; Sigma-Aldrich, St. Louis, MO) containing high glucose (180mg/dL), 1% penicillin streptomycin (PS; Gemini Bio-products, Sacramento, CA) and 20% fetal bovine serum (Gibco, Grand Island, NY). CPA (10 µM) was delivered to the culture medium using dimethyl sulfoxide (DMSO) as a vehicle. Another group was cultured in base media with DMSO as a negative control. Culture media was changed every two days. Cultured arterial rings were compared to freshly isolated coronary arteries as a control.

Proliferation assay

Epicardial conduit coronary arteries were prepared as described above and cultured in 12-well plates at 37°C with 4.6 CO_2 for three days in DMEM containing

normal glucose (100 mg/dL) and 1% PS in the absence of FBS (serum starved conditions). Then, fresh media was added and the culture was maintained for one day in the presence of the selective SERCA activator CDN1163 (10 μM; Neurodon, LLC) and in the presence or absence of CPA (10 μM). Control rings were cultured for the final day in serum free conditions without CDN1163 or CPA.

Histology

Coronary artery segments (2-4 mm in length) were placed in 10% phosphate-buffered formalin for 24-48 hours and then transferred to 70% ethanol. Histology was performed in the Department of Anatomy and Cell Biology at Indiana University School of Medicine (Indianapolis, IN). Verhoeff van-Gieson (VVG) elastin stain was employed for interrogation of medial thickening. Masson's Trichrome (TC) stain was employed for interrogation of extracellular matrix deposition. Images were captured using a LEICA DM 300 inverted microscope and analyzed with Adobe Photoshop CS6 (Adobe Systems, Inc. San Jose, CA).

Immunohistochemistry

Coronary artery segments embedded in paraffin (described above) were transported the Department of Pathology at Indiana University School of Medicine and were processed as previously described (139). Immunostaining was performed using Ki-67 as a proliferation marker. Images were captured using a LEICA DM 300 inverted microscope and analyzed with ImageJ as described in the data supplement.

Statistical Analysis

Statistical analysis was performed using GraphPad Prism 5.0 (San Diego, CA). One-way analysis of variance (ANOVA) with student Newman-Keuls post hoc analysis was performed. Data are represented as mean ± SEM. $p<0.05$ was considered statistically significant.

Results

Cyclopiazonic acid inhibits SERCA-mediated recovery of cytosolic Ca^{2+} following SR Ca^{2+} store depletion with caffeine.

To verify CPA as an inhibitor of SERCA function, we released the SR Ca^{2+} store with caffeine (5 mM Caf in Fig. 3.1A) in the absence of extracellular Ca^{2+} and in the presence or absence of CPA (representative tracings in Fig. 3.1A). Following removal of caffeine, we assessed recovery of cytosolic Ca^{2+} relative to baseline as an index of SERCA function, as previously described (204). CPA effectively abolished the Ca^{2+} undershoot, verifying its use as a specific inhibitor of SERCA activity (Fig. 3.1B).

Cyclopiazonic acid inhibits culture-induced medial thickening.

Medial thickness was assessed in VVG stained arterial segments as a percentage of total external elastic laminar area in fresh (Day 0; Fig. 3.2A) arterial segments, and in segments cultured for seven days in the absence (Fig. 3.2C) and presence (Fig. 3.2D) of CPA. Culturing of arterial segments increased medial area and this increase was prevented with CPA treatment (Fig. 3.2B).

Cyclopiazonic acid treatment does not alter culture-induced collagen deposition.

Collagen deposition was examined in TC stained arterial segments as a percentage of total medial area in fresh (Day 0; Fig. 3.3A) arterial segments and in segments cultured for seven days in the absence (Fig. 3.3C) or presence (Fig. 3.3D) of CPA. Collagen content (blue staining in Figs. 3.3A-C) was increased with culture, but was not altered with CPA treatment (Fig. 3.3B).

CDN1163 stimulation of SERCA induces CSM proliferation.

Following serum starvation, coronary arterial rings were cultured in the absence (Control; Fig. 3.4A) or presence (Fig. 3.4B) of CDN1163, and in the presence of CDN1163 and CPA (Fig. 3.4C) and Ki-67 positive staining was examined as an index of

cell proliferation (black arrows in Figs. 3.4A-C). CDN1163 increased cell proliferation ~3-fold and this effect was blocked by the SERCA inhibitor CPA (Fig. 3.4D).

Discussion

The current study examined SERCA inhibition and activation in an organ culture model of medial thickening and cell proliferation. Specific and direct stimulation of SERCA activity with CDN1163 induced CSM proliferation, while inhibition of SERCA activity with CPA completely abolished culture-induced medial thickening. Taken together, these data suggest that the elevated SERCA activity observed in early CAD (79; 81; 82; 168) causes the induction of the quiescent-to-proliferative phenotypic switch of CSM during the beginning stages of atherosclerotic lesion formation.

An interesting contribution to the discussion of SERCA and CSM proliferation during CAD progression is a series of studies in which gene transfer of SERCA2a halted culture-induced intimal thickening and CSM proliferation (72; 205; 206). While these data are seemingly at odds with earlier findings that elevated SERCA expression and function are associated with increased smooth muscle proliferation (196; 199), a couple of key experimental differences may shed light on the apparent discrepancies. Firstly, human coronary arteries used by the group at Mt. Sinai are obtained from explanted human hearts (72; 205) obtained at transplant. However, 37-46% of explanted hearts have overt CAD (207). Additionally, data from Nissen's group indicate that, in adults between 20-29 years of age, an estimated 66% of individuals have asymptomatic CAD (193). Therefore, it is likely that the group at Mt. Sinai is taking samples at their peak proliferative rate and labeling them "normal." The current study takes arteries with 0% intimal thickness as baseline, thereby eliminating any confounding factor from early CAD-induced CSM proliferation at baseline.

Recently, we found that voltage-gated Ca^{2+} channel function is also increased in early CAD (168; 187), and we previously demonstrated that store-operated Ca^{2+} entry is

elevated in early CAD (126). Interestingly, a recent study in myometrial smooth muscle demonstrated that elevated SERCA function and activity increase store-operated Ca^{2+} entry, thereby depolarizing the sarcolemma and activating L-type voltage-gated channels (208). Future studies should undertake determination of the effect of SERCA upregulation on other Ca^{2+} transporters in organ culture, and determine whether these additional perturbations in Ca^{2+} regulation contribute to CSM de-differentiation.

This study provides evidence of a causal link between SERCA upregulation and CSM proliferation in early, asymptomatic CAD. These data are valuable, as they provide a potential target for early treatment of CAD through modulation of SERCA activity. Additionally, these data provide a potential early step in the cascade of CSM Ca^{2+} handling perturbations in early CAD.

Acknowledgements

The authors would like to thank Dr. Jose Estrada (Indiana University School of Medicine) for generous sharing of coronary tissue.

Conflict of Interest

There are no conflicts of interest to disclose.

Figures

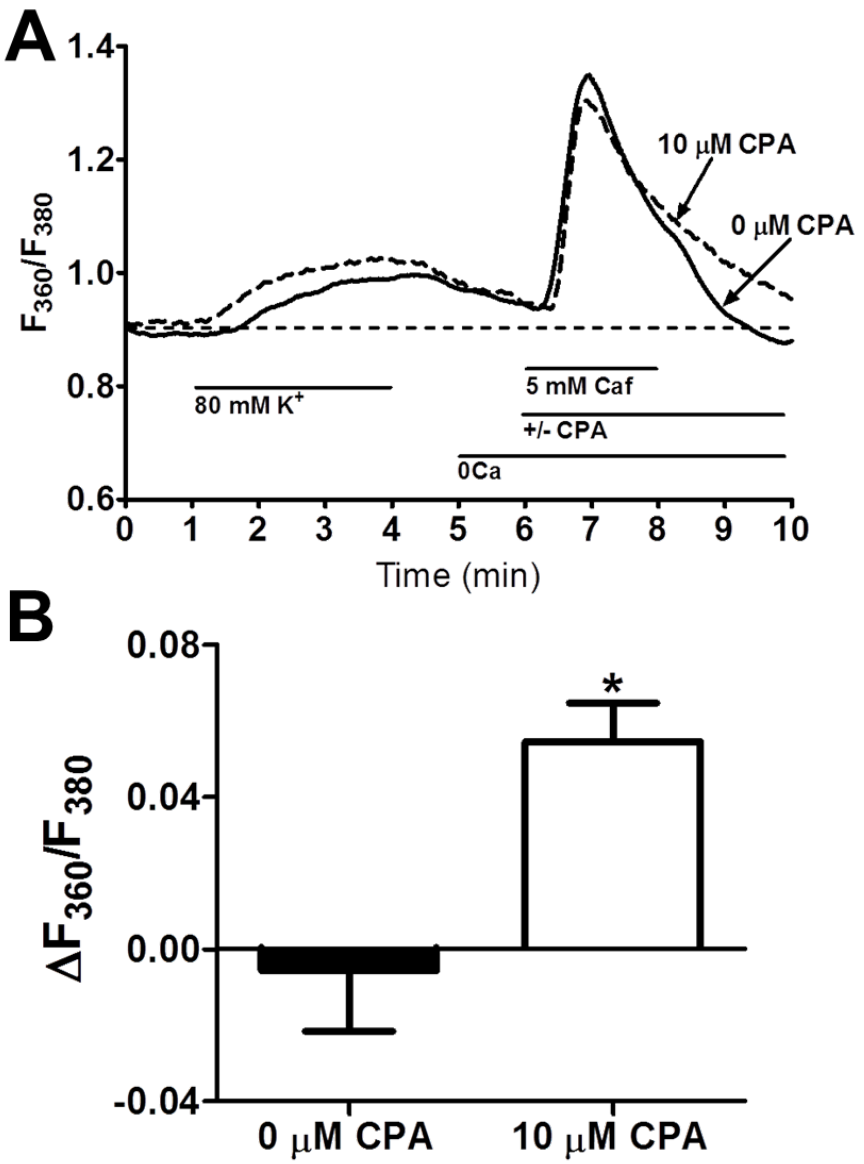

Figure 3.1: Cyclopiazonic acid inhibits SERCA-mediated recovery of cytosolic Ca^{2+} following SR Ca^{2+} store depletion with caffeine. A) Representative tracings obtained from interrogation of fura-2 (2.5 μM)-loaded CSM in the presence and absence of cyclopiazonic acid (CPA). B) CPA (White bar; 10 μM) prevents recovery of cytoplasmic Ca^{2+} to baseline levels. *, $p<0.05$.

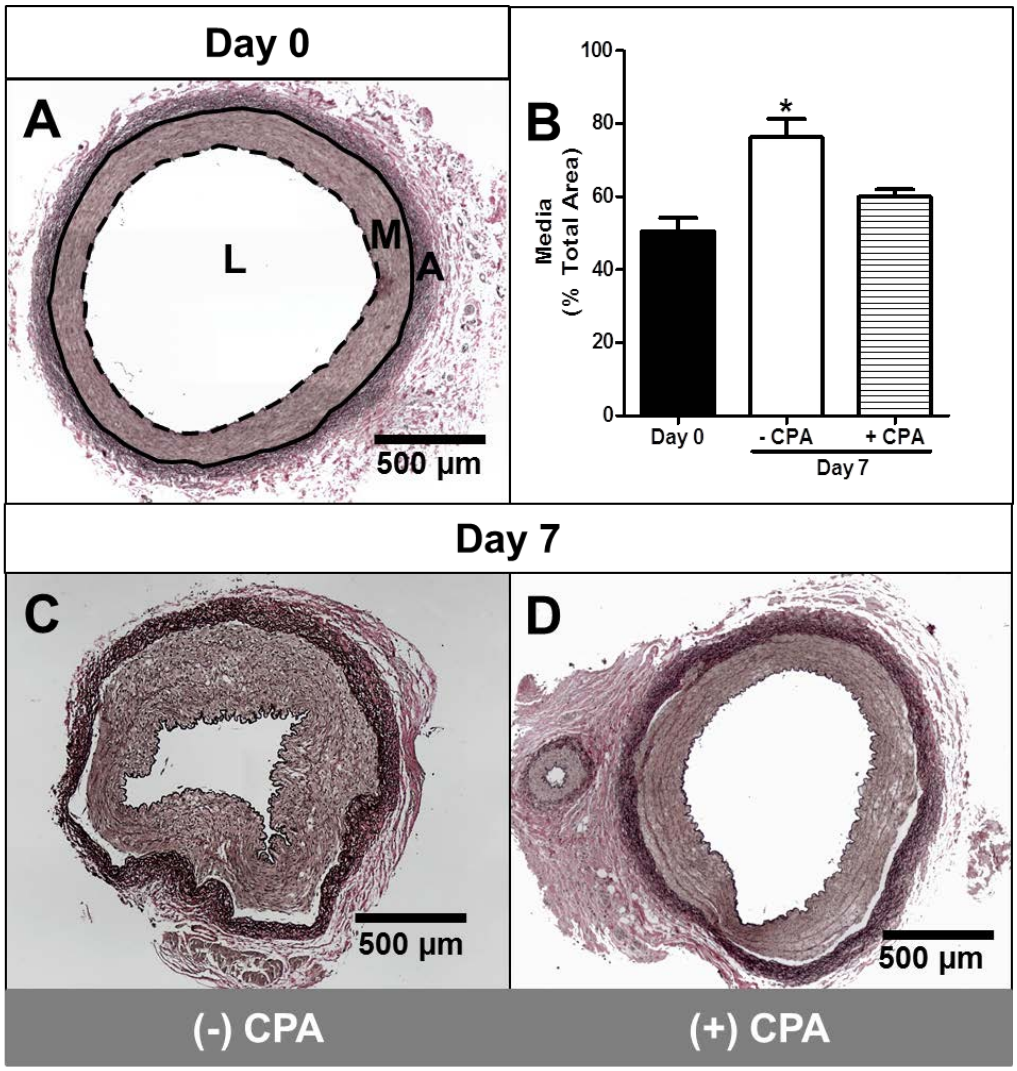

Figure 3.2: Cyclopiazonic acid inhibits culture-induced medial thickening. Verhoeff Van-Gieson's elastin stain was used to identify external (solid black line in A) and internal (dashed black line in A) elastic lamina in order to assess medial area as a percentage of total area inside the external elastic lamina. A) Fresh arterial rings were used as a control (Day 0). L = lumen; M = media; A = adventitia. B) Medial thickening was observed after 7 days in the absence of CPA; however this thickening was prevented by CPA treatment. *, $p < 0.05$. C) Coronary arterial ring cultured for 7 days in the absence of CPA. D) Coronary arterial ring cultured for 7 days in the presence of CPA.

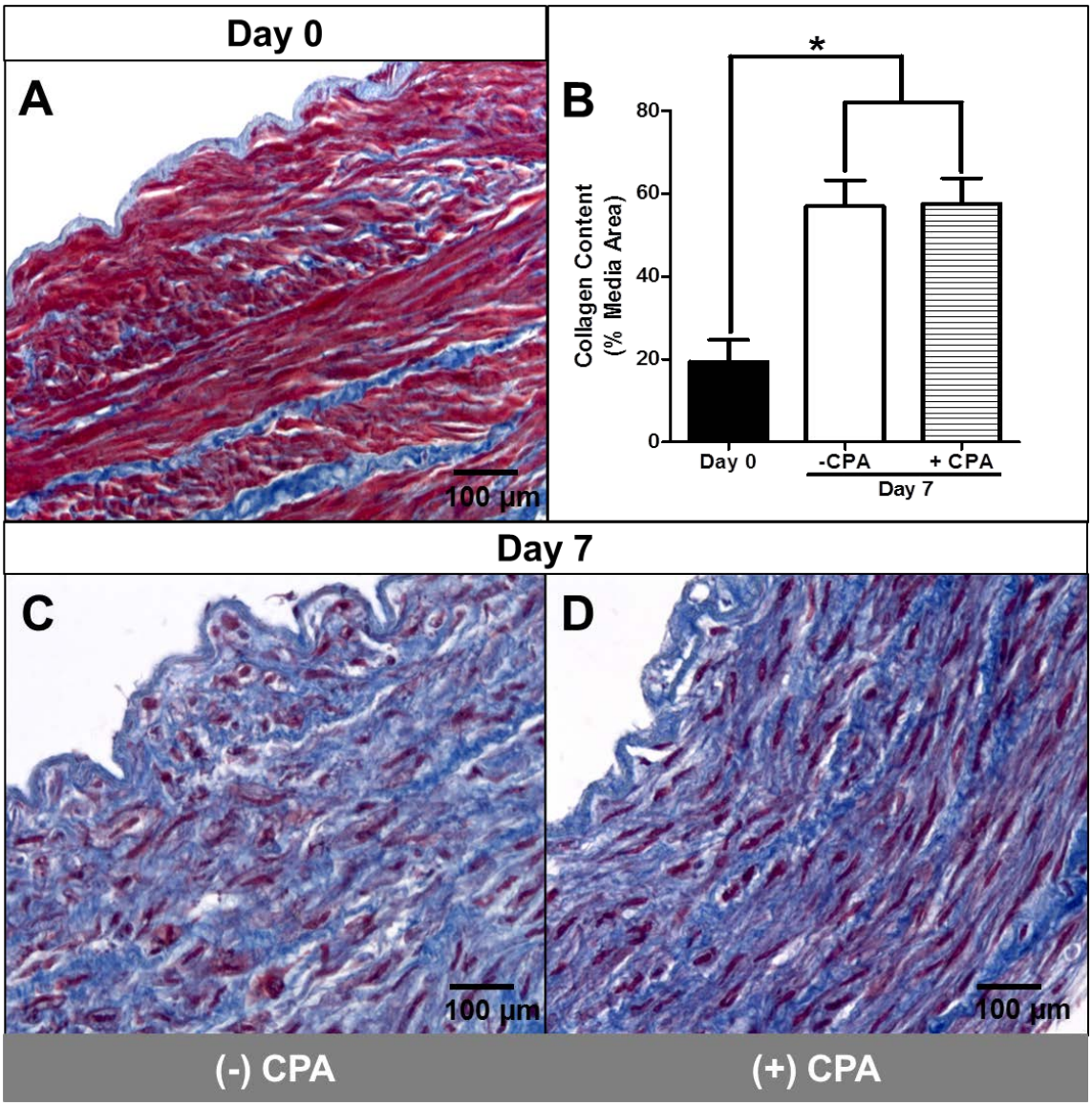

Figure 3.3: Cyclopiazonic acid treatment does not alter culture-induced collagen deposition. Masson's trichrome stain was used to identify collagen deposition (blue in panels A, C, and D) in culture. A) Fresh arterial rings were used as control (Day 0). B) Collagen content was increased after 7 days of culture, and this was not altered with CPA treatment. *, $p < 0.05$. C) Coronary arterial ring cultured for 7 days in the absence of CPA. D) Coronary arterial ring cultured for 7 days in the presence of CPA.

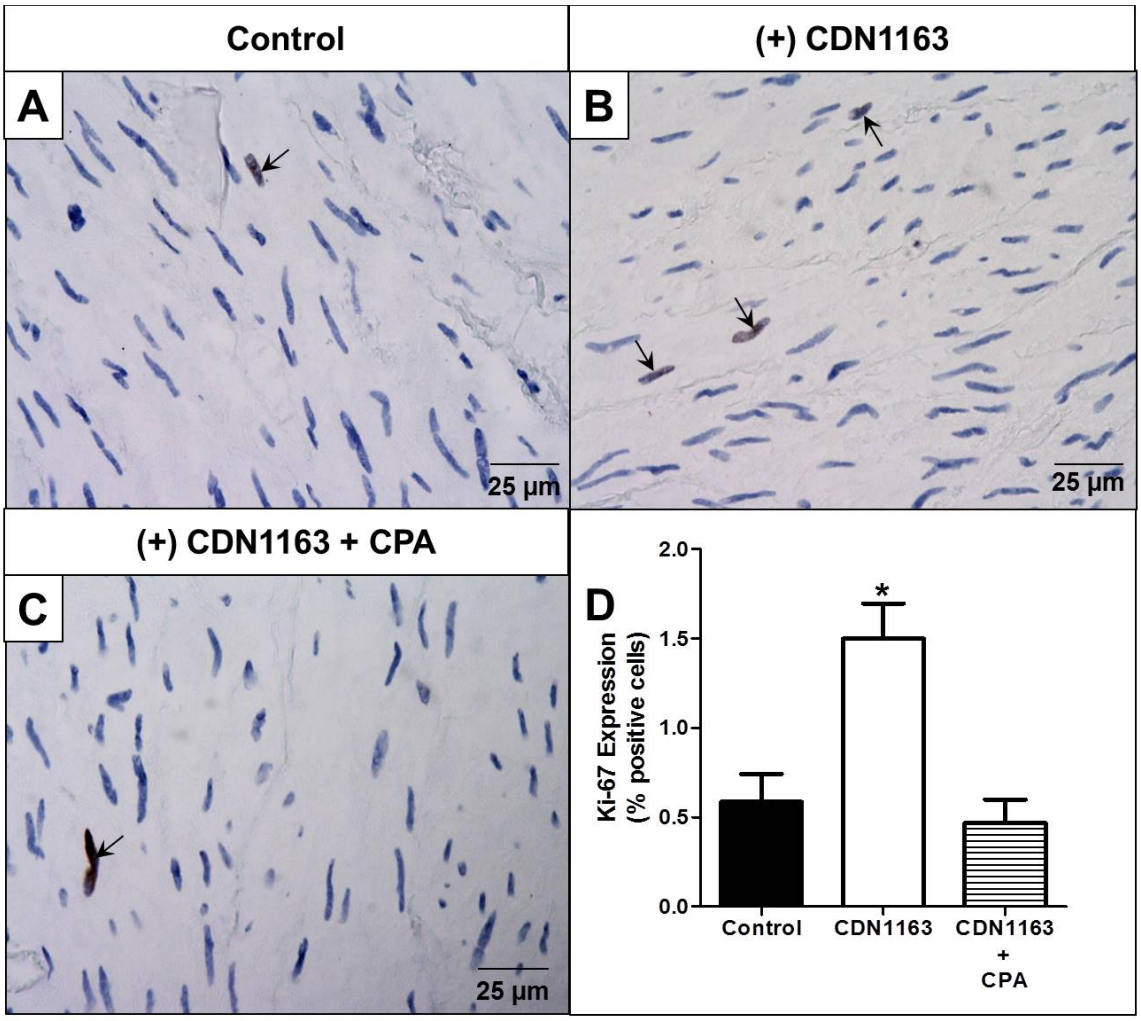

Figure 3.4: CDN1163 stimulation of SERCA induces CSM proliferation. Ki-67 immunostaining was utilized as an index of proliferative activity. Positively stained nuclei are indicated with black arrows in panels A and B. Coronary arterial rings were serum staved for 72 hours. Culture media was changed, and rings were cultured for an additional 24 hours in the absence of serum and in the absence (A) or presence (B) of the SERCA activator, CDN1163. C) CPA was added in conjunction to CDN1163 and cultured for 24 hours. D) CDN1163 induced a ~3-fold increase in proliferation that was abolished by CPA.

CHAPTER 4: METABOLIC SYNDROME ABOLISHES GLUCAGON-LIKE PEPTIDE-1 RECEPTOR AGONIST STIMULATION OF SERCA IN CORONARY SMOOTH MUSCLE

(Published in *Diabetes* 64:3321-3327, 2015. doi: 10.2337/db14-1790)

Abstract

Metabolic syndrome (MetS) doubles the risk of adverse cardiovascular events. Glucagon-like peptide-1 (GLP-1) receptor agonists induce weight loss, increase insulin secretion, and improve glucose tolerance. Studies in healthy animals suggest cardioprotective properties of GLP-1 receptor agonists, perhaps partially mediated by improved sarco-endoplasmic reticulum Ca^{2+} ATPase (SERCA) activity. We examined the acute effect of GLP-1 receptor agonists on coronary smooth muscle cells (CSM) enzymatically isolated from lean, healthy Ossabaw miniature swine. Intracellular Ca^{2+} handling was interrogated with fura-2. The GLP-1 receptor agonist, exenatide, activated SERCA, but did not alter other Ca^{2+} transporters. Further, we tested the hypothesis that chronic, *in vivo* treatment with GLP-1 receptor agonist, AC3174, would attenuate coronary artery disease (CAD) in swine with MetS. MetS was induced in 20 swine by six months feeding of a hypercaloric, atherogenic diet. Swine were then randomized (N=10/group) into placebo or AC3174 treatment groups and continued diet for an additional six months. AC3174 treatment attenuated weight gain, increased insulin secretion, and improved glucose tolerance. Intravascular ultrasound and histology showed no effect of AC3174 on CAD. MetS abolished SERCA activation by GLP-1 receptor agonists. We conclude that MetS confers vascular resistance to GLP-1 receptor agonists, partially through impaired cellular signaling steps involving SERCA.

Background

Metabolic syndrome (MetS) is defined as the presence of three or more of the following five risk factors: obesity, hypertension, glucose intolerance, insulin resistance, and dyslipidemia (169). Obesity, MetS, and type 2 diabetes are all independent risk factors for cardiovascular disease. The presence of MetS doubles risk of experiencing an adverse cardiovascular event (15). Thus, it is important to understand the effect of diabetes and MetS treatment modalities on cardiovascular health.

Insulin-sensitizing drugs and those which enhance insulin secretion from pancreatic beta cells have been employed in the treatment of type 2 diabetes and MetS. Others, such as dipeptidyl peptidase-4 inhibitors, and glucagon-like peptide-1 receptor agonists (exenatide, liraglutide, AC3174, etc.) increase both insulin sensitivity and insulin secretion (33; 34). Recently, insulin-sensitizing thiazolidinediones have been implicated in increased risk of fluid retention, LDL and triglyceride accumulation, heart failure, and myocardial infarction (209-211). Hence, there is great attention on cardiovascular outcomes of anti-diabetic agents and the Food and Drug Administration requires cardiovascular safety profiles for all new agents (212).

Glucagon-like peptide-1 (GLP-1) receptor agonists are attractive treatment options for MetS, because GLP-1 is an endogenous hormone which functions in normal physiology to increase insulin sensitivity, biosynthesis, and secretion (33). Additionally, GLP-1 receptor agonists reduce myocardial infarct size in ischemia/reperfusion injury (112), improve cardiac function in chronic heart failure (103), and attenuate neointimal formation following vascular injury (113). At the cellular level, GLP-1 receptor agonists improve endothelial calcium homeostasis following simulated ischemia/reperfusion (116). Further, GLP-1 receptor agonists improve sarco-endoplasmic reticulum Ca^{2+} ATPase (SERCA) activity in multiple cell types (114; 115). These studies provide rationale for a protective role of GLP-1 in the coronary vasculature.

A recent study revealed impaired GLP-1 stimulation of myocardial glucose uptake in human patients with type 2 diabetes and in MetS swine (91). This finding raises the question of potential resistance to GLP-1 in MetS and type 2 diabetes and highlights the need for rigorous examination of GLP-1 action on coronary artery disease (CAD), specifically in MetS. Given the stimulation of SERCA in macrophages and ventricular myocytes (114; 115) and altered SERCA in coronary smooth muscle (CSM) in MetS and diabetes (79; 82), potentially vaso-protective actions of GLP-1 could be mediated through cellular Ca^{2+} signaling. This study was investigated the effect of GLP-1 receptor agonists on SERCA stimulation in CSM from lean swine and on coronary artery disease (CAD) and CSM SERCA stimulation in MetS.

Methods

Animals

All protocols involving animals were approved by the institutional animal care and use committee at Indiana University School of Medicine, and fully complied with animal use standards (182; 183). Ossabaw miniature swine were separated into two treatment groups: placebo (N=10) and GLP-1 receptor agonist AC3174-treated (N=10; 0.25μg/kg body weight subcutaneously, twice daily; Amylin Pharmaceuticals, San Diego, CA), which displays nearly identical pharmacokinetic and pharmacodynamics profiles as the marketed GLP-1 receptor agonist, exenatide (34). CAD and MetS were induced in both treatment groups as described in the online supplement. One animal in the placebo group died prior to collection of endpoint data.

Isolation of coronary smooth muscle cells

Epicardial coronary arteries were cleaned of adherent tissue and CSM were isolated with a collagenase solution as described (79; 82) .

Measurement of intracellular Ca^{2+}

CSM were loaded with fura-2/AM and whole cell intracellular Ca^{2+} levels were measured as described in the online supplement

Acute in vitro exenatide treatment

CSM from lean, healthy Ossabaw swine or a separate group of swine with MetS and CAD were treated with 100 nM exenatide during assessment of intracellular Ca^{2+}. The selective SERCA inhibitor, cyclopiazonic acid (CPA, 10 μM) was utilized as a negative control for SERCA function.

Intravenous glucose tolerance testing

Intravenous glucose tolerance testing (IVGTT) was performed as described (82; 148) and in the online supplement.

Plasma Lipid, Electrolyte, and Enzyme Assays

Blood samples were obtained at time of IVGTT prior to intravenous injection of glucose. Lipid electrolyte and enzyme content were measured offsite (Antech Diagnostics, West Lafayette, IN).

Intravascular ultrasound

After 12 months on diet, intravascular ultrasound pullbacks were performed as described in the online supplement.

Histology

Coronary arterial rings were placed in phosphate-buffered formalin at time of euthanasia. Hematoxylin & Eosin (H&E), Verhoeff-van Gieson (VVG), and Trichrome (TC) staining were performed on sections of these rings. Plaque burden and collagen content were determined using commercially available software (ImageJ 1.48v, National Institutes of Health, USA) as described (82).

Results

Acute in vitro exenatide treatment in CSM from lean, healthy swine

We investigated the acute effect of the GLP-1 receptor agonist, exenatide, on intracellular Ca^{2+} handling in CSM isolated from lean, healthy Ossabaw swine. SR Ca^{2+} stores were released with caffeine in the absence of extracellular Ca^{2+} in the presence and absence of 100 nM exenatide (Fig. 4.1A), and the subsequent undershoot of cytosolic Ca during recovery was assessed. Exenatide treatment did not alter resting cytosolic Ca^{2+} (Fig. 4.1B) or Ca^{2+} influx through voltage-gated Ca^{2+} channels (Fig. 4.1C). Exenatide elicited improved recovery of cytosolic Ca^{2+} below baseline levels and this effect was completely ablated in the presence of the SERCA inhibitor CPA (Fig. 4.1D). The GLP-1 receptor agonist liraglutide also demonstrated improved recovery of cytosolic Ca^{2+}, which was prevented by the GLP-1 receptor antagonist, exendin (9-39) (Fig. 4.S1). In the presence of caffeine, SERCA buffering of cytosolic Ca^{2+} is functionally inhibited, because of the much more rapid release of Ca^{2+} through ryanodine receptors on the SR membrane. Therefore, we assessed the rate of recovery to 50% recovery to baseline (T_{50}), in the presence of caffeine as a measure of Ca^{2+} extrusion and/or Ca^{2+} uptake into caffeine-insensitive intracellular stores and to 100% recovery to baseline (T_{100}) in the absence of caffeine as another measure of SERCA activation. Exenatide significantly decreased time to 100%, but not 50% recovery to baseline (Fig. 4.1E).

Clinical measurement of MetS in Ossabaw swine

We then investigated the chronic effect of GLP-1 receptor agonism *in vivo*. To examine the effects of diet and GLP-1 receptor treatment on glucose metabolism, kidney function, and plasma electrolytes, blood profiles of these parameters were obtained (Table 4.S1) and IVGTTs were performed. Overall, feeding of an excess calorie, atherogenic diet increased body weight, which was significantly attenuated by AC3174 treatment (Fig. 4.2A). Blood pressure was not altered by diet or AC3174 treatment.

While fasting plasma glucose was not altered by diet or AC3174 treatment (Table 4.S1), IVGTT assessment of glucoregulation revealed improved glucose handling in AC3174 treated swine, compared to placebo (Fig. 4.2B-D). This was corroborated by augmented plasma insulin levels following intravenous glucose challenge in AC3174 treated animals, compared to placebo (Fig. 4.2E-G).

Intravascular ultrasound and histology measurement of CAD

Intravascular ultrasound (IVUS) was employed to examine severity of CAD *in vivo* and was confirmed by histology. Both wall coverage and percent plaque burden were assessed as previously described (82) in placebo and AC3174-treated pigs. AC3174 treatment did not alter CAD severity as indicated by either wall coverage or percent plaque burden (Fig. 4.3C-D). *In vitro*, histological examination of coronary arterial rings revealed no effect of AC3174 treatment on plaque burden (Fig. 4.3E-F; I-J; H), collagen deposition (Fig. 4.3G; K-L).

Effect of chronic, in vivo GLP-1 receptor agonist treatment on CSM Ca^{2+} handling in MetS-induced CAD.

We have previously demonstrated alterations in coronary smooth muscle (CSM) Ca^{2+} handling in MetS-induced CAD (79; 82; 180) . We therefore investigated whether chronic, *in vivo* AC3174 treatment resulted in improved intracellular Ca^{2+} handling in CSM. Fig. 4.4A shows the Ca^{2+} signaling protocol to assess baseline Ca^{2+} levels, sarcoplasmic reticulum (SR) Ca^{2+} store release assessed by the caffeine-induced Ca^{2+} peak in the absence of extracellular Ca^{2+}, and SERCA activity assessed by subsequent recovery of cytosolic Ca^{2+} levels and undershoot of cytosolic [Ca^{2+}] below baseline levels. Chronic AC3174 treatment did not alter intracellular Ca^{2+} handling in CSM from swine with MetS-induced CAD (Fig. 4.4B-D).

Effect of acute, in vitro exenatide treatment on CSM in MetS and CAD

Further, we assessed the acute, direct effect of GLP-1 receptor agonists on Ca^{2+} handling in CSM isolated from swine with MetS and CAD. Cells were exposed to the GLP-1 receptor agonist, exenatide (100 nM), which has an identical pharmacological profile as AC3174 (34) (Fig. 4.4A) for three minutes prior to treatment with high K^+. We again assessed caffeine-induced SR Ca^{2+} store release by peak Ca^{2+} response to caffeine and SERCA activity by the subsequent undershoot of cytosolic Ca^{2+} during recovery. Exenatide did not alter either SR Ca^{2+} store release or the undershoot of cytosolic Ca^{2+} below baseline (Fig 4.4E-F).

Discussion

The principle finding of this study is that MetS confers *vascular* resistance to the effects of GLP-1 receptor agonists. AC3174 did improve several cardiovascular risk factors, such as the metabolic factors, glucose tolerance and insulin secretion, indicating that longer term treatment may have indirect benefits on cardiovascular health. Treatment of MetS and type 2 diabetes is confounded by potential secondary and detrimental cardiovascular effects. Previous studies in lean, healthy animals indicate that GLP-1 receptor agonists provide a potential cardioprotective treatment for type 2 diabetes and MetS (103; 112; 113). In the current study, we examined possible Ca^{2+} regulatory mechanisms for GLP-1 receptor agonist action in CSM from lean, healthy Ossabaw swine. Our finding that GLP-1 receptor agonists exert a positive effect on SERCA activity in coronary smooth muscle from lean Ossabaw swine is in agreement with findings that GLP-1 receptor agonists enhance SERCA activity in other cell types, including endothelial cells (116), macrophages (114), and cardiomyocytes (115), and is the first study examining the effect of GLP-1 receptor agonists in CSM. The kinetics of the Ca^{2+} transient shown in Fig. 4.1E demonstrate a lack of exenatide effect on Ca^{2+} extrusion. We have previously shown these kinetic measurements to be an appropriate

assay of Ca^{2+} extrusion (79). Reduced SERCA activity has been implicated in CSM proliferation and neointimal formation in the progression of CAD (73; 206). One possible mechanism explaining this phenomenon is induction of endoplasmic reticulum (ER) stress. As the single means by which Ca^{2+} may enter the ER, SERCA is a crucial regulator of ER Ca^{2+} homeostasis, and SERCA inhibition elicits an ER stress response through depletion of ER Ca^{2+}[213]. ER stress is associated with development of atherosclerosis (114). Inhibition of ER stress through heightened activation of SERCA could provide a novel means by which to treat CAD.

We also examined the effect of GLP-1 receptor agonists on CAD progression in MetS. This study was needed because of recent evidence of MetS-induced resistance to the cardioprotective effects of GLP-1 (91). The improvement of systemic glucoregulation with AC3174 treatment provides essential positive evidence for GLP-1 receptor agonist action in the Ossabaw swine model of MetS and CAD. Further, we demonstrated that GLP-1 receptor agonist, AC3174 has no effect on MetS-induced CAD. This is in contrast with the recent finding that GLP-1 prevents myocardial ischemia-reperfusion injury (112) and injury-induced neointimal hyperplasia (113), providing evidence that the MetS phenotype itself confers cardiovascular resistance to the beneficial effects of GLP-1. It is important to note that, while AC3174 treatment did not attenuate CAD progression, the absence of adverse effects of AC3174 provide a cardiovascular safety profile for GLP-1 receptor agonists.

Additionally, we examined the acute, direct effect of GLP-1 receptor agonists on intracellular Ca^{2+} regulation in CSM from Ossabaw swine with MetS and CAD who had not received any treatment with GLP-1 receptor agonists. Here, we found that exenatide had no effect on Ca^{2+} regulation in CSM from swine with MetS and CAD. This finding is in contrast with other studies in which GLP-1 receptor agonism resulted in increased SERCA activity (114-116). A study in humans with type 2 diabetes revealed that

exenatide treatment enhanced endothelial-dependent vasodilation (214), although it is important to note that blood cholesterol levels were controlled in these patients. The current study, revealing a lack of effect of GLP-1 receptor agonism on SERCA activity in the setting of MetS corroborates the earlier finding that MetS ablated the effect of GLP-1 receptor agonists in myocardium and highlights the need for additional studies to investigate specific aspects of MetS (obesity, hyperinsulinemia, glucose intolerance, hypertension, and dyslipidemia) that may underlie resistance of the coronary vasculature to GLP-1 receptor agonists.

Acknowledgments

This study was supported in part by Amylin Pharmaceuticals, San Diego, CA, and by National Institutes of Health grant HL062552.

S.L.D. researched and evaluated data and wrote the manuscript. M.L.M. researched data and reviewed and edited the manuscript. L.N.B. and A.F. researched and organized data and reviewed the manuscript. K.A.S. researched data and reviewed the manuscript. M.A., N.C., and M.S. conceptualized the chronic, *in vivo* study, researched data, and reviewed and edited the manuscript. M.S. is the guarantor of this work and, as such, had full access to all the data in the study and takes responsibility for the integrity of the data and the accuracy of the data analysis.

The authors thank James P. Byrd, Brandy Sparks, and Josh Sturek for technical assistance. We also thank Dr. Rebecca S. Bruning, Indiana University School of Medicine, Department of Cellular & Integrative Physiology, for editorial assistance during preparation of the manuscript.

Figures

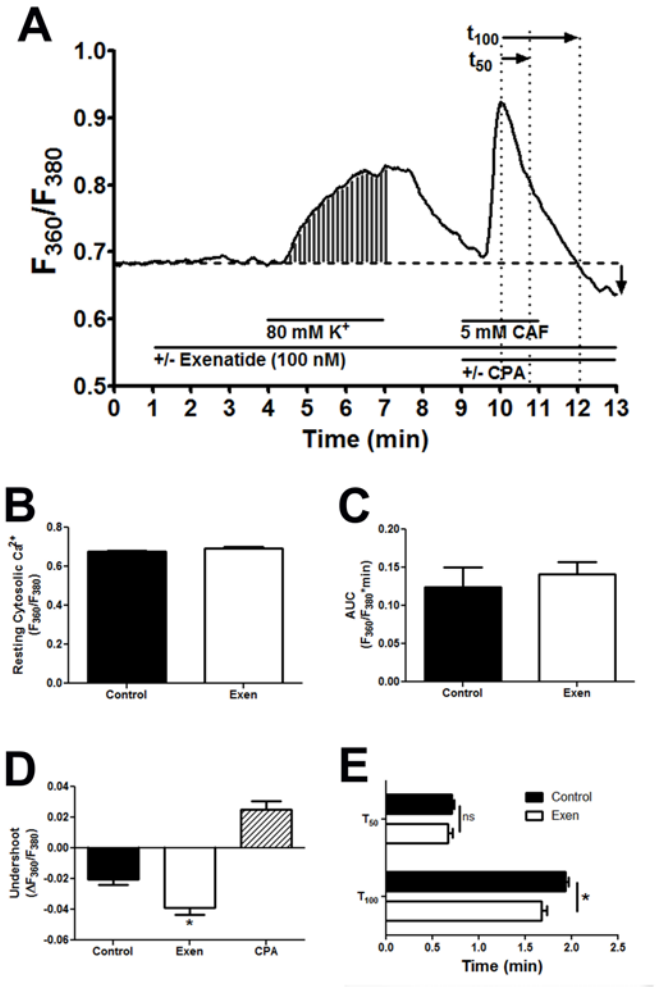

Figure 4.1: Effect of acute exenatide treatment on CSM Ca^{2+} handling in CSM isolated from lean, healthy Ossabaw swine. A) Representative tracing of data from Ca^{2+} imaging protocol. Horizontal dashed line indicates baseline. (Control n = 114 CSM; Exen n = 82 CSM; CPA n = 68 CSM) B) Resting cytosolic Ca^{2+}. C) Area under the curve (AUC) for Ca^{2+} influx during high K^+, corresponding to the shaded region in panel A. D) Undershoot of Ca^{2+} below resting levels, corresponding to the black vertical arrow in panel A. E) Time to half (t_{50}) and total (t_{100}) recovery from caffeine-induced rise in cytosolic Ca^{2+}, corresponding to the horizontal black arrows in panel A.

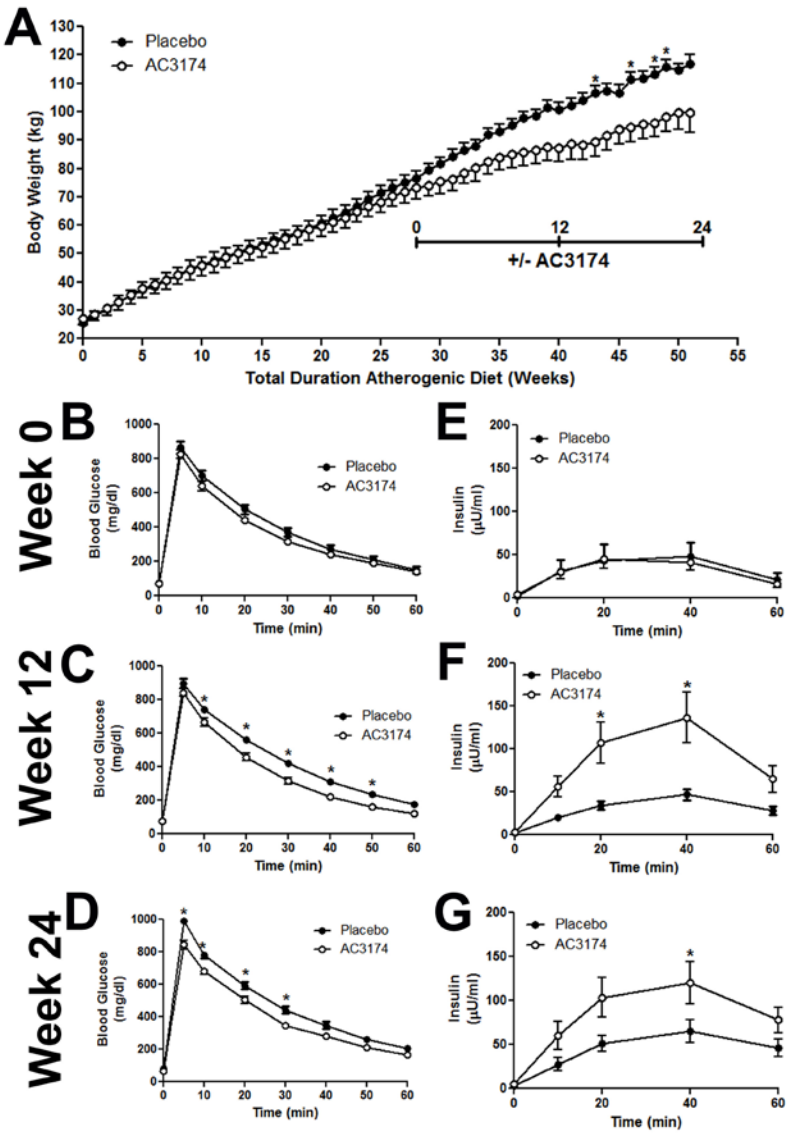

Figure 4.2: AC3174 attenuates weight gain and improves glucose handling in Ossabaw miniature swine. Closed circles = placebo treatment group. Open circles = AC3174 treatment group. A) Weight gain in Ossabaw miniature swine. Inset timeline indicates time on placebo or AC3174 treatment, which corresponds with times in B-D and Table S1. B-D) Time course of plasma glucose responses during IVGTT at B) beginning, C) 12 weeks, and D) 24 weeks of AC3174 treatment. E-G) Time course of plasma insulin responses during IVGTT at E) beginning, F) 12 weeks, and G) 24 weeks of AC3174 treatment.

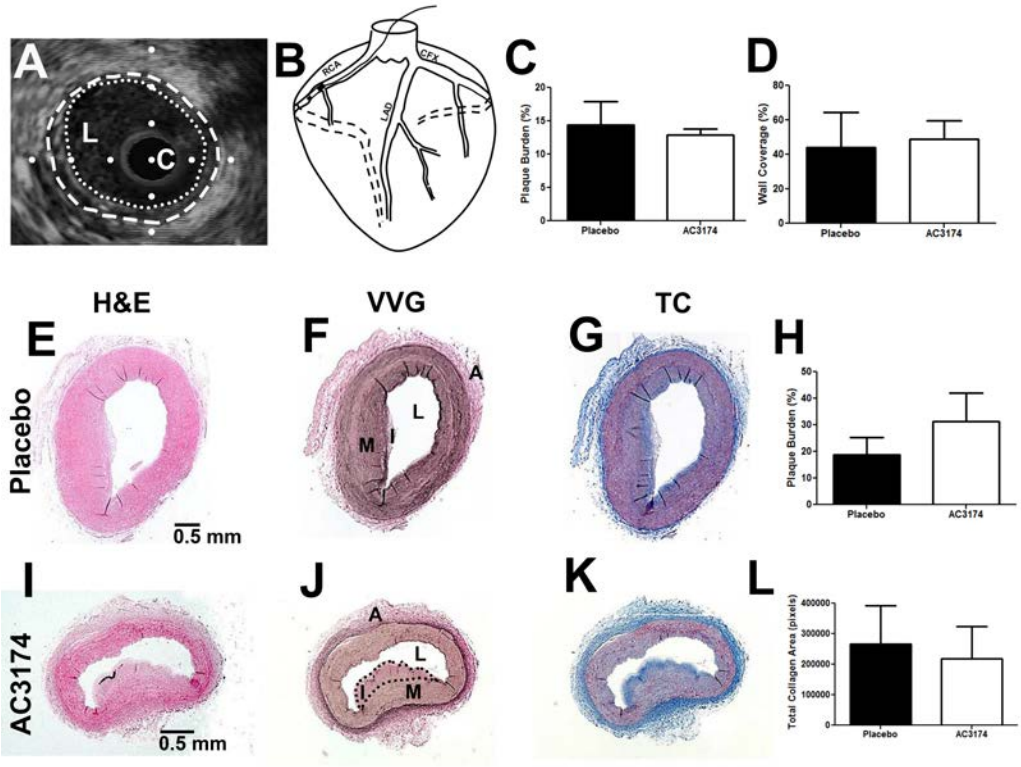

Figure 4.3: AC3174 treatment does not attenuate CAD progression as measured by intravascular ultrasound (IVUS) and histology. A) IVUS image of artery with CAD. Lumen traced in white dashed line. L = Lumen, C = Catheter. Distance between dots is 1 mm. Lumen traced in white dotted line. Arterial wall traced in white dashed line. Atherosclerotic plaque is indicated between dotted and dashed lines. B) The heart and major epicardial coronary arteries. RC = right coronary artery, LAD = left anterior descending, CFX = circumflex. The RC and CFX on the anterior aspect of the heart are shown by the solid lines and the arteries traversing to the posterior aspect of the heart are shown by the dashed lines. The IVUS catheter is shown in the RC positioned for a pullback. C, D) Quantification of IVUS pullbacks performed in the RC in both placebo (n = 6) and AC3174-treated (n = 3) swine. AC3174 did not attenuate CAD as measured by percent plaque burden (panel C) or percent wall coverage (panel D). E-G; I-K: Coronary arterial rings from placebo (n = 4; panels E-G) and AC3174-treated (n = 5; panels I-K) swine. In panels F and J: A = Adventitia; I = Intima; L = Lumen; M = Media. A, E) Coronary artery rings stained with hematoxylin & eosin (H&E). F, J) Coronary artery rings stained with Verhoeff-van Gieson (VVG) stain for elastin. An overt atherosclerotic plaque is traced in panel H. G, K) Coronary artery rings stained with Masson's trichrome (TC) for collagen. H) Graphical representation of plaque burden, (p = 0.35) L) Graphical representation of total collagen area, (p = 0.79).

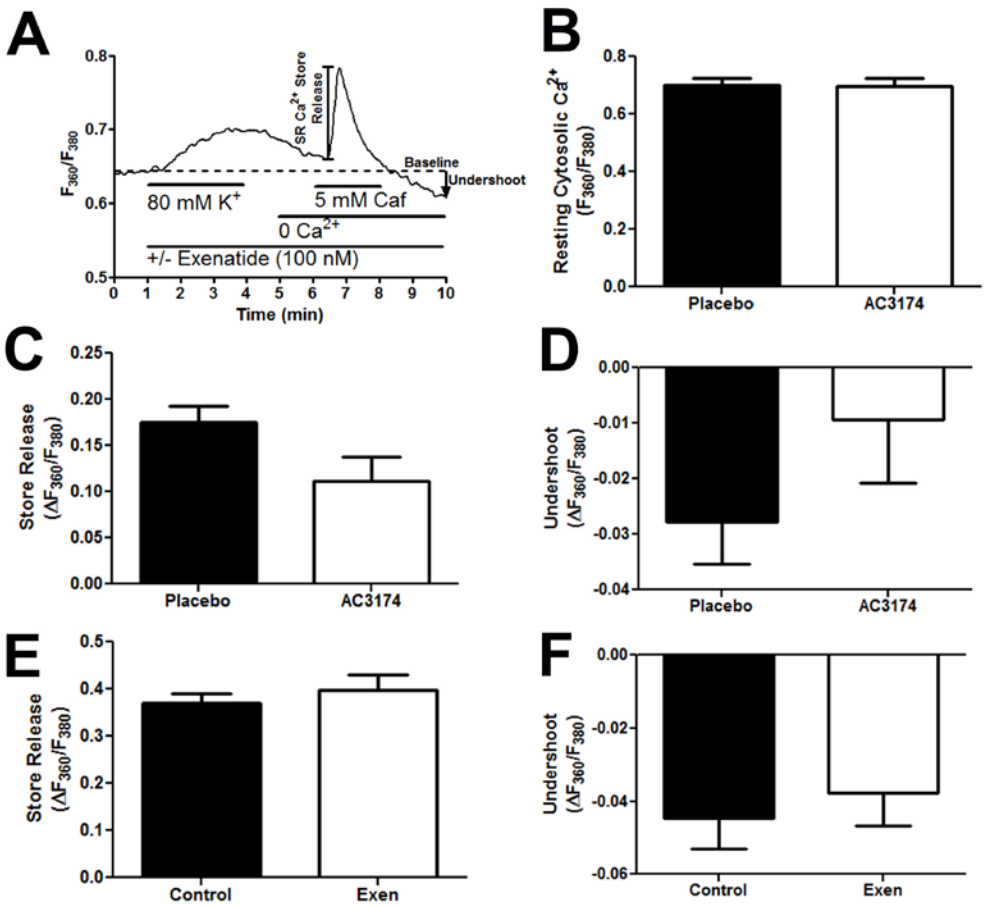

Figure 4.4: Effect of GLP-1R agonists on CSM Ca^{2+} handling in MetS Ossabaw swine. A) Representative tracing of data from Ca^{2+} imaging protocol. Dashed line indicates baseline. B-D) Effect of chronic in vivo AC3174 treatment on CSM Ca^{2+} handling. (Placebo n = 4 swine; AC3174 n = 6 swine) B) Resting cytosolic Ca^{2+} levels. C) Caffeine-induced SR Ca^{2+} store release. Corresponds to brackets in panel A. D) Undershoot of cytosolic Ca^{2+} levels below baseline. Corresponds to black arrow in panel A. E-F) Effect of acute ex vivo exenatide treatment on Ca^{2+} handling in CSM from MetS Ossabaw swine. (0Ca n = 38 CSM; Exen n = 24 CSM) E) Caffeine-induced SR Ca^{2+} store release. Corresponds to brackets in panel A. F) Undershoot of cytosolic Ca^{2+} levels below baseline. Corresponds to black arrow in panel.

Data Supplement

Animals.

Coronary artery disease (CAD) and metabolic syndrome (MetS) were induced in both treatment groups by feeding, once daily for 6 months, 1 kg of atherogenic diet, containing 16% kcal from protein, 41% kcal from complex carbohydrates, 19% kcal from fructose, and 43% kcal from fat, and supplemented with 2.0% cholesterol and 0.7% sodium cholate by weight (KT324, Purina Test Diet, Richmond, IN), as previously described (82; 126; 139). Following 6 months on this diet, swine were placed on placebo or AC3174 treatment twice daily and feeding was altered to 0.5 kg twice daily for an additional six months. Water was provided ad libitum. Six lean, age-matched Ossabaw miniature swine fed a standard chow diet (5L80, Purina Lab Diet, Richmond, IN) were a control group to verify presence of MetS. Coronary smooth muscle (CSM) cells were isolated from additional lean and MetS swine for acute, in vitro assessment of GLP-1 receptor agonist action on intracellular Ca^{2+} handling (see acute in vitro exenatide treatment methods).

Measurement of intracellular Ca^{2+} levels.

CSM were loaded with the fluorescent intracellular Ca^{2+} indicator, fura-2/AM. Fura-2 loaded cells were placed on a coverslip contained in a constant-flow superfusion chamber mounted on an inverted epifluorescence microscope (model TMS-F, Nikon, Melville, NY), with flow maintained at 1-2 ml/min. Whole cell intracellular Ca^{2+} levels were assessed as the 360 nm/380 nm excitation ratio of the fura-2 emission at 510 nm at room temperature (22-25 °C), using the InCa++ Ca^{2+} Imaging System (Intracellular Imaging, Cincinnati, OH) as previously described (63; 79; 82; 126; 160; 184; 201; 215; 216). Basal Ca2+ levels were measured in physiologic salt solution (PSS) composed of

the following (in mM): 2 $CaCl_2$, 138 NaCl, 1 $MgCl_2$, 5 KCl, 10 HEPES, 10 glucose; pH 7.4). Voltage-gated calcium channels were activated by depolarization with high (80 mM) K+ solution (2 $CaCl_2$, 63 NaCl, 1 $MgCl_2$, 80 KCl, 10 HEPES, 10 glucose; pH 7.4). Sarcoplasmic reticulum (SR) Ca^{2+} stores were released with 5 mM caffeine in Ca^{2+}-free solution (138 NaCl, 1 $MgCl_2$, 5 KCl, 10 HEPES, 10-5 M K^+-EGTA, 10 glucose; pH 7.4).

Intravenous glucose tolerance testing.

Briefly, swine were pre-acclimated to sling-restraint. Following an overnight fast, swine were restrained in the low stress sling and baseline blood samples and tail-cuff blood pressures were obtained. Next, glucose (1 g/kg body weight) was administered intravenously as a bolus and timed blood samples were collected. Blood glucose was measured immediately (YSI 2300 STAT Plus Glucose analyzer, YSI Life Sciences, Yellow Springs, OH). Plasma insulin assays were performed offsite (Millipore, Inc., St Charles, MO).

Intravascular ultrasound.

After 12 months on diet, following an overnight fast, swine received 2.2 mg/kg xylazine and 5.5 mg/kg telazol, similar to previous reports (69; 82; 126; 139; 165; 184). Swine were intubated and anesthesia was maintained at 2-4% isoflurane in 100% O2 as a carrier gas. A 7 F introducer sheath was inserted into the right femoral artery and heparin (200 U/kg) was administered. A 7 F guiding catheter (Amplatz L, sizes 0.75-2.0; Corndis, Bridgewater, NJ) was advanced to engage either the right or left coronary ostium. A 3.2 F, 40 MHz IVUS catheter (Boston Scientific, Natick, MA) was advanced over a guide wire and positioned in the coronary artery. Automated IVUS pullbacks were performed at 0.5 mm/sec. Angiography was performed throughout the procedure to assist in catheter placement.

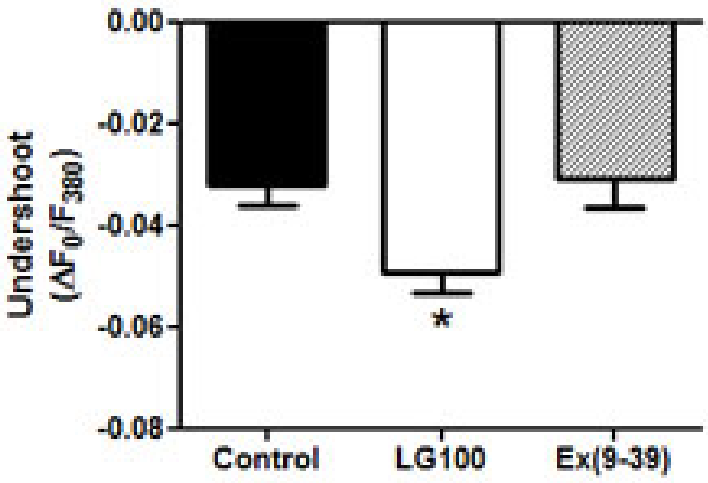

Figure 4.S1: Liraglutide increases SERCA activity in CSM from lean, healthy Ossabaw Swine, and this effect is prevented in the presence of GLP-1 receptor antagonist, Exendin (9-39).

Table 4.S1: Phenotypic Characteristics of Ossabaw Swine Groups.

Parameter	Lean	Placebo			AC3174			Significance, * (p < 0.05)
Week on Treatment		**0**	**12**	**24**	**0**	**12**	**24**	
Body Weight	61 ± 6	75 ± 3	100 ± 2*	116 ± 2*	73 ± 4	87 ± 5	100 ± 6*	Lean < AC3174 < Placebo
Blood Pressure								
Systolic (mmHg)	143 ± 8	149 ± 8	151 ± 4	170 ± 7	132 ± 5	149 ± 6	152 ± 6	None
Diastolic (mmHg)	76 ± 5	79 ± 5	84 ± 3	89 ± 5	74 ± 4	82 ± 5	85 ± 4	None
Mean Arterial Pressure (mmHg)	98 ± 5	102 ± 5	106 ± 2	116 ± 5	93 ± 4	104 ± 5	107 ± 4	None
Carbohydrate Metabolism								
Fasting plasma glucose (mg/dL)	77 ± 5	74 ± 2	78 ± 2	81 ± 2	72 ± 3	73 ± 3	68 ± 2	None
Peak plasma insulin (µU/dL)	88 ± 33	47 ± 17	47 ± 6	67 ± 12	46 ± 10	139 ± 29*	122 ± 25*	Placebo < AC3174
Lipids								
Total cholesterol (mg/dL)	66 ± 10	430 ± 95	420 ± 68	240 ± 20	460 ± 78	369 ± 65	354 ± 61	Lean < Placebo, AC3174
Triglycerides (mg/dL	29 ± 5	67 ± 16	46 ± 6	41 ± 4*	60 ± 6	64 ± 13	74 ± 7*	Lean < Placebo < AC3174
Kidney Function								
BUN (mg/dL)	13 ± 1.0	15 ± 1.4	13 ± 0.9	13 ± 1.2	16 ± 1.2	14 ± 1.4	15 ± 1.2	None
Creatinine (mg/dL)	1.2 ± 0.09	1 ± 0.04	0.9 ± 0.05	1 ± 0.04	1.1 ± 0.09	1 ± 0.07	1 ± 0.04	None
Plasma Proteins								
Total Protein (g/dL)	7.1 ± 0.2	6.2 ± 0.4	6.7 ± 0.2	6.8 ± 0.2	6.4 ± 0.4	6.8 ± 0.7	6.6 ± 0.2	None
Albumin (g/dL)	4 ± 0.2	3.6 ± 0.1	3.6 ± 0.1	3.7 ± 0.2	3.7 ± 0.1	3.9 ± 0.1	3.8 ± 0.1	None
Globulin (g/DL)	3.3 ± 0.2	2.9 ± 0.1	3.1 ± 0.2	3.1 ± 0.1	2.8 ± 0.2	2.9 ± 0.1	2.8 ± 0.1	None
Electrolytes								
Phosphorus (mg/dL)	5.8 ± 0.2	7 ± 0.1*	6.7 ± 0.2	6.2 ± 0.2	6.7 ± 0.2*	6.1 ± 0.2*	6 ± 0.2	Lean < Placebo > AC3174
Calcium (mg/dL)	10.3 ± 0.1	9.7 ± 0.2	9.4 ± 0.2	9.5 ± 0.3	9.7 ± 0.3	9.8 ± 0.3	9.5 ± 0.2	None
Magnesium (mEq/L)	1.6 ± 0.1	1.8 ± 0.1	1.7 ± 0.1	1.6 ± 0.1	1.7 ± 0.1	1.7 ± 0.1	1.6 ± 0.1	None
Sodium (mEq/L)	140 ± 1	140 ± 1	137 ± 2	139 ± 1	141 ± 1	137 ± 2	138 ± 2	None
Potassium (mEq/L)	4.3 ± 0.3	4.2 ± 0.1	4.3 ± 0.1	4 ± 0.1	4.3 ± 0.1	4.2 ± 0.1	3.9 ± 0.1	None
Chloride (mEq/L)	102 ± 1	99 ± 1	97 ± 1	106 ± 8	100 ± 1	97 ± 1	98 ± 1	None
Other								
Creatine Phosphokinase	537 ± 225	422 ± 40	502 ± 56	448 ± 54	364 ± 54	410 ± 72	645 ± 321	None

CHAPTER 5: CONCLUSION

Summary of Findings

The prevalence of metabolic syndrome (MetS) in the United States (US) continues to fuel cardiovascular disease, which takes more lives than any other cause (10; 15-17; 37; 45). In particular, coronary artery disease (CAD) is the underlying cause in 1 out of every 7 deaths in the US (6). Projections to 2030 predict that 40.5% of all US citizens will have some form of cardiovascular disease (38). This rise in cardiovascular disease continues to place an ever-increasing burden on healthcare systems in the US to develop innovative treatment strategies to combat this “silent killer” of Americans.

Coronary smooth muscle (CSM) physiology in the setting of CAD is an important area of current cardiovascular research, and is the focus of this dissertation. In particular, alterations in CSM phenotypes (termed phenotypic modulation) observed during CAD progression have elicited much attention. Recent efforts to organize understanding of developmental, mature, and pathologic CSM phenotypes have been the subject of critical reviews (54; 217; 218). These studies indicate that de-differentiated CSM display enhanced proliferative and secretory capabilities, assisting in formation of a fibrous cap during early CAD pathophysiology. Proliferative CSM may later differentiate into osteogenic CSM, depositing mineral crystals into the atherosclerotic lesion. Ultimately, CSM apoptosis may contribute to plaque rupture and myocardial infarction (219). Fig. 5.1 depicts these phenotypic changes during CAD progression, together with the intracellular Ca^{2+} handling changes described below.

Changes in intracellular Ca^{2+} regulation within CSM have been implicated in CAD pathogenesis, as Ca^{2+} is a ubiquitous second messenger and affects many cellular processes, including CSM contraction, proliferation, and apoptosis. Alterations in Ca^{2+} handling protein function contribute to disrupted cytosolic and compartmental Ca^{2+} concentrations, thus altering normal contractile function, as well as proliferation and

apoptosis pathways. In particular, increased sarcoplasmic reticulum (SR) Ca^{2+} is associated with proliferation in smooth muscle cell lines (66-68) and intact sarco-endoplasmic reticulum Ca^{2+} ATPase (SERCA) function is necessary for CSM proliferation (68). Indeed, SERCA expression and function is increased during early CAD (79; 81; 82; 187). Increased CSM proliferation contributes to CAD progression through assistance with outward remodeling and plaque stabilization in early CAD.

In light of these data, the primary objective of this work was to investigate SERCA function during MetS-induced CAD progression, elucidate a causal role for SERCA upregulation in CSM proliferation, and investigate the effects of secondary SERCA activation with glucagon-like peptide-1 receptor agonists on MetS-induced CAD progression *in vivo*. This was accomplished in three independent studies, outlined in the specific aims below.

Specific Aim 1: Examine the changes in CSM Ca^{2+} regulation during MetS-induced CAD progression. Specifically, examine changes in SR Ca^{2+} handling with increasing CAD severity. In this repeat cross-sectional study, we determined that alterations in CSM Ca^{2+} regulation during CAD progression are transitory and biphasic. During early and clinically insignificant CAD, Ca^{2+} handling by all of the transporters examined was significantly increased. This increased activity by Ca^{2+} transporters occurred concurrently with an observed increase in coronary vasoconstriction. Later in CAD, Ca^{2+} transporter function is dramatically reduced, together with reductions in vasoactivity. Specifically, CSM isolated from plaques of arteries with severe CAD demonstrated a reduced SR Ca^{2+} store, together with reductions in SERCA function, compared both to healthy and mild CAD samples. The reductions in SR Ca^{2+} store and SERCA function were mirrored by reductions in CSM proliferation in arteries with severe CAD, compared to those with mild CAD. These findings support the hypothesis that SERCA function is linked to CSM proliferation, and thereby, plaque formation during CAD progression.

Specific Aim 2: Test the hypothesis that increased SERCA function induces CSM de-differentiation and proliferation in an organ culture model of CAD. The goal of this study was to establish a causal link between upregulation of SERCA function and induction of CSM proliferation in an organ culture model of CAD. Blockade of SERCA with the selective SERCA inhibitor, cyclopiazonic acid (CPA), prevented culture-induced medial thickening. Conversely, stimulation of SERCA with the selective SERCA activator, CDN1163 induced CSM proliferation, as assessed by positive Ki-67 staining. These findings are consistent with the hypothesis that the elevated SERCA function observed in early CAD is a proximal inducer of CSM proliferation.

Specific Aim 3: Investigate the effects of glucagon-like peptide-1 receptor agonists on SERCA stimulation *in vitro* in CSM from lean swine and on CAD and CSM SERCA stimulation in MetS *in vivo*. Here, we examined the effects of GLP-1 receptor agonists both on intracellular Ca^{2+} regulation and on overall CAD progression. We demonstrated that acute treatment of CSM from healthy Ossabaw swine with GLP-1 receptor agonists had a stimulatory effect on SERCA activity. Conversely, acute *in vitro* treatment of CSM from Ossabaw swine with MetS with GLP-1 receptor agonist, or its chronic administration *in vivo* had no effect on SERCA activity. Correspondingly, no alterations in CAD progression were observed with GLP-1 receptor agonist administration. However, we did demonstrate improvement of several metabolic parameters with GLP-1 treatment, including glucose regulation and body weight. These results support the hypothesis that MetS confers cardiovascular resistance to GLP-1 receptor agonists, and suggest that this resistance is mediated, in part, through a lack of SERCA responsiveness to GLP-1 receptor activation.

Future Directions

There is a substantial body of evidence for altered CSM Ca^{2+} regulation in CAD (76-80; 82; 126; 160; 187). In this dissertation I have established a causal link between elevated SERCA function and CSM proliferation. However, a variety of questions remain unanswered regarding additional Ca^{2+} handling anomalies observed in CAD, as well as their effect on further phenotypic modulation during CAD progression.

Intracellular Ca^{2+} handling mechanisms in CSM were discussed in detail in chapter one (Fig. 1.6). Briefly, a number of Ca^{2+} transport proteins are employed to maintain optimal Ca^{2+} concentrations both in the cytosol and in intracellular Ca^{2+} compartments, such as the SR. These include two Ca^{2+} entry channels located on the sarcolemmal membrane: voltage-gated Ca^{2+} channels (VGCC) and transient receptor potential channels (TRP), two sarcolemma-bound extrusion mechanisms: the Na^{+}/Ca^{2+} exchanger (NCX) and the plasma membrane Ca^{2+} ATPase (PMCA), two SR Ca^{2+} release channels: the ryanodine receptor (RyR) and the inositol 1,4,5-trisphosphate receptor (IP_3R), and the sarco-endoplasmic reticulum Ca^{2+} ATPase (SERCA), which is responsible for maintaining optimal SR Ca^{2+} load.

Direct or indirect interaction between Ca^{2+} handling proteins is necessary for maintenance of proper Ca^{2+} concentrations. We have taken advantage of these interactions to study a variety of Ca^{2+} handling events. Indeed, early experiments in our lab and others employed Ca^{2+} influx via VGCCs to load the SR with Ca^{2+} (184; 220-222) and observe subsequent “SR Ca^{2+} unloading” events (63-65; 222-225). A classic example of Ca^{2+} handling protein interaction is that of store-operated Ca^{2+} entry (SOCE), in which depletion of the SR Ca^{2+} store results in a signal to the sarcolemma, triggering Ca^{2+} influx either directly through store-operated Ca^{2+} channels or via reverse-mode NCX activity triggered by Na^{+} influx through TRP channels (126; 226-228). We have previously demonstrated that SOCE is mediated in Ossabaw swine via TRP canonical 1

(TRPC1) (126). Interestingly, an intact SOCE complex is necessary for CSM proliferation (72). I hypothesize that a cycle in which elevated SERCA activity results in SR Ca^{2+} unloading either via IP_3R or RyR-mediated release (229), in turn triggering a compensatory rise in cytosolic Ca^{2+} via SOCE. SERCA function is then further upregulated to sequester additional cytosolic Ca^{2+}, resulting in chronically elevated cytosolic and SR Ca^{2+}, thereby initiating proliferative pathways. Fig. 5.2 illustrates this hypothetical scenario in which both SR Ca^{2+} and cytosolic Ca^{2+} levels are elevated and contribute to CSM proliferation.

CSM dedifferentiation to a proliferative phenotype during CAD is compensatory – in the media, CSM proliferation contributes to outward remodeling of the artery, thus maintaining adequate lumen diameter (43; 230; 231), while in the intima, proliferative CSM serve to stabilize the plaque and protect against plaque rupture (230; 232). Thus, the increased activity of SERCA and other Ca^{2+} transporters in CSM during the early stages of CAD may be protective. Later decreases in the activity of these Ca^{2+} transporters may signal further phenotypic modulation to osteogenic or apoptotic phenotypes, contributing to atherosclerotic plaque destabilization and rupture.

Contributing to plaque destabilization, coronary artery calcification (CAC) involves a shift to an osteogenic phenotype. We recently found that CAC can be detected with positron emission tomography measurement of ^{18}F-sodium fluoride combined with computed tomography in the coronary arteries much earlier than previously reported (233). The amount of early CAC is correlated with early intravascular ultrasound (IVUS) measurements of CAD progression. Early, “spotty” microcalcification is associated with atherosclerotic plaque instability, due to increased incidence of microfractures within the lesion (234-236). Aikawa *et al.* (234) demonstrated that early-stage CAC is spatially associated with inflammation markers, while late-stage calcification does not demonstrate the same association. In an editorial associated with

the Aikawa study (237), Shanahan proposes a model in which early inflammation triggers apoptotic and osteogenic transition of CSM. Later, macrocalcifications engulf inflammatory regions, halting the inflammatory process and resulting in calcified, fibrotic, acellular plaques which are ultimately resistant to rupture. Thus, the early stages of CAC are when atherosclerotic plaques are most susceptible to rupture, and are therefore a crucial area of investigation.

Early studies of CAD identified the presence of extracellular matrix vesicles in calcified arteries using electron microscopy (238; 239). However, until quite recently, it was unknown whether these vesicles were derived from membrane budding or through an exosomal pathway. Recently, however, exosomal pathways were identified in the formation of calcifying extracellular matrix vesicles (56). A recent review by Kapustin and Shanahan (240) summarizes the process of CAC. Under normal physiologic conditions, vesicles produced by CSM contain calcification inhibitors, such as fetuin-A (241), while matrix vesicles released by osteogenic CSM lack these inhibitors (240). The formation of calcifying matrix vesicles is associated with large elevations in cytosolic Ca^{2+} (239). Thus, it is conceivable that alterations in intracellular Ca^{2+} handling mechanisms could contribute to the osteogenic phenotype. In chapter two of this work, we demonstrated that SR Ca^{2+} stores and SERCA activity are reduced in late-stage CAD. Ca^{2+} store depletion due to decreased SERCA activity may contribute to compensatory rises in cytosolic Ca^{2+} through constitutive activation of SOCE mechanisms.

To examine the dual role of SR Ca^{2+} store depletion and activation of SOCE in induction of CAC, future studies will include the culture of arterial rings in media containing elevated phosphate as an initial substrate for calcification. Chronic SR Ca^{2+} store depletion may be attained through continued blockade of SERCA function with cyclopiazonic acid (CPA). TRPC1 expression and SOCE may be assessed in the manner previously described. Calcification may be measured histologically by Von

Kossa staining. Additionally, OsteoSense 680EX may be employed to detect early deposition of hydroxyapatite, as demonstrated by Aikawa *et al.* (234). Chronic depletion of SR Ca^{2+} and the subsequent activation of SOCE is hypothesized to increase deposition of hydroxyapatite. Additionally, knockdown of TRPC1 expression is hypothesized to result in reduced hydroxyapatite deposition. In contrast to the elevations in both SR and cytosolic Ca^{2+} associated with proliferation, the proposed model for calcification describes a depleted SR Ca^{2+} store concurrent with increases in cytosolic Ca^{2+}

Induction of both CSM proliferation and CAC requires elevations in cytosolic Ca^{2+}. In the model described in Fig. 5.2, the elevated SR Ca^{2+} load contributes to increased cytosolic Ca^{2+} through SOCE following SR Ca^{2+} unloading. Concurrently, elevations in SERCA activity may prevent cytosolic Ca^{2+} from attaining the level of "overload" necessary for formation of calcific matrix vesicles and induction of CAC (239; 242; 243). Thus, both increased and decreased SERCA function may contribute to increases in cytosolic Ca^{2+} through SOCE-dependent mechanisms. However, the direction of SERCA regulation (up- vs. down-) may serve as a molecular switch, determining the level of cytosolic Ca^{2+} overload, thereby driving the transition from proliferative to osteogenic CSM.

If reductions in SERCA activity serve as a molecular switch for the proliferative-to-osteogenic transition, then it is necessary to ask what may drive the reduction in SERCA activity. SERCA function is reduced by the enrichment of the SR membrane with cholesterol (244; 245). Under normal, healthy conditions, the SR membrane contains little to no cholesterol (245; 246). However, recent studies suggest that CSM within atherosclerotic lesions may take up cholesterol and become foam cells (43; 247). Indeed, recent lineage tracing studies indicate that proliferative CSM within atherosclerotic lesions transition to macrophage-like cells capable of taking up oxidized

lipoproteins (248-250). Cholesterol uptake by macrophage-like cells results in enrichment of SR membrane with cholesterol, and subsequent inhibition of SERCA (244). Correspondingly, there is ample literature evidence that chronically elevated low-density lipoprotein (LDL) cholesterol increases risk of CAC (251-256). More specifically, apolipoprotein B has been associated with increased CAC (257). Taken together, these data suggest that chronic exposure to elevated LDL results in the uptake of oxidized LDL by CSM, thereby inhibiting SERCA function and inducing calcifying matrix vesicle formation. Future studies should examine CSM SERCA function and incidence of calcification in arterial segments cultured in the presence and absence of oxidized LDL. These studies could provide mechanistic background for interactions between the dyslipidemia associated with MetS, reductions in SERCA function, and induction of CAC. Fig. 5.3 provides an overall working model of the predicted effect of chronically elevated LDL on SERCA function and calcific matrix vesicle formation.

It is also important to note that, concurrently with elevated SERCA and SOCE, VGCC activity is also elevated. While the impetus for increased VGCC activity remains unknown, Berwick *et al*. (76) demonstrated that the elevated VGCC activity contributes to the increased coronary arterial tone observed in early CAD. Additionally, while VGCC activity is elevated in early CAD (187), blockade of VGCCs with diltiazem does not alter CSM proliferation (72). Indeed, VGCC activity is associated with maintenance of a differentiated, contractile phenotype (258), promoting smooth muscle myosin heavy chain expression (179). Thus, increased VGCC activity is unlikely to contribute to the proliferative phenotype modulation, and is likely highly pathogenic, contributing to increased vasoconstriction observed in early CAD. Further studies are necessary to determine whether VGCC activity is localized to microdomains within the sarcolemma, which may contribute to its unique effects during early CAD, when other Ca^{2+} handling proteins are promoting the proliferative phenotype transition. Similar phenomena have

been observed in neurons where N-type and L-type VGCCs are relegated to separate membrane domains, thus participating in “private lines of communication” and serving different roles in neuronal cell signaling (259; 260). Regarding a putative impetus for elevations in VGCC function, Ossabaw swine demonstrate elevated aldosterone secretion with MetS induction (186). Spironolactone, an aldosterone antagonist, inhibits VGCC activity (261). Correspondingly, aldosterone treatment of rat cardiomyocytes with aldosterone resulted in increased Ca^{2+} current which was prevented with spironolactone (262). Thus, increased VGCC activity is likely induced directly by the MetS “milieu” in Ossabaw swine.

Closing Remarks

This dissertation supports an overall working model: During MetS-induced CAD, initial increases in SERCA function drive SOCE-mediated elevations in cytosolic Ca^{2+}, which contributes to CSM proliferation in a compensatory and protective fashion. Long term elevations in LDL cholesterol trigger the uptake of LDL by proliferative CSM residing in the atherosclerotic lesion, resulting in cholesterol enrichment in the SR membrane. Loading of the SR membrane with cholesterol inhibits SERCA function. Reduced SERCA function results in a depleted SR Ca^{2+} store, which drives further SOCE and results in cytosolic Ca^{2+} overload. To compensate for cytosolic Ca^{2+} overload, matrix vesicles are loaded with Ca^{2+} and other calcifying components and released into the extracellular matrix, thus contributing to the induction of CAC.

CSM phenotypic modulation during atherosclerotic CAD progression is complex. Until recently, only two aberrant CSM phenotypes had been identified: proliferative CSM and osteogenic CSM. More recently, however, lineage tracing studies have expanded our understanding of the complexity of CSM modulation within atherosclerotic plaques, adding an additional phenotype – that of macrophage-like CSM which demonstrate impaired cholesterol transport (247), possibly contributing to plaque growth and

progression. As we have here described, a number of CSM Ca^{2+} handling processes are perturbed during CAD progression. We have established increased SERCA function as a causal factor in CSM proliferation. However, the role of reduced SERCA function and well as previously observed alterations in VGCC function, SOCE, and Ca^{2+} extrusion mechanisms in CSM phenotypes has yet to be explored. These alterations in CSM Ca^{2+} may be protective/adaptive or detrimental. Further elucidation of the protective vs. detrimental nature of alterations in CSM Ca^{2+} regulation will enhance our understanding of the specific mechanisms underlying CAD progression, and will allow fine-tuning of patient treatment and care.

Figures

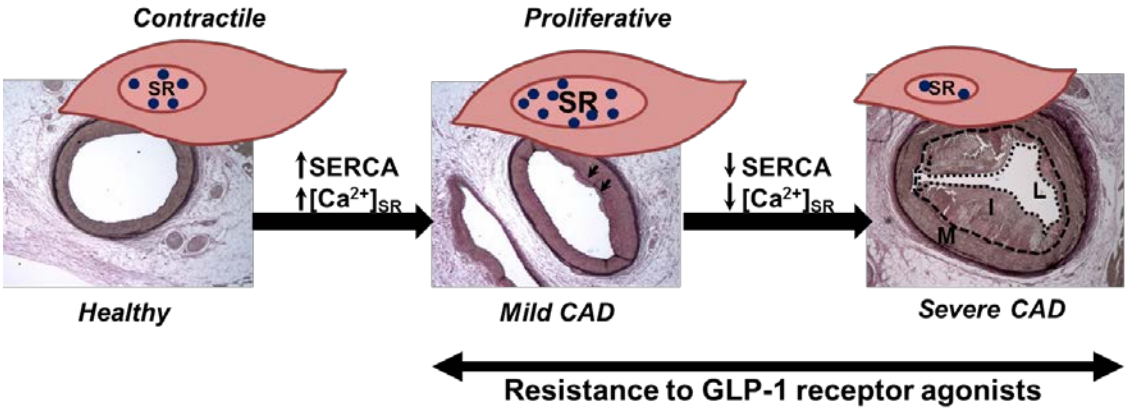

Figure 5.1: CSM phenotypic modulation during CAD progression. Healthy coronary arteries contain primarily contractile CSM. Increases in SERCA function result in elevated SR Ca^{2+} stores, driving the switch to the proliferative CSM phenotype. Later, reductions in SERCA function and SR Ca^{2+} store results in further modulation to additional phenotypes. During CAD progression, CSM fail to respond to GLP-1 receptor-mediated actions on SERCA activity. SR = Sarcoplasmic reticulum. Blue dots = Ca^{2+}.

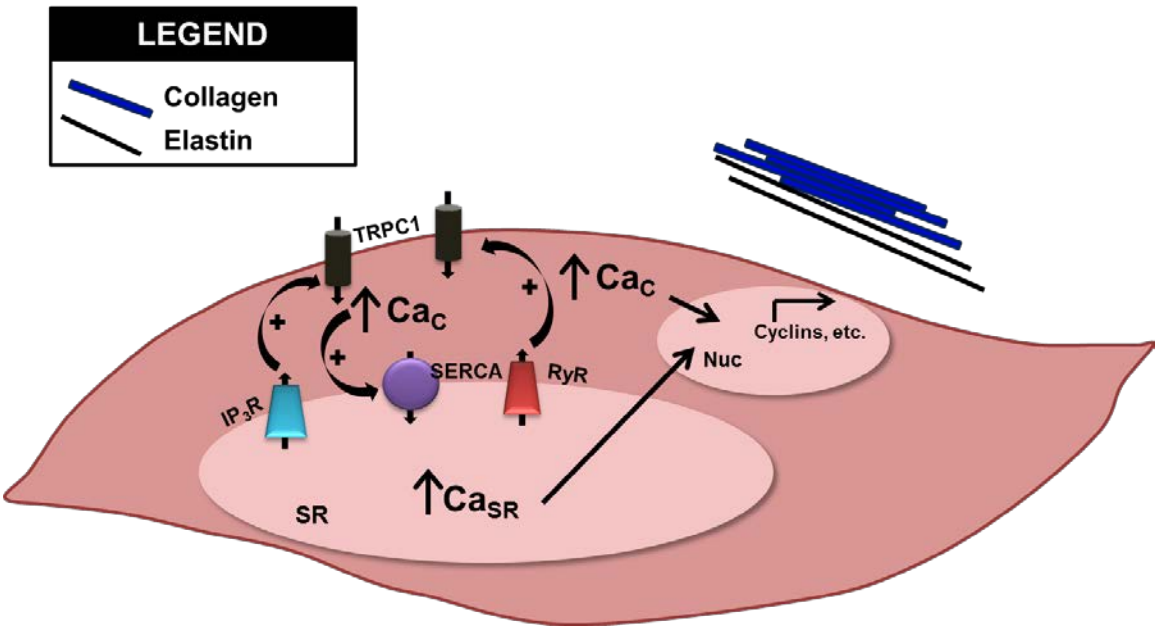

Figure 5.2: Elevated SERCA function drives CSM proliferation. Increased SERCA function in early CAD results in SR Ca^{2+} store overload, triggering SR Ca^{2+} unloading via RyR and/or IP_3R-mediated Ca^{2+} release, thereby activating SOCE through TRPC1. Chronically elevated SR and cytosolic Ca^{2+} contribute to expression of cell cycle proteins and secretion of extracellular matrix proteins, such as collagen and elastin. TRPC1 = Transient receptor potential canonical 6 channel; Ca_C = Cytosolic Ca^{2+}; IP_3R = Inositol 1,4,5-trisphosphate receptor; SERCA = Sarco-endoplasmic reticulum Ca^{2+} ATPase; RyR = Ryanodine receptor; SR = Sarcoplasmic reticulum; Ca_{SR} = SR Ca^{2+}; Nuc = Nucleus.

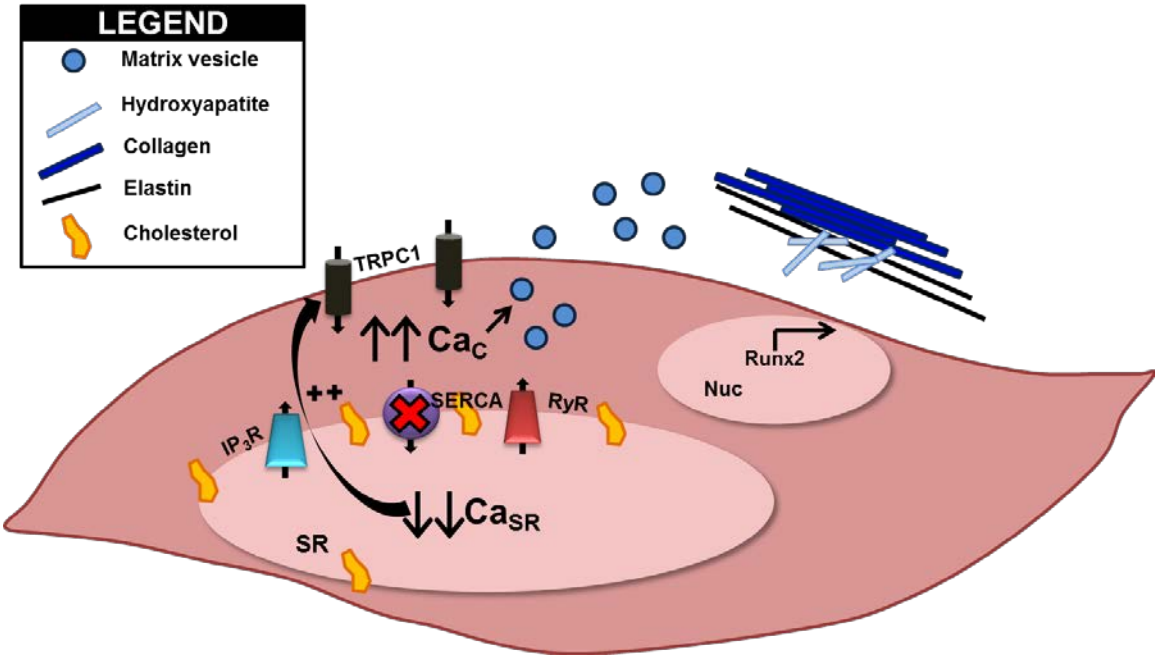

Figure 5.3: Chronic exposure to LDL results in CSM uptake of cholesterol, driving coronary artery calcification. Uptake of cholesterol by CSM results in enrichment of the SR membrane with cholesterol, functionally inhibiting SERCA activity. Drastic depletion of the SR Ca^{2+} store results in constitutive activation of SOCE mechanisms, resulting in cytosolic Ca^{2+} overload and loading of matrix vesicles. Secretion of matrix vesicles results in deposition of hydroxyapatite crystals in the extracellular matrix. TRPC1 = Transient receptor potential canonical 1 channel; Ca_C = Cytosolic Ca^{2+}; IP_3R = Inositol 1,4,5-trisphosphate receptor; SERCA = Sarco-endoplasmic reticulum Ca^{2+} ATPase; RyR = Ryanodine receptor; SR = Sarcoplasmic reticulum; Ca_{SR} = SR Ca^{2+}; Nuc = nucleus.

LIST OF APPENDICES

APPENDIX A

PROTOCOL FOR DISPERSION OF VASCULAR SMOOTH MUSCLE CELLS (VSM)

Michael Sturek Ph.D, MLM, 8/19/13, MLM SLD, 07/25/14

Current Date ___-___-___ Initials_____

1. Conduit coronary arteries of swine are typically used. The artery is classified as proximal, middle, and distal thirds. At euthanasia/tissue collection, grossly dissect vessels by first locating vessel and then making a transverse cut through myocardium near ostium. Remove entire length of conduit artery with minimal adjacent cardiac muscle, fat, etc. attached. Place the tissue into wide-mouth bottle containing ~50-75 ml ice-cold 2CaNa. Place immediately into cooler filled with ice. (NOTE: in the case of overnight transport, store tissue in EH storage media on ice).

[Animal: Pig# _____, Age _____, Time dead _____, Misc. _____]

[**Portion of artery**: Proximal ___, Middle ___, Distal

Artery: LAD___ RCA ___ CFX ___ Other?_____]

[**Date** ____-____-____, Time of storage _____]

2. Clean artery of adherent connective tissue, fat, cardiac muscle, etc. in cell culture hood in 100 x 20 mm culture dish in ~30 ml Low Ca. Treat artery gently (do not stretch excessively, if possible).

****At this point, the artery can be stored in the refrigerator in storage media for 2-5 days, if necessary.**

[Storage media = EH + PS]

[In refrigerator: Date ____-____-____ Time _____]

3. Cut open artery longitudinally to reveal lumen. Pin down the artery with the lumen facing up in a 30 ml Sylgard jar with 2 mL Collagenase solution. (Approximately a 1 cm^2 area of vessel is enough to yield several million SMC.) Pin the artery segment on all corners and at the middle to increase surface area.

4. Place jar in 37° C shaking water bath (100 strokes/min; 5.5 on dial) for 60 min. The jar should be placed so that the long axis of the vessel segment is parallel with the direction of the shaking.

[Collagenase batch: Date made: ____-____-____, Made by: _____]

[**Dispersion 1**: Date ____-____-____,

Time started _____, Time ended _____]

5. Aspirate supernatant and pipette over artery several times to loosen isolated CSM. Place drop of supernatant in 35 mm petri dish on microscope and observe. (At this point expect mostly connective tissue, endothelial cells (EC), etc., but few CSM. EC are round and clump together in bunches). Note appropriately and either: 1) discard_____, 2) save in 15 ml tube for immediate fura-2 or patch-clamp studies_____. If #2, transfer supernatant to 15 mL conical tube and clearly label with pig number and cell fraction. Centrifuge at 900 rpm (**Not RCF**) for 4 min, remove supernatant (**Be careful not to aspirate the pellet!),** then re-suspend pellet in 1 mL of freshly prepared 0.02%BSA in 2CaNa (20 mg BSA/10 mL 2CaNa). Add 2.5µL fura-2 AM and triturate several times. Place in 37° C water bath for ~30-45 mins.

Cell fraction: _____ (Ignore this section if discarded)

[Dye: Fura-2____, Other_____ Dye concentration _____]

[Loading: Date ____-____-____,

Time started _____, Time ended _____]

6. Add another 2 mL Collagenase solution to Sylgard jar and repeat steps 4 and 5 until isolation is complete.

Step 4:

[**Dispersion 2**: Time started _____, Time ended _____]

Step 5:

Cell fraction: _____

[Dye: Fura-2____, Other_____ Dye concentration _____]

[Loading: Date ____-____-____,

Time started _____, Time ended _____]

Step 4:

[**Dispersion 3**: Time started _____, Time ended _____]

Step 5:

Cell fraction: _____

[Dye: Fura-2____, Other_____ Dye concentration _____]

[Loading: Date ____-____-____,

Time started _____, Time ended _____]

7. Centrifuge cells at 900 rpm for 4 min, re-suspend in EH solution and put in 37° C water bath for ~20 min.

   [Time started _____, Time ended _____]

8. Centrifuge cells at 900 rpm for 4 min, re-suspend in 0.02%BSA in 2CaNa and chill on ice. Wrap tubes in foil to protect from light exposure.

NOTES:

1. All steps following fura-2 loading, CSM are light-sensitive. When possible, minimize exposure to light.
2. "Overnight dispersion" - It is also possible to disperse by exposing cells to 2 mL collagenase in bottle at room temp. for »8-10 hours.

APPENDIX B

EXPERIMENTAL SOLUTIONS

8-20-13 ***Collagenase (in Low Ca)***

Component	Concentration	20 ml tot.	10 ml tot.	Stock
Collagenase, CLS II	300 U/mL	20 mg	10 mg	300 U/mg (04-12-12, Worthington)
BSA (Fraction V)	0.2% (wt/vol)	40 mg	20 mg	(09-94, Sigma-Aldrich)
Soybean Trypsin Inhibitor Type SI	0.1%	20 mg	10 mg	2.17 mg trypsin/mg (03-04-14, Worthington)
DNase I, Type IV	459 KUnitz/mL	4 mg	2 mg	2297 KUnitz/mg (06-04-14, Sigma-Aldrich)

[Batch: Date made: ____-____-____, Made by: _____]

1. Adjust pH of Low Ca to 7.55, then add collagenase and pH will be exactly 7.40 filter.

2. Make in 10-20 ml quantities. Each isolation requires at least 4-6 ml collagenase. Remaining collagenase solution may be frozen at -20˚ C for up to 10 days.

8-3-14 ***2 CaNa***

Components	Conc. (mM)	1000 ml total
$CaCl_2$	2	20 ml of 0.1 M
NaCl	138	138 ml of 1.0 M
$MgCl_2$	1	10 ml of 0.1 M
KCl	5	5 ml of 1.0 M
HEPES	10	10 ml of 1.0 M
Glucose	10	1.8 g
pH (with NaOH)	7.4	3-4 ml of 1.0 M

NOTES:

1. Sterile solutions all contain PS and are sterilized by filtration through Millex-GS 0.2 µm filter or Millipore Stericup apparatus.
2. Penicillin Streptomycin (PS) 100 mg/ml (100 U/ml) is added in a 1:100 (vol:vol) ratio to yield a 1% PS solution.

7-9-87 ***Low Ca***

Components	Concentration (mM)	1000 ml total
$CaCl_2$	0.5	5.0 ml of 0.1 M
NaCl	135	135 ml of 1.0 M
$MgCl_2$	1	10 ml of 0.1 M
KCl	5	50 ml of 0.1 M
KH_2PO_4	0.44	4.4 ml of 0.1 M
Na_2HPO_4	0.34	3.4 ml of 0.1 M
$NaHCO_3$	2.6	26 ml of 0.1 M
Amino Acids	1X	20 ml of 50X
Vitamins	1X	10 ml of 100X
Phenol Red	0.001%	2 ml of 0.5%
HEPES	20	20 ml of 1.0 M
Glucose	10	1.8 g
pH	7.4	with NaOH
PS	1%	10 ml

NOTES:

1. Low Ca is exactly like EH, except that the Ca concentration is only 0.5 mM, and no horse serum is used.

2. Low Ca with horse serum may be used to facilitate acquisition of a seal when doing patch-clamp studies.

7-9-87 ***EH (aka Storage media)***

Components	Concentration (mM)	1000 ml total
$CaCl_2$	2.0	20 ml of 0.1 M
NaCl	135	135 ml of 1.0 M
$MgCl_2$	1	10 ml of 0.1 M
KCl	5	50 ml of 0.1 M
KH_2PO_4	0.44	4.4 ml of 0.1 M
Na_2HPO_4	0.34	3.4 ml of 0.1 M
$NaHCO_3$	2.6	26 ml of 0.1 M
Amino Acids	1X	20 ml of 50X
Vitamins	1X	10 ml of 100X
Phenol Red	0.001%	2 ml of 0.5%
HEPES	20	20 ml of 1.0 M
Glucose	10	1.8 g
pH	7.4	with NaOH
PS	1%	10 ml
Horse Serum	2%	20 ml

NOTES:

1. EH media is a type of Eagle's Minimal Essential Medium (EMEM), but also has HEPES as a pH buffer, so that bubbling the solution with O_2 is not necessary for maintenance of pH.

2. Sterile-filter under laminar flow hood with Millipore Stericup system.

8-4-14 ***2Ca80K***

Components	Conc. (mM)	1000 ml total
$CaCl_2$	2	20 ml of 0.1 M
NaCl	63	63 ml of 1.0 M
$MgCl_2$	1	10 ml of 0.1 M
KCl	80	80 ml of 1.0 M
HEPES	10	10 ml of 1.0 M
Glucose	10	1.8 g
pH (with NaOH)	7.4	3-4 ml of 1.0 M

2-29-16 ***0CaNa***

Components	Conc. (mM)	1000 ml total
$CaCl_2$	----	----
NaCl	138	138 ml of 1.0 M
$MgCl_2$	1	10 ml of 0.1 M
KCl	5	5 ml of 1.0 M
HEPES	10	10 ml of 1.0 M
KEGTA	10^{-5} M	1 ml of 0.01 M
Glucose	10	1.8 g
pH (with NaOH)	7.4	5-7 ml of 1.0 M

NOTES:

1. Rationale for low [Ca^{2+}] – Determination of the importance of extracellular Ca^{2+} (presumably Ca^{2+} influx) for a measured increase in intracellular Ca^{2+}.
2. $CaCl_2$ removal does not include equimolar addition of $MgCl_2$ or other ions. We have only used 1 and 5 mM EGTA on cells when achieving a fura-2 RATIO minimum. The cells probably become very leaky to Na^+ and other ions, thus addition of Mg^{2+} would “stabilize” the membrane.
3. Total ml of NaOH added gives number of mM extra Na added; e.g. total [Na^+] for 0CaNa is ~ 143 mM. Note that NaCl increases to 127 mM with –CaNa, 5 EGTA solution to keep [Na^+; at 143 mM as ~16 mM Na^+ used for pH.

8-4-14 ***2Ba80K5Na***

Components	Conc. (mM)	1000 ml total
$BaCl_2$	2	20 ml of 0.1 M
LiCl	63	63 ml of 1.0 M
$MgCl_2$	1	10 ml of 0.1 M
KCl	80	80 ml of 1.0 M
HEPES	10	10 ml of 1.0 M
Glucose	10	1.8 g
pH (with NaOH)	7.4	3-4 ml of 1.0 M

APPENDIX C

PROTOCOL FOR ORGAN CULTURE OF SWINE CORONARY ARTERY RINGS TO INDUCE MEDIAL THICKENING

Mikaela McKenney, Umut Ulge, 07/23/14. Modified, Stacey D. Rodenbeck, 03/22/16

1. Euthanasia per standard protocol. With sterile gloves and tools, remove heart with pericardial sac intact.
2. Lay heart on inside of paper from sterile glove pack and remove pericardial sac with sterile tools.
3. Thoroughly rinse the heart with ice cold sterile-filtered 2CaNa + 2% penicillin/streptomycin (P/S).
4. Grossly dissect the coronary arteries and place in individual appropriately pre-labeled tubes of 2CaNa + 2% P/S. Keep tubes on ice.
5. Transfer collected specimens to lab on ice for dissection under the sterile laminar flow hood.
6. Open the flow hood and turn off U.V. light. Clean surface with 70% ethanol.
7. Thaw a frozen aliquot of 50 mL sterile-filtered Low Ca solution for fine dissection.
8. In flow hood, remove grossly dissected artery and place in Low Ca solution in a sterile culture dish on ice. Finely dissect coronary artery from myocardium and adventitia carefully and gently.
9. Allow clean artery to rest in ice cold Low Ca solution while preparing a 6-well plate with 4-5 mL of sterile phosphate-buffered saline (PBS) in each well.
10. Section cleaned artery into rings of 2-4 mm in length, and place in top left well of prepared 6-well plate.
11. Allow rings to sit in PBS for ~30 seconds, and then transfer clockwise to the next well. Transfer each ring separately and allow excess solution to drip off of the ring into the previous well before transfer. Continue to transfer rings in a

clockwise fashion until all rings have undergone complete 6-well serial "sterilization."

12. Prepare a 12-well plate for culture by filling each well with 2 mL of culture media (Dulbecco's Modified Eagle's Medium (DMEM) + 180 mg/dL glucose + 1% P/S + 20% fetal bovine serum).
13. Set aside arterial segments for cold stored controls.
14. Transfer a single coronary segment into a single well of the prepared 12-well plate.
15. Cover each plate and label appropriately with pig number, date, and culture conditions.
16. Transfer plates to the 37°C incubator. Check that the CO_2 is set to 4.6% and that the tray at the bottom of the incubator is full of distilled water.
17. Change culture media every two days.
18. Culture rings for 7 days to achieve optimal medial thickening.

APPENDIX D

QUANTIFICATION OF MEDIAL AREA IN VERHOEFF VAN-GIESON STAINED CORONARY ARTERIES IN ADOBE PHOTOSHOP CS6

Stacey D. Rodenbeck, 03/22/16

1. Open image of Verhoeff Van-Gieson stained artery (taken with 10X microscope objective) in Adobe Photoshop CS6.
2. Ensure that the measurement log is open: Window > Measurement Log.
3. To set scale: Image > Analysis > Set Measurement Scale > Custom
    a. The ruler tool is automatically selected for this activity. To set pixel length, trace the length of the scale bar.
    b. Type in scale bar length in micrometers (ie: 500) for logical length.
    c. Click OK.
4. Select magnetic lasso tool. Click once at any point along external elastic lamina (EEL) to begin tracing. Release, and drag around the external elastic laminar border. Click to close circle.
5. Click “Record Measurements” in measurement log.
6. Record “Area” value in Excel Spreadsheet as EEL Area.
7. Repeat steps 4-6, tracing along the internal elastic lamina (IEL).
8. Medial area = EEL Area – IEL Area
9. To normalize medial area to artery size, calculate % Medial Area = (Medial Area/EEL Area)*100.

APPENDIX E

QUANTIFICATION OF MEDIAL COLLAGEN IN MASSON'S TRICHROME STAINED CORONARY ARTERY SEGMENTS

Stacey D. Rodenbeck, 03/22/16

1. Open image of Masson's Trichrome stained artery (taken with 10X microscope objective) in Adobe Photoshop CS6.
2. Ensure that the measurement log is open: Window > Measurement Log.
3. To set scale: Image > Analysis > Set Measurement Scale > Custom
    a. The ruler tool is automatically selected for this activity. To set pixel length, trace the length of the scale bar.
    b. Type in scale bar length in micrometers (ie: 500) for logical length.
    c. Click OK.
4. Make a "Background copy" as a new layer by right-clicking on "Background" and selecting "Duplicate Layer." Name this layer "Adventitia".
5. Working from the "Adventitia" layer, select the magnetic lasso tool, and trace along inner border of the blue adventitia, then Ctrl-X (cut) and Ctrl-V (paste) to create a new layer containing the medial layer.
6. Change name of new layer to "Media."
7. In the "Media" Layer, use the magnetic lasso to trace the inner border of the media, and click "Delete," leaving only the media in view.
8. Select both "Adventitia" and "Media" layers concurrently. Using the Magic wand tool, set "tolerance" to 20, and select "Sample All Layers." Click in Adventitia to select blue in both layers. You may add to the selected area by holding down "Shift" as you click.

9. Once you are satisfied that you've selected all of the collagen in both layers, click "Record Measurements" in the measurement log. Record the area measure under "Total Collagen Area" in an Excel file.
10. Deselect the "Media" layer.
11. Working with the "Adventitia" layer only, use the Magic Wand tool to select the adventitial collagen again. Be especially careful to ensure that you select the same amount of the adventitia as you did in step 9.
12. Click "Record Measurements."
13. Record area measure under "Adventitial Collagen Area" in Excel File.
14. Medial Collagen Area = Total Collagen Area – Adventitial Collagen Area.
15. Deselect "Adventitia" layer.
16. Select "Media" layer.
17. Determine medial area by using magic wand tool to click outside of the media. Everything that is not media will be selected. Type Ctrl-shift-I to select the inverse.
18. Click "Record Measurement."
19. Record Area measure as "Medial Area" in Excel file.
20. To express collagen content as a percentage of medial area, % Medial Collagen = (Medial Collagen Area/Medial Area)*100.

APPENDIX F

QUANTIFICATION OF POSITIVE KI-67 STAINED CELLS IN ADOBE PHOTOSHOP CS6

Stacey D. Rodenbeck, 03/22/16.

1. Open image of Ki-67 stained artery segment (taken with 40X microscope objective) in Adobe Photoshop CS6.
2. Ensure that the measurement log is open: Window > Measurement Log.
3. To set scale: Image > Analysis > Set Measurement Scale > Custom
    a. The ruler tool is automatically selected for this activity. To set pixel length, trace the length of the scale bar.
    b. Type in scale bar length in micrometers (ie: 25) for logical length.
    c. Click OK.
4. Cell nuclei positively stained with Ki-67 will be brown. Manually count these, and record the count in an Excel spreadsheet as “Ki-67 Nuclei”
5. Select “Channels” in the right tool bar.
6. Click through the Red, Green, and Blue channels to determine which two channels show the most contrast between them (usually red and blue).
7. Image > Calculations
    a. There will be two sources. Set the channel 1 to “Red” and channel 2 to “blue.
    b. Under “blending” select “subtract.”
    c. Adjust the “offset” so that all cell nuclei are white (usually -110).
    d. Click OK.
8. A new channel will have been created. Label this channel “Nuclei.”
9. With the Nuclei channel selected, Image > Adjustments > Threshold.
    a. Set threshold such that all nuclei are white and background is black.

10. To minimize noise from small particles, Filter > Noise > Median
    a. Adjust “radius” to eliminate smaller particles (usually 5-10).
11. Using the magic wand tool, select white nuclei.
12. Click “Record Measurements”
13. Record “Count” in Excel spreadsheet as “Total Nuclei.”
14. % Positive Nuclei = (Ki-67 Nuclei/Total Nuclei)*100.

LIST OF REFERENCES

1. Ogden CL, Carroll MD, Kit BK, Flegal KM: Prevalence of childhood and adult obesity in the United States, 2011-2012. JAMA 2014;311:806-814

2. Mendis S, Armstrong T, Bettcher D, Branca F, Lauer J, Mace C, Poznyak V, Riley L, Da Costa E Silva V, Stevens G: *Global Status Report on Noncommunicable Diseases 2014*. Geneva, Switzerland, WHO Press, 2014

3. Popkin BM: The world is fat. Sci Am 2007;297:88-95

4. Landgraf K, Rockstroh D, Wagner IV, Weise S, Tauscher R, Schwartze JT, Loffler D, Buhligen U, Wojan M, Till H, Kratzsch J, Kiess W, Bluher M, Korner A: Evidence of early alterations in adipose tissue biology and function and its association with obesity-related inflammation and insulin resistance in children. Diabetes 2015;64:1249-1261

5. Spalding KL, Arner E, Westermark PO, Bernard S, Buchholz BA, Bergmann O, Blomqvist L, Hoffstedt J, Naslund E, Britton T, Concha H, Hassan M, Ryden M, Frisen J, Arner P: Dynamics of fat cell turnover in humans. Nature 2008;453:783-787

6. Mozaffarian D, Benjamin EJ, Go AS, Arnett DK, Blaha MJ, Cushman M, Das SR, de Ferranti S, Despres JP, Fullerton HJ, Howard VJ, Huffman MD, Isasi CR, Jimenez MC, Judd SE, Kissela BM, Lichtman JH, Lisabeth LD, Liu S, Mackey RH, Magid DJ, McGuire DK, Mohler ER, 3rd, Moy CS, Muntner P, Mussolino ME, Nasir K, Neumar RW, Nichol G, Palaniappan L, Pandey DK, Reeves MJ, Rodriguez CJ, Rosamond W, Sorlie PD, Stein J, Towfighi A, Turan TN, Virani SS, Woo D, Yeh RW, Turner MB: Heart Disease and Stroke Statistics-2016 Update: A Report From the American Heart Association. Circulation 2015;133:e38-e360

7. Neel JV: Diabetes mellitus: a "thrifty" genotype rendered detrimental by "progress"? Am J Hum Genet 1962;14:353-362

8. Levine JA: Lethal sitting: homo sedentarius seeks answers. Physiology (Bethesda) 2014;29:300-301

9. O'Rourke R W: Metabolic thrift and the genetic basis of human obesity. Ann Surg 2014;259:642-648

10. Alberti KG, Eckel RH, Grundy SM, Zimmet PZ, Cleeman JI, Donato KA, Fruchart JC, James WP, Loria CM, Smith SC, Jr.: Harmonizing the metabolic syndrome: a joint interim statement of the International Diabetes Federation Task Force on Epidemiology and Prevention; National Heart, Lung, and Blood Institute; American Heart Association; World Heart Federation; International Atherosclerosis Society; and international association for the Study of Obesity. Circulation 2009;120:1640-1645

11. Alberti KG, Zimmet PZ: Definition, diagnosis and classification of diabetes mellitus and its complications. Part 1: diagnosis and classification of diabetes mellitus provisional report of a WHO consultation. Diabet Med 1998;15:539-553

12. Beltran-Sanchez H, Harhay MO, Harhay MM, McElligott S: Prevalence and trends of metabolic syndrome in the adult U.S. population, 1999-2010. J Am Coll Cardiol 2013;62:697-703

13. Hales CN, Barker DJ: Type 2 (non-insulin-dependent) diabetes mellitus: the thrifty phenotype hypothesis. Diabetologia 1992;35:595-601

14. Rinaudo P, Wang E: Fetal programming and metabolic syndrome. Annu Rev Physiol 2012;74:107-130

15. Gami AS, Witt BJ, Howard DE, Erwin PJ, Gami LA, Somers VK, Montori VM: Metabolic syndrome and risk of incident cardiovascular events and death: a systematic review and meta-analysis of longitudinal studies. J Am Coll Cardiol 2007;49:403-414

16. Grundy SM: Pre-diabetes, metabolic syndrome, and cardiovascular risk. J Am Coll Cardiol 2012;59:635-643

17. Mottillo S, Filion KB, Genest J, Joseph L, Pilote L, Poirier P, Rinfret S, Schiffrin EL, Eisenberg MJ: The metabolic syndrome and cardiovascular risk a systematic review and meta-analysis. J Am Coll Cardiol 2010;56:1113-1132

18. Hutcheson R, Rocic P: The metabolic syndrome, oxidative stress, environment, and cardiovascular disease: the great exploration. Exp Diabetes Res 2012;2012:271028

19. Sturek M, Tune JD, Alloosh M: Ossabaw Island miniature swine: metabolic syndrome and cardiovascular assessment. In *Swine in the Laboratory: Surgery, Anesthesia, Imaging, and Experimental Techniques,* 3rd Edition ed. Swindle MM, Ed. Boca Raton, CRC Press, 2015, p. 451-465

20. Lam DW, LeRoith D: The worldwide diabetes epidemic. Curr Opin Endocrinol Diabetes Obes 2012;19:93-96

21. American Diabetes Association: Diagnosis and classification of diabetes mellitus. Diabetes Care 2014;37 Suppl 1:S81-90

22. Lin Y, Sun Z: Current views on type 2 diabetes. J Endocrinol 2010;204:1-11

23. American Diabetes Association: Economic costs of diabetes in the U.S. in 2012. Diabetes Care 2013;36:1033-1046

24. Menke A, Casagrande S, Geiss L, Cowie CC: Prevalence of and Trends in Diabetes Among Adults in the United States, 1988-2012. JAMA 2015;314:1021-1029

25. LeRoith D: Beta-cell dysfunction and insulin resistance in type 2 diabetes: role of metabolic and genetic abnormalities. Am J Med 2002;113 Suppl 6A:3S-11S

26. Riddle MC: Tactics for type II diabetes. Endocrinol Metab Clin North Am 1997;26:659-677

27. Inzucchi SE, Bergenstal RM, Buse JB, Diamant M, Ferrannini E, Nauck M, Peters AL, Tsapas A, Wender R, Matthews DR: Management of hyperglycemia in type 2 diabetes, 2015: a patient-centered approach: update to a position statement of the American Diabetes Association and the European Association for the Study of Diabetes. Diabetes Care 2015;38:140-149

28. Gin H, Messerchmitt C, Brottier E, Aubertin J: Metformin improved insulin resistance in type I, insulin-dependent, diabetic patients. Metabolism 1985;34:923-925

29. Butterfield WJ: The effects of phenformin on peripheral glucose utilization and insulin action in obesity and diabetes mellitus. Ann N Y Acad Sci 1968;148:724-733

30. Mehnert H: Metformin, the rebirth of a biguanide: mechanism of action and place in the prevention and treatment of insulin resistance. Exp Clin Endocrinol Diabetes 2001;109 Suppl 2:S259-264

31. Madison LL, Combes B, Unger RH, Kaplan N: The relationship between the mechanism of action of the sulfonylureas and the secretion of insulin into the portal circulation. Ann N Y Acad Sci 1959;74:548-556

32. Proks P, Reimann F, Green N, Gribble F, Ashcroft F: Sulfonylurea stimulation of insulin secretion. Diabetes 2002;51 Suppl 3:S368-376

33. Drucker DJ: The biology of incretin hormones. Cell Metabolism 2006;3:153-165

34. Hargrove DM, Kendall ES, Reynolds JM, Lwin AN, Herich JP, Smith PA, Gedulin BR, Flanagan SD, Jodka CM, Hoyt JA, McCowen KM, Parkes DG, Anderson CM: Biological activity of AC3174, a peptide analog of exendin-4. Regul Pept 2007;141:113-119

35. Tune JD: *Coronary Circulation*. Morgan & Claypool, 2014

36. Sturek M, Mokelke EA, Sindermann JR, Adam LP, March KL: Molecular and cellular physiology of differentiated vascular smooth muscle. In *Cardiovascular Medicine,* Third Edition ed. Willerson JT, Cohn JN, Wellens HJJ, Holmes DR, Eds. London, Springer-Verlag, 2006, p. 1511-1523

37. Murphy SL, Kochanek KD, Xu J, Heron M: Deaths: Final Data for 2012. Natl Vital Stat Rep 2015;63:1-117

38. Heidenreich PA, Trogdon JG, Khavjou OA, Butler J, Dracup K, Ezekowitz MD, Finkelstein EA, Hong Y, Johnston SC, Khera A, Lloyd-Jones DM, Nelson SA, Nichol G, Orenstein D, Wilson PW, Woo YJ: Forecasting the future of cardiovascular disease in the United States: a policy statement from the American Heart Association. Circulation 2011;123:933-944

39. Trogdon JG, Finkelstein EA, Nwaise IA, Tangka FK, Orenstein D: The economic burden of chronic cardiovascular disease for major insurers. Health promotion practice 2007;8:234-242

40. Stary HC, Chandler AB, Dinsmore RE, Fuster V, Glagov S, Insull W, Jr., Rosenfeld ME, Schwartz CJ, Wagner WD, Wissler RW: A definition of advanced types of atherosclerotic lesions and a histological classification of atherosclerosis. A report from the Committee on Vascular Lesions of the Council on Arteriosclerosis, American Heart Association. Circulation 1995;92:1355-1374

41. Cocker MS, Mc Ardle B, Spence JD, Lum C, Hammond RR, Ongaro DC, McDonald MA, Dekemp RA, Tardif JC, Beanlands RS: Imaging atherosclerosis with hybrid [18F]fluorodeoxyglucose positron emission tomography/computed tomography imaging: what Leonardo da Vinci could not see. J Nucl Cardiol 2012;19:1211-1225

42. McEvoy JW, Blaha MJ, Defilippis AP, Budoff MJ, Nasir K, Blumenthal RS, Jones SR: Coronary artery calcium progression: an important clinical measurement? A review of published reports. J Am Coll Cardiol 2010;56:1613-1622

43. Tabas I, Garcia-Cardena G, Owens GK: Recent insights into the cellular biology of atherosclerosis. J Cell Biol 2015;209:13-22

44. Lakka HM, Laaksonen DE, Lakka TA, Niskanen LK, Kumpusalo E, Tuomilehto J, Salonen JT: The metabolic syndrome and total and cardiovascular disease mortality in middle-aged men. JAMA 2002;288:2709-2716

45. Kim JY, Mun HS, Lee BK, Yoon SB, Choi EY, Min PK, Yoon YW, Hong BK, Rim SJ, Kwon HM: Impact of metabolic syndrome and its individual components on the presence and severity of angiographic coronary artery disease. Yonsei Med J 2010;51:676-682

46. Creed KE: Functional diversity of smooth muscle. Br Med Bull 1979;35:243-247

47. Smith GL, Austin C, Crichton C, Wray S: A review of the actions and control of intracellular pH in vascular smooth muscle. Cardiovasc Res 1998;38:316-331

48. Somlyo AP, Somlyo AV, Kitazawa T, Bond M, Shuman H, Kowarski D: Ultrastructure, function and composition of smooth muscle. Ann Biomed Eng 1983;11:579-588

49. Somlyo AP, Somlyo AV: Smooth muscle structure and function. In *The Heart and Cardiovascular System* Fozzard HA, al. e, Eds. New York, Raven Press, Ltd., 1992, p. 1295-1324

50. Smolensky AV, Ford LE: Filament lattice changes in smooth muscle assessed using birefringence. Can J Physiol Pharmacol 2005;83:933-940

51. Seow CY: Myosin filament assembly in an ever-changing myofilament lattice of smooth muscle. Am J Physiol Cell Physiol 2005;289:C1363-1368

52. Somlyo AV, Somlyo AP: Electromechanical and pharmacomechanical coupling in vascular smooth muscle. J Pharmacol Exp Ther 1968;159:129-145

53. Farley JM, Miles PR: Role of depolarization in acetylcholine-induced contractions of dog trachealis muscle. J Pharmacol Exp Ther 1977;201:199-205

54. Owens GK, Kumar MS, Wamhoff BR: Molecular regulation of vascular smooth muscle cell differentiation in development and disease. Physiol Rev 2004;84:767-801

55. Chamley-Campbell J, Campbell GR, Ross R: The smooth muscle cell in culture. Physiol Rev 1979;59:1-61

56. Kapustin AN, Chatrou ML, Drozdov I, Zheng Y, Davidson SM, Soong D, Furmanik M, Sanchis P, De Rosales RT, Alvarez-Hernandez D, Shroff R, Yin X, Muller K, Skepper JN, Mayr M, Reutelingsperger CP, Chester A, Bertazzo S, Schurgers LJ, Shanahan CM: Vascular smooth muscle cell calcification is mediated by regulated exosome secretion. Circ Res 2015;116:1312-1323

57. Speer MY, Yang HY, Brabb T, Leaf E, Look A, Lin WL, Frutkin A, Dichek D, Giachelli CM: Smooth muscle cells give rise to osteochondrogenic precursors and chondrocytes in calcifying arteries. Circ Res 2009;104:733-741

58. Dineen SL, Neeb ZP, Obukhov AG, Sturek M: Transient receptor potential channels in metabolic syndrome-induced coronary artery disease. In *Vascular Ion Channels in Physiology and Disease* Levitan I, Dopico AM, Eds. New York, NY, Springer 2016

59. Poburko D, Liao CH, van Breemen C, Demaurex N: Mitochondrial regulation of sarcoplasmic reticulum Ca2+ content in vascular smooth muscle cells. Circ Res 2009;104:104-112

60. Wray S, Burdyga T: Sarcoplasmic reticulum function in smooth muscle. Physiol Rev 2010;90:113-178

61. Michalak M, Robert Parker JM, Opas M: Ca2+ signaling and calcium binding chaperones of the endoplasmic reticulum. Cell Calcium 2002;32:269-278

62. Smith CD, Wang A, Vembaiyan K, Zhang J, Xie C, Zhou Q, Wu G, Chen SR, Back TG: Novel carvedilol analogues that suppress store-overload-induced Ca2+ release. J Med Chem 2013;56:8626-8655

63. Witczak CA, Sturek M: Training-induced sarcoplasmic reticulum Ca^{2+} unloading occurs without Ca^{2+} influx. Med Sci Sports Exerc 2005;37:1119-1125

64. Stehno-Bittel L, Laughlin MH, Sturek M: Exercise training alters Ca release from coronary smooth muscle sarcoplasmic reticulum. Am J Physiol Heart Circ Physiol 1990;259:H643-H647

65. Stehno-Bittel L, Sturek M: Spontaneous sarcoplasmic reticulum calcium release and extrusion from bovine, not porcine, coronary artery smooth muscle. J Physiol (Lond) 1992;451:49-78

66. Ghosh TK, Bian JH, Short AD, Rybak SL, Gill DL: Persistent intracellular calcium pool depletion by thapsigargin and its influence on cell growth. J Biol Chem 1991;266:24690-24697

67. Short AD, Bian J, Ghosh TK, Waldron RT, Rybak SL, Gill DL: Intracellular Ca2+ pool content is linked to control of cell growth. Proc Natl Acad Sci U S A 1993;90:4986-4990

68. Waldron RT, Short AD, Meadows JJ, Ghosh TK, Gill DL: Endoplasmic reticulum calcium pump expression and control of cell growth. J Biol Chem 1994;269:11927-11933

69. Mokelke EA, Dietz NJ, Eckman DM, Nelson MT, Sturek M: Diabetic dyslipidemia and exercise affect coronary tone and differential regulation of conduit and microvessel K^+ current. Am J Physiol Heart Circ Physiol 2005;288:H1233-H1241

70. Marsden PA, Danthuluri NR, Brenner BM, Ballermann BJ, Brock TA: Endothelin action on vascular smooth muscle involves inositol trisphosphate and calcium mobilization. Biochem Biophys Res Commun 1989;158:86-93

71. Periasamy M, Kalyanasundaram A: SERCA pump isoforms: their role in calcium transport and disease. Muscle Nerve 2007;35:430-442

72. Bobe R, Hadri L, Lopez JJ, Sassi Y, Atassi F, Karakikes I, Liang L, Limon I, Lompre AM, Hatem SN, Hajjar RJ, Lipskaia L: SERCA2a controls the mode of agonist-induced intracellular Ca2+ signal, transcription factor NFAT and proliferation in human vascular smooth muscle cells. J Mol Cell Cardiol 2011;50:621-633

73. Lipskaia L, Hadri L, Le PP, Esposito B, Atassi F, Liang L, Glorian M, Limon I, Lompre AM, Lehoux S, Hajjar RJ: SERCA2a gene transfer prevents intimal proliferation in an organ culture of human internal mammary artery. Gene Ther 2012;

74. Lipskaia L, Bobe R, Chen J, Turnbull IC, Lopez JJ, Merlet E, Jeong D, Karakikes I, Ross AS, Liang L, Mougenot N, Atassi F, Lompre AM, Tarzami ST, Kovacic JC, Kranias E, Hajjar RJ, Hadri L: Synergistic role of protein phosphatase inhibitor 1 and sarco/endoplasmic reticulum Ca2+ -ATPase in the acquisition of the contractile phenotype of arterial smooth muscle cells. Circulation 2014;129:773-785

75. Dally S, Bredoux R, Corvazier E, Andersen JP, Clausen JD, Dode L, Fanchaouy M, Gelebart P, Monceau V, Del Monte F, Gwathmey JK, Hajjar R, Chaabane C, Bobe R, Raies A, Enouf J: Ca2+-ATPases in non-failing and failing heart: evidence for a novel cardiac sarco/endoplasmic reticulum Ca2+-ATPase 2 isoform (SERCA2c). Biochem J 2006;395:249-258

76. Berwick Z, Dick G, O'Leary H, Bender S, Goodwill A, Moberly S, Owen M, Miller S, Obukhov A, Tune J: Contribution of electromechanical coupling between KV and CaV1.2 channels to coronary dysfunction in obesity. Basic Res Cardiol 2013;108:370

77. Knudson JD, Dincer UD, Bratz IN, Sturek M, Dick GM, Tune JD: Mechanisms of coronary dysfunction in obesity and insulin resistance. Microcirculation 2007;14:317-338

78. Borbouse L, Dick GM, Asano S, Bender SB, Dincer UD, Payne GA, Neeb ZP, Bratz IN, Sturek M, Tune JD: Impaired function of coronary BK_{Ca} channels in metabolic syndrome. Am J Physiol Heart Circ Physiol 2009;297:H1629-H1637

79. Witczak CA, Wamhoff BR, Sturek M: Exercise training prevents Ca^{2+} dysregulation in coronary smooth muscle from diabetic dyslipidemic Yucatan swine. J Appl Physiol 2006;101:752-762

80. Bowles DK, Heaps CL, Turk JR, Maddali KK, Price EM: Hypercholesterolemia inhibits L-type calcium current in coronary macro-, not microcirculation. J Appl Physiol 2004;96:2240-2248

81. Hill BJF, Price EM, Dixon JL, Sturek M: Increased calcium buffering in coronary smooth muscle cells from diabetic dyslipidemic pigs. Atherosclerosis 2003;167:15-23

82. Neeb ZP, Edwards JM, Alloosh M, Long X, Mokelke EA, Sturek M: Metabolic syndrome and coronary artery disease in Ossabaw compared with Yucatan swine. Comp Med 2010;60:300-315

83. Gefel D, Hendrick GK, Mojsov S, Habener J, Weir GC: Glucagon-like peptide-I analogs: effects on insulin secretion and adenosine 3',5'-monophosphate formation. Endocrinology 1990;126:2164-2168

84. Wheeler MB, Lu M, Dillon JS, Leng XH, Chen C, Boyd AE, 3rd: Functional expression of the rat glucagon-like peptide-I receptor, evidence for coupling to both adenylyl cyclase and phospholipase-C. Endocrinology 1993;133:57-62

85. Ding WG, Renstrom E, Rorsman P, Buschard K, Gromada J: Glucagon-like peptide I and glucose-dependent insulinotropic polypeptide stimulate Ca2+-induced secretion in rat alpha-cells by a protein kinase A-mediated mechanism. Diabetes 1997;46:792-800

86. Tsien RW, Bean BP, Hess P, Lansman JB, Nilius B, Nowycky MC: Mechanisms of calcium channel modulation by beta-adrenergic agents and dihydropyridine calcium agonists. J Mol Cell Cardiol 1986;18:691-710

87. Tiaho F, Richard S, Lory P, Nerbonne JM, Nargeot J: Cyclic-AMP-dependent phosphorylation modulates the stereospecific activation of cardiac Ca channels by Bay K 8644. Pflugers Arch 1990;417:58-66

88. Li CF, Wang JH, Colyer J: Immunological detection of phospholamban phosphorylation states facilitates the description of the mechanism of phosphorylation and dephosphorylation. Biochemistry 1990;29:4535-4540

89. Jackson WA, Colyer J: Translation of Ser16 and Thr17 phosphorylation of phospholamban into Ca 2+-pump stimulation. Biochem J 1996;316 (Pt 1):201-207

90. Montrose-Rafizadeh C, Avdonin P, Garant MJ, Rodgers BD, Kole S, Yang H, Levine MA, Schwindinger W, Bernier M: Pancreatic glucagon-like peptide-1 receptor couples to multiple G proteins and activates mitogen-activated protein kinase pathways in Chinese hamster ovary cells. Endocrinology 1999;140:1132-1140

91. Moberly S, Mather K, Berwick Z, Owen M, Goodwill A, Casalini E, Hutchins G, Green M, Ng Y, Considine R, Perry K, Chisholm R, Tune J: Impaired cardiometabolic responses to glucagon-like peptide 1 in obesity and type 2 diabetes mellitus. Basic Res Cardiol 2013;108:365

92. Buteau J, Foisy S, Rhodes CJ, Carpenter L, Biden TJ, Prentki M: Protein kinase Czeta activation mediates glucagon-like peptide-1-induced pancreatic beta-cell proliferation. Diabetes 2001;50:2237-2243

93. Hansen L, Deacon CF, Orskov C, Holst JJ: Glucagon-like peptide-1-(7-36)amide is transformed to glucagon-like peptide-1-(9-36)amide by dipeptidyl peptidase IV in the capillaries supplying the L cells of the porcine intestine. Endocrinology 1999;140:5356-5363

94. Deacon CF, Nauck MA, Toft-Nielsen M, Pridal L, Willms B, Holst JJ: Both subcutaneously and intravenously administered glucagon-like peptide I are rapidly degraded from the NH2-terminus in type II diabetic patients and in healthy subjects. Diabetes 1995;44:1126-1131

95. Eng J, Kleinman WA, Singh L, Singh G, Raufman JP: Isolation and characterization of exendin-4, an exendin-3 analogue, from Heloderma suspectum venom. Further evidence for an exendin receptor on dispersed acini from guinea pig pancreas. J Biol Chem 1992;267:7402-7405

96. Thorens B, Porret A, Buhler L, Deng SP, Morel P, Widmann C: Cloning and functional expression of the human islet GLP-1 receptor. Demonstration that exendin-4 is an agonist and exendin-(9-39) an antagonist of the receptor. Diabetes 1993;42:1678-1682

97. Greig NH, Holloway HW, De Ore KA, Jani D, Wang Y, Zhou J, Garant MJ, Egan JM: Once daily injection of exendin-4 to diabetic mice achieves long-term beneficial effects on blood glucose concentrations. Diabetologia 1999;42:45-50

98. Young AA, Gedulin BR, Bhavsar S, Bodkin N, Jodka C, Hansen B, Denaro M: Glucose-lowering and insulin-sensitizing actions of exendin-4: studies in obese diabetic (ob/ob, db/db) mice, diabetic fatty Zucker rats, and diabetic rhesus monkeys (Macaca mulatta). Diabetes 1999;48:1026-1034

99. Nauck M: Incretin therapies: highlighting common features and differences in the modes of action of glucagon-like peptide-1 receptor agonists and dipeptidyl peptidase-4 inhibitors. Diabetes Obes Metab 2016;18:203-216

100. Kolterman OG, Buse JB, Fineman MS, Gaines E, Heintz S, Bicsak TA, Taylor K, Kim D, Aisporna M, Wang Y, Baron AD: Synthetic exendin-4 (exenatide) significantly reduces postprandial and fasting plasma glucose in subjects with type 2 diabetes. J Clin Endocrinol Metab 2003;88:3082-3089

101. Sheu WH, Brunell SC, Blase E: Efficacy and tolerability of exenatide twice daily and exenatide once weekly in Asian versus White patients with type 2 diabetes mellitus: A pooled analysis. Diabetes Res Clin Pract 2016;114:160-172

102. Trautmann ME, Han J, Ruggles J: Early Pharmacodynamic Effects of Exenatide Once Weekly in Type 2 Diabetes Are Independent of Weight Loss: A Pooled Analysis of Patient-Level Data. Clin Ther 2016;

103. Liu Q, Anderson C, Broyde A, Polizzi C, Fernandez R, Baron A, Parkes DG: Glucagon-like peptide-1 and the exenatide analogue AC3174 improve cardiac function, cardiac remodeling, and survival in rats with chronic heart failure. Cardiovasc Diabetol 2010;9:76

104. Liu Q, Adams L, Broyde A, Fernandez R, Baron AD, Parkes DG: The exenatide analogue AC3174 attenuates hypertension, insulin resistance, and renal dysfunction in Dahl salt-sensitive rats. Cardiovasc Diabetol 2010;9:32

105. MacDonald PE, El-Kholy W, Riedel MJ, Salapatek AM, Light PE, Wheeler MB: The multiple actions of GLP-1 on the process of glucose-stimulated insulin secretion. Diabetes 2002;51 Suppl 3:S434-S442

106. Gromada J, Ding WG, Barg S, Renstrom E, Rorsman P: Multisite regulation of insulin secretion by cAMP-increasing agonists: evidence that glucagon-like peptide 1 and glucagon act via distinct receptors. Pflugers Arch 1997;434:515-524

107. Leech CA, Holz GG, Habener JF: Signal transduction of PACAP and GLP-1 in pancreatic beta cells. Ann N Y Acad Sci 1996;805:81-92

108. Holz GG, Kuhtreiber WM, Habener JF: Pancreatic beta-cells are rendered glucose-competent by the insulinotropic hormone glucagon-like peptide-1(7-37). Nature 1993;361:362-365

109. Salapatek AM, MacDonald PE, Gaisano HY, Wheeler MB: Mutations to the third cytoplasmic domain of the glucagon-like peptide 1 (GLP-1) receptor can functionally uncouple GLP-1-stimulated insulin secretion in HIT-T15 cells. Mol Endocrinol 1999;13:1305-1317

110. Holz GG, Leech CA, Heller RS, Castonguay M, Habener JF: cAMP-dependent mobilization of intracellular Ca2+ stores by activation of ryanodine receptors in pancreatic beta-cells. A Ca2+ signaling system stimulated by the insulinotropic hormone glucagon-like peptide-1-(7-37). J Biol Chem 1999;274:14147-14156

111. Gromada J, Dissing S, Bokvist K, Renstrom E, Frokjaer-Jensen J, Wulff BS, Rorsman P: Glucagon-like peptide I increases cytoplasmic calcium in insulin-secreting beta TC3-cells by enhancement of intracellular calcium mobilization. Diabetes 1995;44:767-774

112. Timmers L, Henriques JP, de Kleijn DP, Devries JH, Kemperman H, Steendijk P, Verlaan CW, Kerver M, Piek JJ, Doevendans PA, Pasterkamp G, Hoefer IE: Exenatide Reduces Infarct Size and Improves Cardiac Function in a Porcine Model of Ischemia and Reperfusion Injury. J Am Coll Cardiol 2009;53:501-510

113. Hirata Y, Kurobe H, Nishio C, Tanaka K, Fukuda D, Uematsu E, Nishimoto S, Soeki T, Harada N, Sakaue H, Kitagawa T, Shimabukuro M, Nakaya Y, Sata M: Exendin-4, a glucagon-like peptide-1 receptor agonist, attenuates neointimal hyperplasia after vascular injury. Eur J Pharmacol 2013;699:106-111

114. Liang CP, Han S, Li G, Tabas I, Tall AR: Impaired MEK signaling and SERCA expression promote ER stress and apoptosis in insulin-resistant macrophages and are reversed by exenatide treatment. Diabetes 2012;61:2609-2620

115. Younce CW, Burmeister MA, Ayala JE: Exendin-4 attenuates high glucose-induced cardiomyocyte apoptosis via inhibition of endoplasmic reticulum stress and activation of SERCA2a. Am J Physiol Cell Physiol 2013;304:C508-C518

116. Dokken BB, Weber CS, Mitchell JL, Gold JM, Lynch RM: Glucagon-like peptide-1 modulates calcium homeostasis in human coronary microvascular endothelial cells after ischemia and reperfusion. Journal of Endocrinology, Diabetes & Obesity 2014;2:1025-1031

117. Bell LN, Lee L, Saxena R, Bemis KG, Wang M, Theodorakis JL, Vuppalanchi R, Alloosh M, Sturek M, Chalasani N: Serum proteomic analysis of diet-induced steatohepatitis and metabolic syndrome in the Ossabaw miniature swine. Am J Physiol Gastrointest Liver Physiol 2010;298:G746-G754

118. Bender SB, Tune JD, Borbouse L, Long X, Sturek M, Laughlin MH: Altered mechanism of adenosine-induced coronary arteriolar dilation in early-stage metabolic syndrome. Exp Biol Med (Maywood) 2009;234:683-692

119. Berwick ZC, Dick GM, Moberly SP, Kohr MC, Sturek M, Tune JD: Contribution of voltage-dependent K^+ channels to metabolic control of coronary blood flow. J Mol Cell Cardiol 2012;52:912-919

120. Bonin EA, Mariani A, Swain J, Bingener J, Sumiyama K, Knipschield M, Sebo TJ, Gostout CJ: Laparoscopic ultrasound-assisted liposuction for lymph node dissection: a pilot study. Surg Endosc 2012;26:1963-1970

121. Boullion RD, Mokelke EA, Wamhoff BR, Otis CR, Wenzel J, Dixon JL, Sturek M: Porcine model of diabetic dyslipidemia: Insulin and feed algorithms for mimicking diabetes in humans. Comp Med 2003;53:42-52

122. Bratz IN, Dick GM, Tune JD, Edwards JM, Neeb ZP, Dincer UD, Sturek M: Impaired capsaicin-induced relaxation of coronary arteries in a porcine model of the metabolic syndrome. Am J Physiol Heart Circ Physiol 2008;294:H2489-H2496

123. Clark BA, Alloosh M, Wenzel JW, Sturek M, Kostrominova TY: Effect of diet-induced obesity and metabolic syndrome on skeletal muscles of Ossabaw miniature swine. Am J Physiol Endocrinol Metab 2011;300:E848-E857

124. Dincer UD: Cardiac beta-adrenoceptor expression is markedly depressed in Ossabaw swine model of cardiometabolic risk. Int J Gen Med 2011;4:493-499

125. Dyson MC, Alloosh M, Vuchetich JP, Mokelke EA, Sturek M: Components of metabolic syndrome and coronary artery disease in female Ossabaw swine fed excess atherogenic diet. Comp Med 2006;56:35-45

126. Edwards JM, Neeb ZP, Alloosh MA, Long X, Bratz IN, Peller CR, Byrd JP, Kumar S, Obukhov AG, Sturek M: Exercise training decreases store-operated Ca^{2+} entry associated with metabolic syndrome and coronary atherosclerosis. Cardiovasc Res 2010;85:631-640

127. Elmadhun NY, Sabe AA, Lassaletta AD, Chu LM, Kondra K, Sturek M, Sellke FW: Metabolic syndrome impairs notch signaling and promotes apoptosis in chronically ischemic myocardium. J Thorac Cardiovasc Surg 2014;148:1048-1055

128. Elmadhun NY, Lassaletta AD, Chu LM, Sellke FW: Metformin alters the insulin signaling pathway in ischemic cardiac tissue in a swine model of metabolic syndrome. J Thorac Cardiovasc Surg 2013;145:258-266

129. Faris RJ, Boddicker RL, Walker-Daniels J, Li J, Jones DE, Spurlock ME: Inflammation in response to n3 fatty acids in a porcine obesity model. Comp Med 2012;62:495-503

130. Flum DR, Devlin A, Wright AS, Figueredo E, Alyea E, Hanley PW, Lucas MK, Cummings DE: Development of a porcine Roux-en-Y gastric bypass survival model for the study of post-surgical physiology. Obes Surg 2007;17:1332-1339

131. Hamamdzic D, Wilensky RL: Porcine models of accelerated coronary atherosclerosis: role of diabetes mellitus and hypercholesterolemia. Journal of diabetes research 2013;2013:761415

132. Handa RK, Evan AP, Connors BA, Johnson CD, Liu Z, Alloosh M, Sturek M, Evans-Molina C, Mandeville JA, Gnessin E, Lingeman JE: Shock wave lithotripsy targeting of the kidney and pancreas does not increase the severity of metabolic syndrome in a porcine model. J Urol 2014;192:1257-1265

133. Handa RK, Liu Z, Connors BA, Alloosh M, Basile DP, Tune JD, Sturek M, Evan AP, Lingeman JE: Effect of renal shock wave lithotripsy on the development of metabolic syndrome in a juvenile swine model: a pilot study. J Urol 2015;193:1409-1416

134. Kreutz RP, Alloosh M, Mansour K, Neeb Z, Kreutz Y, Flockhart DA, Sturek M: Morbid obesity and metabolic syndrome in Ossabaw miniature swine are associated with increased platelet reactivity. Diabetes Metab Syndr Obes 2011;4:99-105

135. Lassaletta AD, Chu LM, Robich MP, Elmadhun NY, Feng J, Burgess TA, Laham RJ, Sturek M, Sellke FW: Overfed Ossabaw swine with early stage metabolic syndrome have normal coronary collateral development in response to chronic ischemia. Basic Res Cardiol 2012;107:243

136. Lee L, Alloosh M, Saxena R, Van Alstine W, Watkins BA, Klaunig JE, Sturek M, Chalasani N: Nutritional model of steatohepatitis and metabolic syndrome in the Ossabaw miniature swine. Hepatology 2009;50:56-67

137. Li ZL, Woollard JR, Ebrahimi B, Crane JA, Jordan KL, Lerman A, Wang SM, Lerman LO: Transition From Obesity to Metabolic Syndrome Is Associated With Altered Myocardial Autophagy and Apoptosis. Arterioscl Throm Vas 2012;32:1132-1141

138. Li ZL, Woollard JR, Wang SM, Korsmo MJ, Ebrahimi B, Grande JP, Textor SC, Lerman A, Lerman LO: Increased glomerular filtration rate in early metabolic syndrome is associated with renal adiposity and microvascular proliferation. Am J Physiol-Renal 2011;301:F1078-F1087

139. McKenney ML, Schultz KA, Boyd JH, Byrd JP, Alloosh M, Teague SD, Arce-Esquivel AA, Fain JN, Laughlin MH, Sacks HS, Sturek M: Epicardial adipose excision slows the progression of porcine coronary atherosclerosis. J Cardiothorac Surg 2014;9:2-12

140. Newell-Fugate AE, Taibl JN, Clark SG, Alloosh M, Sturek M, Krisher RL: Effects of diet-induced obesity on metabolic parameters and reproductive function in female Ossabaw minipigs. Comp Med 2014;64:44-49

141. Owen MK, Witzmann FA, McKenney ML, Lai X, Berwick ZC, Moberly SP, Alloosh M, Sturek M, Tune JD: Perivascular adipose tissue potentiates contraction of coronary vascular smooth muscle: influence of obesity. Circulation 2013;128:9-18

142. Padilla J, Jenkins NT, Lee S, Zhang H, Cui J, Zuidema MY, Zhang C, Hill MA, Perfield JW, 2nd, Ibdah JA, Booth FW, Davis JW, Laughlin MH, Rector RS: Vascular transcriptional alterations produced by juvenile obesity in Ossabaw swine. Physiol Genomics 2013;45:434-446

143. Payne GA, Borbouse L, Kumar S, Neeb Z, Alloosh M, Sturek M, Tune JD: Epicardial Perivascular Adipose-Derived Leptin Exacerbates Coronary Endothelial Dysfunction in Metabolic Syndrome via a Protein Kinase C-beta Pathway. Arterioscl Throm Vas 2010;30:1711-1717

144. Pedersen R, Ingerslev H-C, Salicio SC, Sturek M, Alloosh M, Christoffersen BO, Moesgaard SG, Larsen N, Boye M: Characterization of gut microbiota in Ossabaw and Göttingen minipigs as models of obesity and metabolic syndrome. PLoS One 2012;8:e56612

145. Rodgaard T, Stagsted J, Christoffersen BO, Cirera S, Moesgaard SG, Sturek M, Alloosh M, Heegaard PM: Orosomucoid expression profiles in liver, adipose tissues and serum of lean and obese domestic pigs, Gottingen minipigs and Ossabaw minipigs. Vet Immunol Immunopathol 2013;151:325-330

146. Sabe AA, Elmadhun NY, Sadek AA, Chu LM, Bianchi C, Sellke FW: Differential effects of atorvastatin on autophagy in ischemic and nonischemic myocardium in Ossabaw swine with metabolic syndrome. J Thorac Cardiovasc Surg 2014;148:3172-3178

147. Sham JG, Simianu VV, Wright AS, Stewart SD, Alloosh M, Sturek M, Cummings DE, Flum DR: Evaluating the mechanisms of improved glucose homeostasis after bariatric surgery in Ossabaw miniature swine. Journal of diabetes research 2014;2014:526972

148. Sturek M, Alloosh M, Wenzel J, Byrd JP, Edwards JM, Lloyd PG, Tune JD, March KL, Miller MA, Mokelke EA, Brisbin IL, Jr.: Ossabaw Island miniature swine: cardiometabolic syndrome assessment. In *Swine in the Laboratory: Surgery, Anesthesia, Imaging, and Experimental Techniques,* 2nd Edition ed. Swindle MM, Ed. Boca Raton, CRC Press, 2007, p. 397-402

149. Talbott CW, See MT, Kaminsky P, Bixby D, Sturek M, Brisbin IL, Kadzere C: Enhancing pork flavor and fat quality with swine raised in sylvan systems Potential niche-market application for the Ossabaw hog. Renew Agr Food Syst 2006;21:183-191

150. Toedebusch RG, Roberts MD, Wells KD, Company JM, Kanosky KM, Padilla J, Jenkins NT, Perfield JW, 2nd, Ibdah JA, Booth FW, Rector RS: Unique transcriptomic signature of omental adipose tissue in Ossabaw swine: a model of childhood obesity. Physiol Genomics 2014;46:362-375

151. Trasino SE, Dawson HD, Urban JF, Jr., Wang TT, Solano-Aguilar G: Feeding probiotic Lactobacillus paracasei to Ossabaw pigs on a high-fat diet prevents cholesteryl-ester accumulation and LPS modulation of the Liver X receptor and inflammatory axis in alveolar macrophages. J Nutr Biochem 2013;24:1931-1939

152. Trask AJ, Katz PS, Kelly AP, Galantowicz ML, Cismowski MJ, West TA, Neeb ZP, Berwick ZC, Goodwill AG, Alloosh M, Tune JD, Sturek M, Lucchesi PA: Dynamic micro- and macrovascular remodeling in coronary circulation of obese Ossabaw pigs with metabolic syndrome. J Appl Physiol (1985) 2012;113:1128-1140

153. Wastney M, Lee W, Jackson GS, Alloosh M, Sturek M, Lachcik P, Peacock M, Martin B, Weaver CM: Soft tissue calcification in the Ossabaw miniature pig: experimental and kinetic modeling studies. Osteoporos Int 2013;24:2123-2126

154. Witczak CA, Mokelke EA, Boullion RD, Wenzel J, Keisler DH, Sturek M: Noninvasive measures of body fat percentage in male Yucatan swine. Comp Med 2005;55:445-451

155. Zhang X, Li ZL, Woollard JR, Eirin A, Ebrahimi B, Crane JA, Zhu XY, Pawar AS, Krier JD, Jordan KL, Tang H, Textor SC, Lerman A, Lerman LO: Obesity-metabolic derangement preserves hemodynamics but promotes intrarenal adiposity and macrophage infiltration in swine renovascular disease. Am J Physiol Renal Physiol 2013;305:F265-F276

156. Fullenkamp AM, Bell LN, Robbins RD, Lee L, Saxena R, Alloosh M, Klaunig JE, Mirmira RG, Sturek M, Chalasani N: Effect of different obesogenic diets on pancreatic histology in Ossabaw miniature swine. Pancreas 2011;40:438-443

157. Habegger KM, Penque BA, Sealls W, Tackett L, Bell LN, Blue EK, Gallagher PJ, Sturek M, Alloosh MA, Steinberg HO, Considine RV, Elmendorf JS: Fat-induced membrane cholesterol accrual provokes cortical filamentous actin destabilization and glucose transport dysfunction in skeletal muscle. Diabetologia 2012;55:457-467

158. Otis CR, Wamhoff BR, Sturek M: Hyperglycemia-induced insulin resistance in diabetic dyslipidemic Yucatan swine. Comp Med 2003;53:53-64

159. Potu RB, Lu H, Adeola O, Ajuwon KM: Metabolic markers in Ossabaw pigs fed high fat diets enriched in regular or low alpha-linolenic acid soy oil. Nutr Metab (Lond) 2013;10:27

160. Witczak CA, Sturek M: Exercise prevents diabetes-induced impairment in superficial buffer barrier in porcine coronary smooth muscle. J Appl Physiol 2004;96:1069-1079

161. Dixon JL, Shen S, Vuchetich JP, Wysocka E, Sun GY, Sturek M: Increased atherosclerosis in diabetic dyslipidemic swine: protection by atorvastatin involves decreased VLDL triglycerides but minimal effects on the lipoprotein profile. J Lipid Res 2002;43:1618-1629

162. Hanhineva K, Barri T, Kolehmainen M, Pekkinen J, Pihlajamaki J, Vesterbacka A, Solano-Aguilar G, Mykkanen H, Dragsted LO, Urban JF, Jr., Poutanen K: Comparative nontargeted profiling of metabolic changes in tissues and biofluids in high-fat diet-fed Ossabaw pig. J Proteome Res 2013;12:3980-3992

163. Mokelke EA, Hu Q, Song M, Toro L, Reddy HK, Sturek M: Altered functional coupling of coronary K^+ channels in diabetic dyslipidemic pigs is prevented by exercise. J Appl Physiol 2003;95:1179-1193

164. Lee DL, Wamhoff BR, Katwa LC, Reddy HK, Voelker DJ, Dixon JL, Sturek M: Increased endothelin-induced Ca^{2+} signaling, tyrosine phosphorylation, and coronary artery disease in diabetic dyslipidemic swine are prevented by atorvastatin. J Pharmacol Exp Ther 2003;306:132-140

165. Long X, Bratz IN, Alloosh M, Edwards JM, Sturek M: Short-term exercise training prevents micro- and macrovascular disease following coronary stenting. J Appl Physiol (1985) 2010;108:1766-1774

166. Long X, Mokelke EA, Neeb ZP, Alloosh M, Edwards JM, Sturek M: Adenosine receptor regulation of coronary blood flow in Ossabaw miniature swine. J Pharmacol Exp Ther 2010;335:781-787

167. Rector RS, Thomas TR, Liu Y, Henderson KK, Holiman DA, Sun GY, Sturek M: Effect of exercise on postprandial lipemia following a higher calorie meal in Yucatan miniature swine. Metabolism 2004;53:1021-1026

168. McKenney ML, Kohr MC, Alloosh M, Schultz KA, Tune JD, Bell LN, Sturek M: Dysfunction of coronary smooth muscle Ca^{2+} regulation in the progression of metabolic syndrome and coronary artery disease in Ossabaw miniature swine (abstract). FASEB J 2012;26

169. Go AS, Mozaffarian D, Roger VL, Benjamin EJ, Berry JD, Blaha MJ, Dai S, Ford ES, Fox CS, Franco S, Fullerton HJ, Gillespie C, Hailpern SM, Heit JA, Howard VJ, Huffman MD, Judd SE, Kissela BM, Kittner SJ, Lackland DT, Lichtman JH, Lisabeth LD, Mackey RH, Magid DJ, Marcus GM, Marelli A, Matchar DB, McGuire DK, Mohler ER, III, Moy CS, Mussolino ME, Neumar RW, Nichol G, Pandey DK, Paynter NP, Reeves MJ, Sorlie PD, Stein J, Towfighi A, Turan TN, Virani SS, Wong ND, Woo D, Turner MB: Heart disease and stroke statistics--2014 update: a report from the American Heart Association. Circulation 2014;129:e28-e292

170. Libby P, Ridker PM, Hansson GK: Progress and challenges in translating the biology of atherosclerosis. Nature 2011;473:317-325

171. Rader DJ, Daugherty A: Translating molecular discoveries into new therapies for atherosclerosis. Nature 2008;451:904-913

172. Jiang H, Stephens NL: Calcium and smooth muscle contraction. Mol Cell Biochem 1994;135:1-9

173. House SJ, Potier M, Bisaillon J, Singer HA, Trebak M: The non-excitable smooth muscle: calcium signaling and phenotypic switching during vascular disease. Pflugers Arch 2008;456:769-785

174. Kruse HJ, Bauriedel G, Heimerl J, Hofling B, Weber PC: Role of L-type calcium channels on stimulated calcium influx and on proliferative activity of human coronary smooth muscle cells. J Cardiovasc Pharmacol 1994;24:328-335

175. Nilsson J, Sjolund M, Palmberg L, Von Euler AM, Jonzon B, Thyberg J: The calcium antagonist nifedipine inhibits arterial smooth muscle cell proliferation. Atherosclerosis 1985;58:109-122

176. Pauly RR, Bilato C, Sollott SJ, Monticone R, Kelly PT, Lakatta EG, Crow MT: Role of calcium/calmodulin-dependent protein kinase II in the regulation of vascular smooth muscle cell migration. Circulation 1995;91:1107-1115

177. Lundberg MS, Curto KA, Bilato C, Monticone RE, Crow MT: Regulation of vascular smooth muscle migration by mitogen-activated protein kinase and calcium/calmodulin-dependent protein kinase II signaling pathways. J Mol Cell Cardiol 1998;30:2377-2389

178. Hill-Eubanks DC, Werner ME, Heppner TJ, Nelson MT: Calcium signaling in smooth muscle. Cold Spring Harb Perspect Biol 2011;3:a004549

179. Wamhoff BR, Bowles DK, McDonald OG, Sinha S, Somlyo AP, Somlyo AV, Owens GK: L-type voltage-gated Ca2+ channels modulate expression of smooth muscle differentiation marker genes via a rho kinase/myocardin/SRF-dependent mechanism. Circ Res 2004;95:406-414

180. Sturek M: Ca^{2+} regulatory mechanisms of exercise protection against coronary artery disease in metabolic syndrome and diabetes. J Appl Physiol 2011;111:573-586

181. Wang HW, Langohr IM, Sturek M, Cheng JX: Imaging and quantitative analysis of atherosclerotic lesions by CARS-based multimodal nonlinear optical microscopy. Arterioscler Thromb Vasc Biol 2009;29:1342-1348

182. Institute for Laboratory Animal Research: *Guide for the care and use of laboratory animals*. Washington, D.C., National Academy Press, 2010

183. AVMA Panel on Euthanasia.American Veterinary Medical Association: 2000 Report of the AVMA panel on euthanasia. JAVMA 2001;218:669-696

184. Heaps CL, Sturek M, Price EM, Laughlin MH, Parker JL: Sarcoplasmic reticulum Ca(2+) uptake is impaired in coronary smooth muscle distal to coronary occlusion. Am J Physiol Heart Circ Physiol 2001;281:H223-H231

185. McKenney-Drake ML, Rodenbeck SD, Owen MK, Schultz KA, Alloosh M, Tune JD, Sturek M: Repeat cross-sectional data on the progression of the metabolic syndrome in Ossabaw miniature swine. Data in Brief 2016;7:1393-1395

186. Alloosh M, Pratt JH, Sturek M, Basile DP: Elevated renin and enhanced adrenal steroidogenesis in the Ossabaw miniature swine model of the metabolic syndrome (abstract). FASEB J 2008;22:736.737

187. McKenney-Drake ML, Rodenbeck SD, Owen MK, Schultz KA, Alloosh M, Tune JD, Sturek M: Biphasic alterations in coronary smooth muscle Ca2+ regulation in a repeat cross-sectional study of coronary artery disease severity in metabolic syndrome. Atherosclerosis 2016;249:1-9

188. Gould KL, Lipscomb K, Hamilton GW: Physiologic basis for assessing critical coronary stenosis. Instantaneous flow response and regional distribution during coronary hyperemia as measures of coronary flow reserve. Am J Cardiol 1974;33:87-94

189. Stary HC: Evolution and progression of atherosclerotic lesions in coronary arteries of children and young adults. Arteriosclerosis 1989;9:I19-I32

190. Tanaka K, Masuda J, Imamura T, Sueishi K, Nakashima T, Sakurai I, Shozawa T, Hosoda Y, Yoshida Y, Nishiyama Y, et al.: A nation-wide study of atherosclerosis in infants, children and young adults in Japan. Atherosclerosis 1988;72:143-156

191. Imakita M, Yutani C, Strong JP, Sakurai I, Sumiyoshi A, Watanabe T, Mitsumata M, Kusumi Y, Katayama S, Mano M, Baba S, Mannami T, Masuda J, Sueishi K, Tanaka K: Second nation-wide study of atherosclerosis in infants, children and young adults in Japan. Atherosclerosis 2001;155:487-497

192. Berenson GS, Srinivasan SR, Bao W, Newman WP, 3rd, Tracy RE, Wattigney WA: Association between multiple cardiovascular risk factors and atherosclerosis in children and young adults. The Bogalusa Heart Study. N Engl J Med 1998;338:1650-1656

193. Tuzcu EM, Kapadia SR, Tutar E, Ziada KM, Hobbs RE, McCarthy PM, Young JB, Nissen SE: High prevalence of coronary atherosclerosis in asymptomatic teenagers and young adults - Evidence from intravascular ultrasound. Circulation 2001;103:2705-2710

194. Hong YM: Atherosclerotic cardiovascular disease beginning in childhood. Korean circulation journal 2010;40:1-9

195. Hill-Eubanks DC, Gomez MF, Stevenson AS, Nelson MT: NFAT regulation in smooth muscle. Trends Cardiovasc Med 2003;13:56-62

196. Magnier-Gaubil C, Herbert JM, Quarck R, Papp B, Corvazier E, Wuytack F, Levy-Toledano S, Enouf J: Smooth muscle cell cycle and proliferation. Relationship between calcium influx and sarco-endoplasmic reticulum Ca2+ATPase regulation. J Biol Chem 1996;271:27788-27794

197. Pozzan T, Rizzuto R, Volpe P, Meldolesi J: Molecular and cellular physiology of intracellular calcium stores. Physiol Rev 1994;74:595-636

198. van Breemen C, Saida K: Cellular mechanisms regulating $[Ca^{2+}]_i$ smooth muscle. Annu Rev Physiol 1989;51:315-329

199. Magnier C, Papp B, Corvazier E, Bredoux R, Wuytack F, Eggermont J, Maclouf J, Enouf J: Regulation of sarco-endoplasmic reticulum Ca2+-ATPases during platelet-derived growth factor-induced smooth muscle cell proliferation. J Biol Chem 1992;267:15808-15815

200. Kang S, Dahl R, Hsieh W, Shin AC, Zsebo KM, Buettner C, Hajjar RJ, Lebeche D: Small Molecular Allosteric Activator of the Sarco/Endoplasmic Reticulum Ca2+-ATPase (SERCA) Attenuates Diabetes and Metabolic Disorders. J Biol Chem 2015;

201. Hill BJF, Wamhoff BR, Sturek M: Functional nucleotide receptor expression and sarcoplasmic reticulum morphology in dedifferentiated porcine coronary smooth muscle cells. J Vasc Res 2001;38:432-443

202. Wamhoff BR, Bowles DK, Dietz NJ, Hu Q, Sturek M: Exercise training attenuates coronary smooth muscle phenotypic modulation and nuclear Ca^{2+} signaling. Am J Physiol Heart Circ Physiol 2002;283:H2397-H2410

203. Edwards JM, Alloosh MA, Long XL, Dick GM, Lloyd PG, Mokelke EA, Sturek M: Adenosine A_1 receptors in neointimal hyperplasia and in-stent stenosis in Ossabaw miniature swine. Coron Artery Dis 2008;19:27-31

204. Dineen SL, McKenney ML, Bell LN, Fullenkamp AM, Schultz KA, Alloosh M, Chalasani N, Sturek M: Metabolic Syndrome Abolishes Glucagon-Like Peptide 1 Receptor Agonist Stimulation of SERCA in Coronary Smooth Muscle. Diabetes 2015;64:3321-3327

205. Lipskaia L, Hadri L, Le Prince P, Esposito B, Atassi F, Liang L, Glorian M, Limon I, Lompre AM, Lehoux S, Hajjar RJ: SERCA2a gene transfer prevents intimal proliferation in an organ culture of human internal mammary artery. Gene Ther 2013;20:396-406

206. Lipskaia L, del Monte F, Capiod T, Yacoubi S, Hadri L, Hours M, Hajjar RJ, Lompre AM: Sarco/endoplasmic reticulum Ca2+-ATPase gene transfer reduces vascular smooth muscle cell proliferation and neointima formation in the rat. Circ Res 2005;97:488-495

207. Lund LH, Edwards LB, Kucheryavaya AY, Dipchand AI, Benden C, Christie JD, Dobbels F, Kirk R, Rahmel AO, Yusen RD, Stehlik J, International Society for H, Lung T: The Registry of the International Society for Heart and Lung Transplantation: Thirtieth Official Adult Heart Transplant Report--2013; focus theme: age. J Heart Lung Transplant 2013;32:951-964

208. Noble D, Borysova L, Wray S, Burdyga T: Store-operated Ca(2)(+) entry and depolarization explain the anomalous behaviour of myometrial SR: effects of SERCA inhibition on electrical activity, Ca(2)(+) and force. Cell Calcium 2014;56:188-194

209. Masoudi FA, Inzucchi SE, Wang Y, Havranek EP, Foody JM, Krumholz HM: Thiazolidinediones, metformin, and outcomes in older patients with diabetes and heart failure: an observational study. Circulation 2005;111:583-590

210. Nesto RW, Bell D, Bonow RO, Fonseca V, Grundy SM, Horton ES, Le Winter M, Porte D, Semenkovich CF, Smith S, Young LH, Kahn R: Thiazolidinedione use, fluid retention, and congestive heart failure: a consensus statement from the American Heart Association and American Diabetes Association. Diabetes Care 2004;27:256-263

211. Masoudi FA: Improving drug safety surveillance: lessons from rosiglitazone. Circ Cardiovasc Qual Outcomes 2010;3:444-446

212. Center for Drug Evaluation and Research: Guidance for Industry: Diabetes Mellitus - Evaluating Cardiovascular Risk in New Antidiabetic Therapies to Treat Type 2 Diabetes.
http://www.fda.gov/downloads/drugs/guidancecomplianceregulatoryinformation/guidances/ucm071627.pdf, 2008

213. Yoshida I, Monji A, Tashiroa K, Nakamura K, Inoue R, Kanba S: Depletion of intracellular Ca2+ store itself may be a major factor in thapsigargin-induced ER stress and apoptosis in PC12 cells. Neurochemistry International 2006;48:696-702

214. Nystrom T, Gutniak MK, Zhang Q, Zhang F, Holst JJ, Ahren B, Sjoholm A: Effects of glucagon-like peptide-1 on endothelial function in type 2 diabetes patients with stable coronary artery disease. Am J Physiol Endocrinol Metab 2004;287:E1209-E1215

215. Hill BJF, Dixon JL, Sturek M: Effect of atorvastatin on intracellular calcium uptake in coronary smooth muscle cells from diabetic pigs fed an atherogenic diet. Atherosclerosis 2001;159:117-124

216. Hill BJF, Katwa LC, Wamhoff BR, Sturek M: Enhanced endothelin(A) receptor-mediated calcium mobilization and contraction in organ cultured porcine coronary arteries. J Pharmacol Exp Ther 2000;295:484-491

217. Nguyen AT, Gomez D, Bell RD, Campbell JH, Clowes AW, Gabbiani G, Giachelli CM, Parmacek MS, Raines EW, Rusch NJ, Speer MY, Sturek M, Thyberg J, Towler DA, Weiser-Evans MC, Yan C, Miano JM, Owens GK: Smooth muscle cell plasticity: fact or fiction? Circ Res 2013;112:17-22

218. Gomez D, Owens GK: Smooth muscle cell phenotypic switching in atherosclerosis. Cardiovasc Res 2012;95:156-164

219. Rudijanto A: The role of vascular smooth muscle cells on the pathogenesis of atherosclerosis. Acta Med Indones 2007;39:86-93

220. Sturek M, Kunda K, Hu Q: Sarcoplasmic reticulum buffering of myoplasmic calcium in bovine coronary artery smooth muscle. J Physiol 1992;451:25-48

221. Heaps CL, Bowles DK, Sturek M, Laughlin MH, Parker JL: Enhanced L-type Ca^{2+} channel current density in coronary smooth muscle of exercise trained swine is compensated to limit myoplasmic net Ca^{2+} accumulation. J Physiol 2000;528:435-445

222. Jones JJ, Dietz NJ, Heaps CL, Parker JL, Sturek M: Calcium buffering in coronary smooth muscle after chronic occlusion and exercise training. Cardiovasc Res 2001;51:359-367

223. Underwood FB, Laughlin MH, Sturek M: Altered control of calcium in coronary smooth muscle cells by exercise training. Med Sci Sports Exerc 1994;26:1230-1238

224. Miyashita Y, Sollott SJ, Cheng L, Kinsella JL, Koh E, Lakatta EG, Froehlich JP: Redistribution of intracellular Ca^{2+} stores after β-adrenergic stimulation of rat tail artery SMC. Am J Physiol Heart Circ Physiol 1997;272:H244-H255

225. Van Breemen C: Calcium requirement for activation of intact aortic smooth muscle. J Physiol (Lond) 1977;272:317-329

226. Poburko D, Liao CH, Lemos VS, Lin E, Maruyama Y, Cole WC, van Breemen C: Transient receptor potential channel 6-mediated, localized cytosolic [Na+] transients drive Na+/Ca2+ exchanger-mediated Ca2+ entry in purinergically stimulated aorta smooth muscle cells. Circ Res 2007;101:1030-1038

227. Putney JW, Jr.: Capacitative calcium entry revisited. Cell Calcium 1990;11:611-624

228. Clapham DE: Calcium signaling. Cell 1995;80:259-268

229. Stehno-Bittel L, Laughlin MH, Sturek M: Exercise training depletes sarcoplasmic reticulum calcium in coronary smooth muscle. J Appl Physiol (1985) 1991;71:1764-1773

230. Alexander MR, Owens GK: Epigenetic control of smooth muscle cell differentiation and phenotypic switching in vascular development and disease. Annu Rev Physiol 2012;74:13-40

231. Glagov S, Weisenberg E, Zarins CK, Stankunavicius R, Kolettis GJ: Compensatory enlargement of human atherosclerotic coronary arteries. N Engl J Med 1987;316:1371-1375

232. Galis ZS, Khatri JJ: Matrix metalloproteinases in vascular remodeling and atherogenesis: the good, the bad, and the ugly. Circ Res 2002;90:251-262

233. McKenney-Drake ML, Territo PR, Salavati A, Houshmand S, Persohn S, Liang Y, Alloosh M, Moe SM, Weaver CM, Alavi A, Sturek M: ^{18}F-NaF PET imaging of early coronary artery calcification. JACC Cardiovasc Imaging 2016;9:627-628

234. Aikawa E, Nahrendorf M, Figueiredo JL, Swirski FK, Shtatland T, Kohler RH, Jaffer FA, Aikawa M, Weissleder R: Osteogenesis Associates With Inflammation in Early-Stage Atherosclerosis Evaluated by Molecular Imaging In Vivo. Circulation 2007;116:2841-2850

235. Vengrenyuk Y, Carlier S, Xanthos S, Cardoso L, Ganatos P, Virmani R, Einav S, Gilchrist L, Weinbaum S: A hypothesis for vulnerable plaque rupture due to stress-induced debonding around cellular microcalcifications in thin fibrous caps. P Natl Acad Sci USA 2006;103:14678-14683

236. Ehara S, Kobayashi Y, Yoshiyama M, Shimada K, Shimada Y, Fukuda D, Nakamura Y, Yamashita H, Yamagishi H, Takeuchi K, Naruko T, Haze K, Becker AE, Yoshikawa J, Ueda M: Spotty Calcification Typifies the Culprit Plaque in Patients With Acute Myocardial Infarction. Circulation 2004;110:3424-3429

237. Shanahan CM: Inflammation Ushers in Calcification: A Cycle of Damage and Protection? Circulation 2007;116:2782-2785

238. Tanimura A, McGregor DH, Anderson HC: Matrix vesicles in atherosclerotic calcification. Proc Soc Exp Biol Med 1983;172:173-177

239. Kapustin AN, Davies JD, Reynolds JL, McNair R, Jones GT, Sidibe A, Schurgers LJ, Skepper JN, Proudfoot D, Mayr M, Shanahan CM: Calcium regulates key components of vascular smooth muscle cell-derived matrix vesicles to enhance mineralization. Circ Res 2011;109:e1-e12

240. Kapustin AN, Shanahan CM: Emerging roles for vascular smooth muscle cell exosomes in calcification and coagulation. J Physiol 2016;(In Press)

241. Reynolds JL, Skepper JN, McNair R, Kasama T, Gupta K, Weissberg PL, Jahnen-Dechent W, Shanahan CM: Multifunctional roles for serum protein fetuin-a in inhibition of human vascular smooth muscle cell calcification. J Am Soc Nephrol 2005;16:2920-2930

242. Fleckenstein-Grun G, Frey M, Thimm F, Hofgartner W, Fleckenstein A: Calcium overload--an important cellular mechanism in hypertension and arteriosclerosis. Drugs 1992;44 Suppl 1:23-30

243. Anderson HC: The role of matrix vesicles in physiological and pathological calcification. Curr Opin Orthop 2007;18:428-433

244. Li Y, Ge M, Ciani L, Kuriakose G, Westover EJ, Dura M, Covey DF, Freed JH, Maxfield FR, Lytton J, Tabas I: Enrichment of endoplasmic reticulum with cholesterol inhibits sarcoplasmic-endoplasmic reticulum calcium ATPase-2b activity in parallel with increased order of membrane lipids: implications for depletion of endoplasmic reticulum calcium stores and apoptosis in cholesterol-loaded macrophages. J Biol Chem 2004;279:37030-37039

245. Autzen HE, Siuda I, Sonntag Y, Nissen P, Moller JV, Thogersen L: Regulation of the Ca(2+)-ATPase by cholesterol: a specific or non-specific effect? Mol Membr Biol 2015;32:75-87

246. van Meer G, Voelker DR, Feigenson GW: Membrane lipids: where they are and how they behave. Nat Rev Mol Cell Biol 2008;9:112-124

247. Allahverdian S, Chehroudi AC, McManus BM, Abraham T, Francis GA: Contribution of intimal smooth muscle cells to cholesterol accumulation and macrophage-like cells in human atherosclerosis. Circulation 2014;129:1551-1559

248. Rosenfeld ME: Converting smooth muscle cells to macrophage-like cells with KLF4 in atherosclerotic plaques. Nat Med 2015;21:549-551

249. Feil S, Fehrenbacher B, Lukowski R, Essmann F, Schulze-Osthoff K, Schaller M, Feil R: Transdifferentiation of vascular smooth muscle cells to macrophage-like cells during atherogenesis. Circ Res 2014;115:662-667

250. Shankman LS, Gomez D, Cherepanova OA, Salmon M, Alencar GF, Haskins RM, Swiatlowska P, Newman AA, Greene ES, Straub AC, Isakson B, Randolph GJ, Owens GK: KLF4-dependent phenotypic modulation of smooth muscle cells has a key role in atherosclerotic plaque pathogenesis. Nat Med 2015;21:628-637

251. Demer LL: Cholesterol in vascular and valvular calcification. Circulation 2001;104:1881-1883

252. Hoeg JM, Feuerstein IM, Tucker EE: Detection and quantitation of calcific atherosclerosis by ultrafast computed tomography in children and young adults with homozygous familial hypercholesterolemia. Arterioscler Thromb 1994;14:1066-1074

253. Pohle K, Maffert R, Ropers D, Moshage W, Stilianakis N, Daniel WG, Achenbach S: Progression of aortic valve calcification: association with coronary atherosclerosis and cardiovascular risk factors. Circulation 2001;104:1927-1932

254. Callister TQ, Raggi P, Cooil B, Lippolis NJ, Russo DJ: Effect of HMG-Coa reductase inhibitors on coronary artery disease as assessed by electron-beam computed tomography. New Engl J Med 1998;339:1972-1978

255. Bild DE, Folsom AR, Lowe LP, Sidney S, Kiefe C, Westfall AO, Zheng ZJ, Rumberger J: Prevalence and correlates of coronary calcification in black and white young adults: the Coronary Artery Risk Development in Young Adults (CARDIA) Study. Arterioscler Thromb Vasc Biol 2001;21:852-857

256. Schmermund A, Baumgart D, Mohlenkamp S, Kriener P, Pump H, Gronemeyer D, Seibel R, Erbel R: Natural history and topographic pattern of progression of coronary calcification in symptomatic patients: An electron-beam CT study. Arterioscler Thromb Vasc Biol 2001;21:421-426

257. Wilkins JT, Li RC, Sniderman A, Chan C, Lloyd-Jones DM: Discordance Between Apolipoprotein B and LDL-Cholesterol in Young Adults Predicts Coronary Artery Calcification: The CARDIA Study. J Am Coll Cardiol 2016;67:193-201

258. Lounsbury KM: Preventing stenosis by local inhibition of KCa3.1: a finger on the phenotypic switch. Arterioscler Thromb Vasc Biol 2008;28:1036-1038

259. Wheeler DG, Groth RD, Ma H, Barrett CF, Owen SF, Safa P, Tsien RW: Ca_v1 and Ca_v2 Channels Engage Distinct Modes of Ca^{2+} Signaling to Control CREB-Dependent Gene Expression. Cell 2012;149:1112-1124

260. Catterall WA: Voltage-gated calcium channels. Cold Spring Harb Perspect Biol 2011;3:a003947

261. Mironneau J: Calcium channel antagonist effects of spironolactone, an aldosterone antagonist. Am J Cardiol 1990;65:K7-K8

262. Wagner M, Rudakova E, Volk T: Aldosterone-induced changes in the cardiac L-type Ca(2+) current can be prevented by antioxidants in vitro and are absent in rats on low salt diet. Pflugers Arch 2008;457:339-349

CURRICULUM VITAE

Stacey Dineen Rodenbeck

EDUCATION

2012 B.S. Biology
Indiana University Southeast
School of Natural Sciences
New Albany, IN

2012 A.A. Chemistry
Indiana University Southeast
School of Natural Sciences
New Albany, IN

2016 Ph.D. Physiology; Minor: Cardiovascular Science
Indiana University
Department of Cellular & Integrative Physiology
Indianapolis, IN
Mentor: Michael Sturek, Ph.D.

Doctoral Dissertation

Coronary Artery Disease in Metabolic Syndrome: A Role for the Sarcoplasmic Reticulum Ca^{2+} ATPase

Research Committee

Michael Sturek, Ph.D. – Professor and Chair, Indiana University School of Medicine, Department of Cellular & Integrative Physiology

Richard Day, Ph.D. – Professor, Indiana University School of Medicine, Department of Cellular & Integrative Physiology

Carmella Evans-Molina, MD/Ph.D. – Assistant Professor of Medicine, Indiana University School of Medicine, Department of Medicine

Kieren J. Mather, MD – Professor of Medicine, Indiana University School of Medicine, Department of Medicine

Johnathan D. Tune, Ph.D. – Professor, Indiana University School of Medicine, Department of Cellular & Integrative Physiology

Awards/Fellowships

2011 McCullough Research Fellowship for Undergraduate Students, Indiana University Southeast

2011 Outstanding Biology Student Award, Indiana University Southeast, School of Natural Sciences; Department of Biology

2011 Dr. Claude D. Baker Scholarship for Undergraduate Students, Indiana University Southeast

2012 Indiana University School of Medicine Graduate Division University Fellowship

2014 Indiana Physiological Society Presentation Award

2014 Moenkhaus Physiology Graduate Fellowship for Academic Excellence, Indiana University School of Medicine; Department of Cellular & Integrative Physiology

2016 Society for Experimental Biology and Medicine Young Investigator Award

Grant Support

AHA 15PRE25280001: Midwest Affiliate Winter 2015 Predoctoral Fellowship, American Heart Association; 2015-Present.

TEACHING EXPERIENCE

Lectures

Fall 2013
BIOL L101Introduction to Biological Sciences, Indiana University Southeast
"Circulatory Systems"

Spring 2013
BIOL L101 Introduction to Biological Sciences, Indiana University Southeast
"*Circulatory Systems"*

BIOL 55700 Physiology II, Indiana University Purdue University Indianapolis
"*Physiology of Circulation"*

Fall 2014
BIOL L317 Developmental Biology, Indiana University Southeast
"The Third Week of Development"
"Cardiovascular System Development"

PHSL F503 Human Physiology, Indiana University School of Medicine
"*Cardiovascular System Design"*
"ECG and the Cardiac Cycle"
"Cardiac Output"

Teaching/Laboratory Assistantships

Spring 2014

GRAD G735 Cardiovascular, Respiratory, and Renal Physiology
Teaching Assistant, ECG Analysis,
Indiana University School of Medicine
Indianapolis, IN

Medical Physiology
Teaching Assistant, ECG Analysis,
Indiana University School of Medicine
Indianapolis, IN

Spring 2015

Medical Physiology
Teaching Assistant, ECG Analysis,
Indiana University School of Medicine,
Indianapolis, IN

GRAD G735 Cardiovascular, Respiratory, and Renal Physiology
Teaching Assistant
Indiana University School of Medicine
Indianapolis, IN

Service/Outreach

January 2013: Student Ambassador; IBMG recruitment weekend, Indiana University School of Medicine Graduate Division, Indianapolis, IN

January 2014: Student Ambassador; IBMG recruitment weekend, Indiana University School of Medicine Graduate Division, Indianapolis, IN

January 2014: Science fair judge; St. Malachy Science Fair, St. Malachy School, Brownsburg, IN

February 2014: Student Ambassador; IBMG recruitment weekend, Indiana University School of Medicine Graduate Division, Indianapolis, IN

August 2014: Student Mentor; IBMG new student orientation, Indiana University School of Medicine Graduate Division, Indianapolis, IN
"Think, Talk, Study Like a Graduate Student" (In collaboration with Gail Gardiner)

October 2014: Panelist; Graduate School Panel Discussion, Department of Biology; School of Natural Sciences; Indiana University Southeast

January 2015: Science fair judge; St. Malachy Science Fair, St. Malachy School, Brownsburg, IN

January 2015: Student Ambassador; IBMG recruitment weekend, Indiana University School of Medicine Graduate Division, Indianapolis IN

February 2015: Student Ambassador; IBMG recruitment weekend, Indiana University School of Medicine Graduate Division, Indianapolis, IN

Mentoring

Summer, 2014: Medical Student, Summer Research Program, Indiana University School of Medicine, Indianapolis, IN

Spring, 2015: Ph.D. Rotation Students (3), IBMG Program, Indiana University School of Medicine, Indianapolis, IN

Spring, 2015: Masters Student, Department of Cellular & Integrative Physiology, Indiana University School of Medicine, Indianapolis, IN

Summer, 2015: Ph.D. Rotation Student, Biomedical Engineering Department, Purdue University, West Lafayette, IN

PROFESSIONAL ORGANIZATIONS

Memberships

Indiana Physiological Society, 2013-present
American Physiological Society, 2013-present
Society for Experimental Biology and Medicine, 2013-present

PUBLICATIONS

Manuscripts

1) Yoder SM, **Dineen SL**, Wang Z, Thurmond DC. YES, a SRC Family Kinase, Is a Proximal Glucose-specific Activator of Cell Division Cycle Control Protein 42 (Cdc42) in Pancreatic Islet β Cells. *JBC* 286(16):11476-87. 2014.

2) **Dineen SL**, McKenney ML, Bell LN, Fullenkamp AM, Schultz KA, Alloosh M, Chalasani N, Sturek M. Metabolic syndrome abolishes glucagon-like peptide-1 receptor agonist stimulation of SERCA in coronary smooth muscle. *Diabetes* 64(9):3321-27. 2015.
***Highlighted with full commentary**:* Davies MG, New Insights on the Role of SERCA During Vessel Remodeling in Metabolic Syndrome. *Diabetes* 64(9):3066-68. 2015.

3) McKenney-Drake ML*, **Rodenbeck SD***, Owen MK, Schultz KA, Tune JD, Sturek M. Biphasic alterations in coronary smooth muscle Ca^{2+} regulation in a repeat cross-sectional study of coronary artery disease severity in metabolic syndrome, *Atherosclerosis* 2016 (In Press).

4) McKenney-Drake ML*, **Rodenbeck SD***, Owen MK, Schultz KA, Tune JD, Sturek M. Repeat cross-sectional data on the progression of the metabolic syndrome in Ossabaw miniature swine, *Data in Brief* 2016 (In Press).

5) **Rodenbeck SD***, Zarse CA*, McKenney-Drake ML, Bruning RS, Sturek M, Chen NX, Moe SM. Disrupted intracellular calcium homeostasis of vascular smooth muscle cells in a rat model of chronic kidney disease, (Under Review).

6) **Rodenbeck SD**, Barnard AL, Sturek M. SERCA activator CDN1163 induces coronary smooth muscle proliferation in an organ culture model of coronary artery disease, (In Preparation).

7) Bruning RS, **Rodenbeck SD**, Alloosh M, Sturek M. Effect of metabolic syndrome and advancing age on vascular smooth muscle, (In Preparation).

8) McKenney-Drake ML, **Rodenbeck SD**, Bruning RS, Yancey KW, Alloosh M, Sacks H, Sturek M. Removal of coronary epicardial adipose tissue attenuates progression of coronary artery disease in Ossabaw swine (In Preparation).

Book Chapters and Reviews

1) **Dineen SL**, Neeb ZP, Obukhov AG, and Sturek M. Transient receptor potential channels in metabolic syndrome-induced coronary artery disease. *Ion Channels in Vascular Disease.* I. Levitan and A.M. Dopico (Eds). New York, NY: Springer, (In Press, 2016).

2) Sturek M, **Dineen SL**, Bruning RS and Alloosh MA. Animal research models in metabolic syndrome and cardiovascular disease. *Compr Physiol* (In prep): 2016

Abstracts

1) **Dineen SL**, McKenney ML, and Sturek M. An *in vitro* model of coronary artery disease and the changes in intracellular calcium regulation during its progression. *FASEB J* 27:lb652. 2013.

2) **Dineen SL**, McKenney ML, and Sturek M. Glucagon-like peptide-1 (GLP-1) receptor agonist, exenatide, enhances Ca^{2+} buffering by SERCA in coronary smooth muscle cells from lean, healthy Ossabaw swine. *FASEB J* 28:700.3. 2014.

3) McKenney ML, **Dineen SL**, Noblet JN, Tune JD, and Sturek M. Increased Ca^{2+}-activated Ca^{2+} influx and impaired Ca^{2+} buffering in coronary smooth muscle from metabolic syndrome Ossabaw swine. *FASEB J* 28:1076.2. 2014.

4) Zarse CA, McKenney ML, **Dineen SL,** Sturek M, Chen NX, and Moe SM. Intracellular Ca^{2+} signaling is altered in vascular smooth muscle cells (VSMC) in chronic kidney disease. *J Am Soc Nephrol* 25:232A, 2014.

5) **Dineen SL** and Sturek M. Assessment of endoplasmic reticulum stress by graded sarcoplasmic reticulum Ca^{2+} store depletion in coronary smooth muscle. *FASEB J* 29:638.2. 2015.

6) **Rodenbeck SD**, Barnard AL, and Sturek M. SERCA inhibition attenuates medial thickening in an organ culture model of coronary artery disease. *FASEB J (In Press)*

PRESENTATIONS

Invited Seminars

1) **Dineen SL**. Top-down Cardiovascular Pathophysiology: Investigating Coronary Artery Disease from Whole Animal Phenotype to Intracellular Mechanism. Invited

Seminar, Department of Biological Sciences, Butler University, October 2014, Indianapolis, IN

Oral Presentations

1) **Dineen SL**, McKenney ML, and Sturek M. Exenatide specifically enhances Ca^{2+} buffering by SERCA in coronary smooth muscle cells from lean, healthy Ossabaw swine. Oral presentation, 4th Annual Meeting of the Indiana Physiological Society, February, 2014, Evansville, IN

2) **Dineen SL**, McKenney ML, and Sturek M. Exenatide specifically enhances Ca^{2+} buffering by SERCA in coronary smooth muscle cells from lean, healthy Ossabaw swine. Oral presentation, Indiana Academy of Science, March 2014, Indianapolis, IN

Poster Presentations

1) **Dineen SL**, Rollins JM, and Kirchner G. Determining the Source of Kanamycin Resistance in a *Halobacillus blutaparonensis* Isolate. Poster presentation, Indiana Academy of Science, March 2012, West Lafayette, IN

2) **Dineen SL**, McKenney ML, and Sturek M. An *in vitro* model of coronary artery disease and the changes in intracellular calcium regulation during its progression. Poster presentation, 3rd Annual Meeting of the Indiana Physiological Society, February, 2013, Indianapolis, IN

3) **Dineen SL**, McKenney ML, and Sturek M. An *in vitro* model of coronary artery disease and the changes in intracellular calcium regulation during its progression. Poster presentation, Experimental Biology 2013, Boston, MA

4) **Dineen SL**, McKenney ML, and Sturek M. Exenatide specifically enhances Ca^{2+} buffering by SERCA in coronary smooth muscle cells from lean, healthy Ossabaw swine. Poster presentation, Experimental Biology 2014, San Diego, CA

5) **Dineen SL** and Sturek M. Altered sarcoplasmic reticulum Ca^{2+} storage in coronary smooth muscle with increasing severity of coronary artery disease. Poster Presentation, 5th Annual Meeting of the Indiana Physiological Society, February, 2015, Indianapolis, IN

6) **Dineen SL** and Sturek M. Assessment of endoplasmic reticulum stress by graded sarcoplasmic reticulum Ca^{2+} store depletion in coronary smooth muscle. Poster Presentation, Experimental Biology 2015, Boston, MA

7) **Rodenbeck SD**, Barnard AL, and Sturek M. SERCA inhibition attenuates medial thickening in an organ culture model of coronary artery disease. Poster Presentation, Experimental Biology 2016, San Diego, CA